MOLECULAR SIZE AND CONFIGURATION OF CARBOXYMETHYL CELLULOSE IN AQUEOUS SOLUTIONS

by

Gullapalli Sitaramaiah, M.Sc.

A thesis submitted to the Faculty of Graduate Studies and Research of McGill University in partial fulfilment of the requirements for the degree of Doctor of Philosophy.

Department of Chemistry,
McGill University,
Montreal, Canada.

April, 1961.

ACKNOWLEDGMENTS

The author takes this opportunity to express his gratitude and thanks to:

Dr. S.G. Mason for his encouragement and valuable suggestions at all times;

Dr. D.A.I. Goring for his able direction and constant advice;

Dr. R. St.J. Manley for valuable discussions;

Dr. R.F. Robertson for allowing use of the ultracentrifuge in his laboratory;

and the Pulp and Paper Research Institute of Canada for laboratory accomodation and equipment.

Acknowledgment is made with thanks to:

The Defence Research Board of Canada for financial assistance (1958-59).

The Visking Division of Union Carbide Co. for a fellowship during 1959-60.

The Pulp and Paper Research Institute of Canada for two summer grants in 1959 and 1960.

McGill University for a summer grant in 1958 and a graduate fellowship during 1960-61.

and The Mead Foundation for a research grant in 1960-61.

FOREWORD

This thesis describes an investigation on the molecular size and configuration of carboxymethyl cellulose in aqueous solutions. The work forms a part of a current series of macromolecular studies in Wood and Cellulose Chemistry.

The thesis opens with a Preface and General Introduction. There follows the main text of the thesis which is divided into three Parts. These are written in the form of scientific papers and are to be submitted for publication with little or no modification. Each of the Parts has its own Abstract, Introduction, Experimental and Results, Discussion, References, Tables and Figures.

The main text of the thesis ends with Concluding Remarks, Claims for Original Research and Suggestions for Further Work.

Additional details of experimental procedure, equipment and data are given in a series of Appendices.

CONTENTS

CONTENTS Continued

CONTENTS Continued

APPENDICES

LIST OF TABLES

Part I

Part II

Part III

LIST OF TABLES Continued

Appendix I

Appendix II

Appendix III

Appendix V

Appendix VI

LIST OF TABLES Appendix VI Continued

LIST OF FIGURES

Part I

Part II

LIST OF FIGURES Continued

Part III

Appendix I

Appendix II

Appendix III

LIST OF FIGURES Appendix III Continued

Appendix IV

Appendix V

LIST OF SYMBOLS

$\mathring{A}$	Angstrom unit (10^{-8} cm.)
A_2	Second virial coefficient
a	A constant in the simplified equation for polyelectrolyte expansion in Hermans–Overbeek theory
$\underline{a}$	Exponent in Mark Howinck equation
b	Effective bond length
b'	Exponent in sedimentation–molecular weight relationship
b_o	Bond length of a glucose unit
C	Calibration constant for light scattering apparatus
C_o	Fringe shift in diffusion
c	Concentration in $g.dl.^{-1}$
D	Diffusion constant
D_o	Diffusion constant at zero concentration and 25^oC
D_m	Diffusion constant by second moment method
D_A	Diffusion constant by 'area' method
e	Electronic charge
F_o	Frictional constant
F_H	Hydrodynamic compressive force
F_E	Electrostatic repulsive force
G	Shear rate in $sec.^{-1}$
g.	gms.
$\underline{g}$	Acceleration due to gravity
H	Optical constant in light scattering equation relating the turbidity-concentration ratio to molecular weight

h	Height defining pressure head in a viscometer
I_E	Ionic strength
I_{90}	Intensity of light scattered at 90^o angle
K	A constant in light scattering equation
K	Constant in the intrinsic viscosity molecular weight equation
K_m	Constant in Staudinger's intrinsic viscosity-molecular weight equation
$\underline{K}$	Reciprocal of Debye width of double layer
k	Arbitrary constant in Zimm's light scattering equation
k	Boltzmann constant
k'	Huggins coefficient
k_s	Constant in the concentration dependence equation of sedimentation
k_s'	A second constant in the above equation
l	Depth of the diffusion cell
M	Molecular weight
M_w	Weight average molecular weight
M_o	Monomer weight
M_{sD}	Sedimentation-diffusion molecular weight
$M_{s\eta}$	Sedimentation-viscosity molecular weight
M_{LS}	Molecular weight by light scattering
N	Avogadro's number
n	Refractive index
n_o	Refractive index of solvent
Q	Surface charge density
q	Porod-Kratky persistence length

R_θ	Raleigh ratio at angle θ
$\overline{R}^2$	Mean square end to end distance of polymer chain
R_s	Radius of a hydrodynamic sphere
r_η	Radius of an equivalent sphere in viscosity assuming random coil model
r_o^2	Mean square end to end distance at high ionic strength
r	Capillary radius of the viscometer
r_{max}	Maximum extension of polymer molecule
$\overline{s}_z^2$	Square of z-average radius of gyration
s_m	Maximum-ordinate sedimentation constant
s_o	Sedimentation constant at zero concentration and 25°C
s	Sedimentation constant
$[s]$	Sedimentation constant extrapolated to zero molecular weight
T	Absolute temperature
t	Time in seconds
t_o	Flow time of solvent in the viscometer
t_s	Flow time of solution in the viscometer
$\bar{v}$	Partial specific volume
x_m	Distance of maximum ordinate
x	Distance in the direction of diffusion
V_R	Repulsive energy of two charged spheres
Z	Degree of polymerization
$\underline{Z}$	Number of charges per polyion
Z*	Dissymmetry in light scattering
$[Z^*]$	Intrinsic dissymmetry

α	Molecular expansion factor
α	A function of the axial ratio of a particle
β	Magnification factor in diffusion
δ	Half the distance of closest approach of particles in doublet collisions
ϵ	Dielectric constant
η_o, η_s	Viscosity of solvent and solution
η_{rel}	Relative viscosity
η_{sp}	Specific viscosity
$[\eta]$	Intrinsic viscosity
$[\eta]_o$	Intrinsic viscosity at zero shear rate
$[\eta]_{500}$	Intrinsic viscosity at a shear rate of 500 $sec.^{-1}$
θ	Angle between transmitted and scattered beams
λ	Wavelength of light (5461 Å)
λ	$x/\sqrt{t}$ in diffusion
ρ_s, ρ_o	Density of solution and solvent
ρ	Density of the medium
σ	Shielding ratio in hydrodynamic theories
τ	Turbidity of solutions by spectrophotometer or by light scattering
$\phi(\sigma)$, $\psi(\sigma)$	Volume factors in hydrodynamic theories
Λ	A constant deduced by Burgers for spheres in doublet collisions
ψ_o	Surface potential
ω	Angular velocity of ultracentrifuge rotor
ζ	Monomer frictional constant

PREFACE

Dilute solutions of cellulose derivatives exhibit special features because of the characteristically high extensions of the cellulose chain molecule as shown in the earlier work on cellulose trinitrate by Huque, Goring and Mason. In the present investigation these studies have been extended to aqueous solutions of carboxymethyl cellulose which are of particular interest because the macromolecules can ionize. In addition to the possibility of configurational changes with increasing molecular weight, the charged groups cause high extension of the cellulose chains at low ionic strength due to electrostatic interaction. Although such polyelectrolyte expansion has been studied in some detail for individual samples by earlier workers, a systematic investigation of the hydrodynamic behavior over a series of fractions of carboxymethyl cellulose is lacking.

The aim of the present investigation was to undertake a general configurational study of a stiff chain polyelectrolyte in contrast to a flexible chain polyelectrolyte, by techniques used to elucidate the solution properties of polymers. Further this investigation was expected to lead to a better understanding of the behavior of cellulose derivatives in solution, particularly for the cellulose ethers, which so far have received considerably less attention than the cellulose esters such as the trinitrate.

Sodium carboxymethyl cellulose was fractionated by precipitating with ethanol from aqueous solution. Eight fractions covering a range of

viscosities were selected for a detailed measurement. The techniques of viscometry, light scattering, velocity sedimentation and diffusion were employed.

Viscosity measurements were made in a four-bulb Ubbelohde capillary viscometer. Intrinsic viscosities were computed at a shear rate of 500 $sec.^{-1}$ over a range of ionic strengths.

Extensive light scattering measurements were made and the weight average molecular weights were obtained. However, the light scattering molecular weights, although reproducible, were anomalously high because of the presence of molecular aggregates.

Sedimentation and diffusion constants were measured and the sedimentation-diffusion molecular weights were calculated from Svedberg's equation.

After a general introduction, the original content of the Thesis is presented in three Parts. Part I deals with the intrinsic hydrodynamic properties of the various fractions. Exponents are determined from the logarithmic dependence of the intrinsic viscosity, sedimentation and diffusion constants on the molecular weight. These exponents are then used to elucidate the configurational behavior of the macromolecule with changes in ionic strength. The polyelectrolyte theories of Hermans and Overbeek and of Flory are applied to interpret the large increases of intrinsic viscosity with decrease in ionic strength. Finally, the recently published approximations of Marrinan and Hermans to the Debye-Bueche and

Kirkwood-Riseman hydrodynamic relationships are used to compute the monomer frictional constant at different molecular weights. The monomer frictional constant is compared with an approximate, comparative value derived from the diffusion constant of sucrose.

Part II of the thesis is concerned with the concentration dependence of the reduced viscosity. The Huggins constant was found to vary widely over a range of ionic strengths and molecular weights. This is interpreted in terms of the secondary electroviscous effect applied to doublet collisions of the macromolecules, analogous to the detailed studies of Mason and co-workers on the collision of the particles in sheared suspensions. A theoretical relationship is derived and tested for the surface charge density on the basis of the equilibrium between the hydrodynamic compressive force and the electrostatic repulsive force when the colliding macromolecules form a doublet.

In the third part, the concentration dependence of sedimentation is considered. Here the changes in the slope constant with molecular weight and ionic strength are treated both by the electrostatic theory of Tiselius and by the excluded volume theory of Wales and Van Holde. It is shown that the latter is predominant in determining the degree of concentration dependence of sedimentation at ionic strengths down to 0.001 M.

After a brief section on concluding remarks, several appendices are listed which give further details of the techniques used. The Thesis ends with tables containing the prime data on which the work is based.

GENERAL INTRODUCTION

In this section a short outline of the general background to the macromolecular studies of cellulose and derivatives is given. Some of the more important investigations so far undertaken on CMC are also briefly presented here. Finally, a brief account of the hydrodynamic theories as well as certain special aspects of the experimental techniques are given in order to anticipate the interpretation of the results.

Cellulose

Cellulose occurs abundantly in nature and is the major component in the vegetable kingdom. For this reason cellulose and its derivatives have been intensively investigated. A detailed survey of our present knowledge in this field has been given in several excellent monographs (1,2,3).

The chemical structure of cellulose is well-established. The cellulose molecule is a polymer resulting from 1-4 polycondensation of β-glucose units. The number of glucose residues in a molecule of cellulose may be of the order of several thousand.

Within a cellulose fibre the chain molecules are bound laterally to one another by hydrogen bonds in such a way as to form crystallites separated by amorphous regions. The dimensions of the crystallite unit cell are 8.35 x 10.3 x 7.9 Å. In the direction of the fibre axis two $C_6H_{10}O_5$ units occur within 10.3 Å. The insolubility of cellulose in aqueous solvents is due to its highly crystalline and hydrogen-bonded

structure. Also the reactivity of cellulose in the amorphous regions is greater than in the crystallites.

The problem of the size of the undegraded cellulose molecule has attracted great interest. In this respect the recent work of Timell et al (4) has shown that celluloses prepared from a wide variety of plants have degrees of polymerization (D.P.) of between 6,000 and 10,500. The celluloses were studied as their trinitrates, prepared by non-degradative nitration of cottons, woods, bast fibres and grasses.

In solution the molecules of cellulose and derivatives have been shown to possess a threadlike form (5). Staudinger (6) pointed out the utility of viscosity measurements on dilute solutions of polymers and gave a useful empirical relationship for the molecular weight, M of long chain molecules

$$[\eta] = K_m M \qquad \ldots(1)$$

where $[\eta]$ is the intrinsic viscosity and K_m is a proportionality constant. In later work Eq. (1) was modified by Mark and Howinck to include an exponent to the molecular weight. For synthetic polymers the exponent in general had the value of 0.6 - 0.8. However, in the case of investigations on cellulose derivatives (7-13) it has been shown that the exponent in the intrinsic viscosity molecular weight relationship was approximately unity, which suggests that the cellulose molecule has an extended configuration in solution.

At Uppsala, Svedberg and co-workers (5) investigated cellulose and a number of its derivatives with a view to determine the molecular weight distribution. Extensive measurements were made by sedimentation velocity and equilibrium in the ultracentrifuge. Nitrocellulose and cellulose in cuprammonium received special attention. Gralen (14) determined molecular weights of cellulose and derivatives by sedimentation and diffusion and observed that polydispersity increased with the increase in molecular weight. Jullander (15) studied the molecular weight distribution and polydispersity of various nitrocelluloses. Bryde and Ranby (16) investigated the molecular properties of native and wood celluloses nitrated under mild conditions. Mosimann (17) showed in the case of nitrocelluloses that the sedimentation equilibrium method can be applied only at low concentrations and moderate molecular weights.

The investigations in recent years have been mainly concerned with the elucidation of the configurational properties of the cellulose macromolecule in solution. Holtzer, Benoit and Doty (11), from a light scattering study of cellulose trinitrate, showed that the ratio of the mean square radius of gyration to the molecular weight increased with the increase of molecular weight and reached a constant value at a molecular weight of about 400,000. A similar trend was noted by Hunt, Newman, Scheraga and Flory (7) as well as Huque, Goring and Mason (18). This behavior was considered to arise from the unusual chain stiffness displayed by the cellulose macromolecule in solution. Manley (13) studied the molecular configuration of ethyl hydroxyethyl cellulose and observed that this cellulose ether showed greater flexibility than the esters. Recently Krigbaum and Sperling (19) reported

that cellulose tricaproate exhibited properties characteristic of inflexible macromolecules. It is interesting to note that investigations on the configuration of cellulose esters by far outweigh similar studies on the ethers.

Cellulose Ethers

Among the cellulose derivatives, the ethers of cellulose are relatively recent and have been studied less than the organo-soluble celluloses such as the trinitrate. The principal water-soluble cellulose ethers are the methyl, ethyl, hydroxyethyl and carboxymethyl celluloses.

Sodium Carboxymethyl Cellulose

Sodium carboxymethyl cellulose is prepared (1) by reacting sodium monochloroacetate with cellulose in the presence of excess sodium hydroxide. The monomer is designated by the structural formula shown in Fig. 1. Generally and in this thesis the term'carboxymethyl cellulose' (CMC) is used to mean the sodium salt of carboxymethyl cellulose.

In the etherification, the reactivity of the positions of substitution was discussed in detail by Timell (20) who found that the 6-position was most reactive. Recently Croon et al (21-24) investigated the distribution of substituents in methyl, ethyl, hydroxyethyl and carboxymethyl celluloses by hydrolysing the ethers to monomers and fractionating the hydrolysates on a carbon column. In a recent study of partially substituted carboxymethyl celluloses, Croon and Purves (24) found all possible arrangements of the carboxymethyl group in the products of carboxymethylation to D.S. 0.75, 0.90 and 0.98.

Fig. 1

Structural formula for a substituted monomer of carboxymethyl cellulose, D.S. = 1

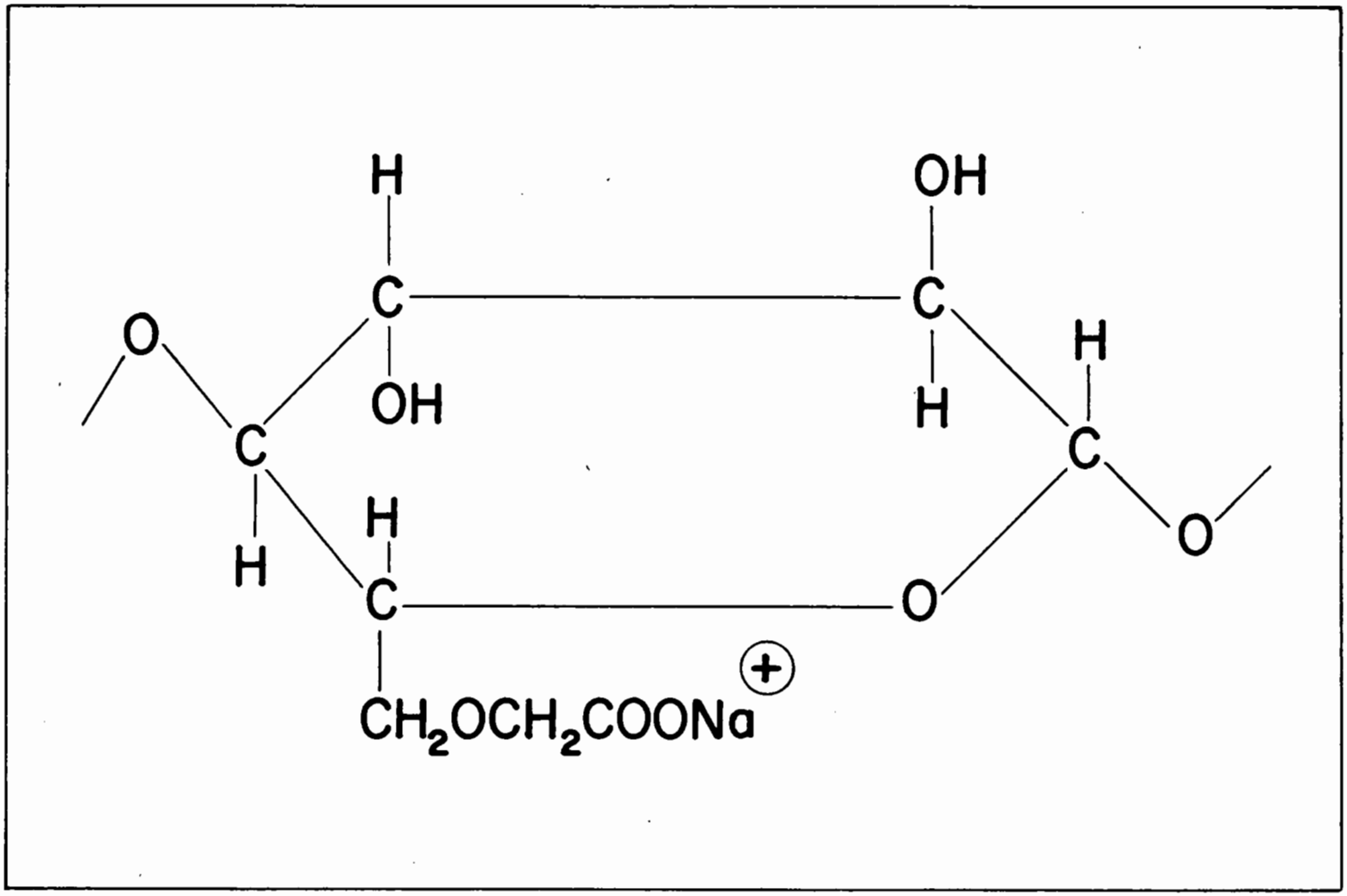
H
OH
C
C
O
H
OH
H
C
C
H
H
O
H
C
O
O
CH2OCH2COONa
+

Solutions of carboxymethyl cellulose can be made in well-agitated water. The solutions are thixotropic and the viscosity depends on the rate of shear and other variables. When dissolved in water, the macromolecule behaves as a protective colloid (1). Also it has film-forming properties. The high viscosity of CMC solutions is an advantage where a thickening agent is needed. The industrial grades of CMC occur in the range of D.S. of 0.7 - 1.2, although the theoretical upper limit of D.S. is three.

In aqueous solution, sodium carboxymethyl cellulose shows typical polyelectrolyte properties. A marked decrease in the reduced viscosity occurs when the solution is made more concentrated or when a salt such as sodium chloride is added. When the sodium ion is removed by ion-exchange or dialysis CMC becomes a weak acid with an ionization constant of 3×10^{-5} (25). The acid form of CMC becomes insoluble when overdried. The pH of precipitation of the acid form increases with the decrease of D.S. A water dispersion of the free acid form can be made by treatment with ion-exchange resins.

Earlier Physico-Chemical Studies of CMC

Various samples of sodium carboxymethyl cellulose have been studied by a number of investigators. Akkerman, Pals and Hermans (26) investigated the dependence of intrinsic viscosity on shear rate for a sample having an average molecular weight of 150,000 and a degree of substitution of 0.55. Their results indicate that, in aqueous sodium chloride, this sample is non-Newtonian, i.e. the intrinsic viscosity decreases with increase of shear rate, at concentrations as low as 0.01 g./100 ml. Basu and Das Gupta (27)

have made a viscosity study on a sample having D.S. of 0.38 and molecular weight of about 40,000 and showed that the sample showed a polyelectrolyte effect i.e. the reduced viscosity increased on dilution.

Allgen and Roswall (28) carried out a dielectric study on a sample of D.S. 0.5 and molecular weight of 460,000. Their results indicate that the molecules are rigid and also a strong interaction between the molecules occurs especially at concentrations above 0.01 $g.dl.^{-1}$ MacLennan (29) investigated the polyelectrolytic behavior of two samples of CMC having a D.S. of 0.83 and 0.5, by measurements of intrinsic viscosity, extinction angle and double refraction of flow. At concentrations necessary to measure the extinction angles a concentration effect was observed which was attributed to particle interactions. The viscosity, extinction angle and birefringence data indicated that the addition of sodium chloride to the polyelectrolyte solutions caused the polyions to contract.

Pals and Hermans (30) investigated the viscosity behavior of sodium carboxymethyl cellulose in detail. Three samples of CMC of D.P. 725, 391 and 325, and of D.S. of 0.42 - 0.56 were used. To obtain reliable intrinsic viscosities, an isoionic dilution technique was developed in which the effective ionic strength is kept constant. The shear dependence of the intrinsic viscosity was observed to vary approximately between 5-15%. It was shown that the viscosity results were approximately of the same magnitude as predicted by the Hermans-Overbeek theory (31).

Schneider and Doty (32) used an unfractionated sample of CMC of D.S. 1.15 and molecular weight of 400,000 and studied by viscosity and light

scattering the change of molecular properties with ionic strength. It was found that the root mean square end-to-end distance increased by 45% in the range of ionic strength, 0.5 - 0.005 investigated. The expansion predicted by Hermans-Overbeek as well as Flory (33) theories was considerably greater than this and hence it was concluded that the existing theories are inadequate to predict the true polyelectrolyte expansion. Trap and Hermans (34) also studied by light scattering the molecular size and configuration of CMC. Good agreement of the effective molecular radius calculated from light scattering with the value from viscosity by Pals and Hermans (30) was noted. Also it was shown that the theory of Katchalsky and Lifson (35) was inadequate to interpret the data.

Fujita and Homma (36) studied the shear dependence of viscosity of CMC solutions by using the same fractions as Pals and Hermans (30), and observed that the intrinsic viscosity obtained from reduced viscosity concentration graphs at constant shear rates was independent of shear rate. Recently Longsworth and Hermans (37) measured the conductivity of potassium salts of carboxymethyl cellulose. When the concentration of $K^{(+)}$ and $Cl^{(-)}$ ions in solution was kept constant, the specific conductivity generally decreased with increasing polymer concentration. The experimental data were interpreted in terms of a theory in which the charge resulting from relaxation effects was treated as a surface charge. Napjus and Hermans (38) carried out conductance and electrophoresis studies on CMC. The electrophoretic mobilities extrapolated to zero polymer content were found to be independent of ionic strength. Further, the radius of a glucose unit was derived as equal to 1 $\mathring{A}$.

With the exception of the work of Pals and Hermans (30), studies on the fractionation of CMC are lacking. To the author's knowledge, no investigation has yet been published in which the hydrodynamic parameters are interpreted in terms of changes in molecular weight, as has been reported for many other high polymers including cellulose trinitrate (7). From such studies on CMC the Kirkwood-Riseman (39) and Debye-Bueche (40) theories could be tested for a stiff chain polyelectrolyte.

Hydrodynamic Theories

Current theories on the hydrodynamic behavior of polymer molecules in solution take into consideration the interaction of the chain elements in flow and assume a constant hydrodynamic radius of the monomer unit. Also assumed is the linear relation

$$\overline{R}^2 = Z\, b^2 \qquad \ldots(2)$$

for the mean square end to end distance, $\overline{R}^2$ of the polymer molecule. In Eq. (2) b is the effective bond length and Z is the degree of polymerization. In the validity range of Eq. (2) the theories can be applied to the determination of molecular dimensions.

In the treatment of Debye and Bueche (40) (D.B.) the coiled macromolecule is replaced by a porous sphere of radius, R_s uniformly filled with resisting points equal to the number of monomer units in the molecule. The hydrodynamic interaction within the sphere is defined by a shielding ratio, σ. Then the flow of solvent through the aggregate of resisting points lead to the results

$$[\eta] = \frac{4\pi}{3} \frac{N}{M} R_s^3 \phi(\sigma) \quad \ldots(3)$$

$$[s] = \frac{s_o \eta_o}{(1-\bar{v}\rho)} = \frac{M}{6\pi R_s N \psi(\sigma)} \quad \ldots(4)$$

$$D = \frac{kT}{6\pi \eta_o R_s \psi(\sigma)} \quad \ldots(5)$$

where the symbols have the same significance, as given in the glossary.

In its physical assumptions the Kirkwood-Riseman (K.R.) theory is more rigorous. The model used is that of hampered flow through beads arranged as in a random coil. The hydrodynamic interaction between the different parts of the molecule is calculated directly on the basis of the classical hydrodynamic equations of motion. The relations obtained are

$$[\eta] = \frac{N \zeta b^2 Z}{36 \cdot \eta_o \cdot M_o} F(\lambda_o Z^{\frac{1}{2}}) \quad \ldots(6)$$

$$D = \frac{kT}{Z\zeta} \left[1 + 8/3 \lambda_o Z^{\frac{1}{2}}\right] \quad \ldots(7)$$

$$s = \frac{M_o}{\zeta} (1-\bar{v}\rho) \left[1 + 8/3 \lambda_o Z^{\frac{1}{2}}\right] \quad \ldots(8)$$

in which ζ and M_o are the frictional constant and molecular weight of the monomer. And $\lambda_o = \zeta/(6\pi^3)^{\frac{1}{2}} \eta_o b$.

In the Flory (33) treatment the frictional constant is related to the intrinsic viscosity and the sedimentation constant and the relationship is given as

$$s_o [\eta]^{1/3}/M^{2/3} = \phi^{1/3} P^{-1} N^{-1} (1-\bar{v}\rho)/\eta_o \quad \ldots(9)$$

where $(\phi^{1/3}_{P-1})$ is a universal constant for polymers and has a value of 2.6×10^{6}.

Experimental Methods

The molecular size and configuration of CMC was investigated by the techniques of viscometry, light scattering sedimentation and diffusion. With the exception of diffusion, the methods have been described in publications from this laboratory. However, some special features in each of them may be mentioned briefly.

Light Scattering

Striations were observed in the light scattering of cellulose trinitrate by Huque et al (18), and 4-O-methylglucuronoxylans by Timell and Goring (41). In this respect Manley (13) observed, in the case of ethyl hydroxyethyl cellulose, light scattering molecular weights which are higher by a factor of three than the sedimentation-diffusion molecular weights. Manley attributed the high molecular weights to large aggregates present in solution. Recently Abe and Prins (42) reported light scattering molecular weights up to 13 times higher than those obtained by Archibald sedimentation technique. In the present work similar difficulties were encountered and, as shown in a later section, the light scattering data could not be used.

Viscosity

In the concentration dependence of the reduced viscosity of poly-

electrolytes, unusually high values of Huggins coefficient, k' were reported for CMC (30,36). Values of k' as high as 400 were observed by Goring and Rezanowich (43), for lignin sulfonates.

Sedimentation

The charge effects in sedimentation were investigated by Tiselius (44). An equation was derived which predicted the decrease of sedimentation rate due to the potential developed in the cell. Pedersen (45), who made a systematic investigation of this problem recently, pointed out that the decrease in sedimentation was partly due to the primary charge effect and partly to changes in configuration of the molecule.

For a wide variety of vinyl polymers Wales and Van Holde (46) interpreted the concentration dependence of sedimentation by the theory of molecular size. In Part III of the thesis these two approaches have been used to interpret the concentration dependence of sedimentation of CMC over a range of molecular weights and ionic strengths.

Diffusion

The usual diffusion techniques employed are so time consuming that comparatively few diffusion studies on macromolecules are available. The Zeiss Diffusion Interferomater used in this work is a bench type instrument. With the micro diffusion cells it has the advantage of giving reasonably accurate diffusion constants in runs of only a few hours. It is also normal in diffusion measurements to work at four or five concentrations in order to

obtain the diffusion constant at zero concentration by extrapolation. However, the Boltzmann (47) technique has been used in the present work which allows the computation of the diffusion constant at zero concentration with a single run at only one concentration. Further details are given in later sections of the Thesis.

REFERENCES

1. E. Ott and H.M. Spurlin, High Polymers, Vol. V, Interscience (1955).
2. E. Heuser, The Chemistry of Cellulose, John Wiley (1944).
3. E. Hagglund, Chemistry of Wood, Academic Press (1951).
4. T. Timell, Svensk Papperstidn. 60, 836 (1957).
5. T. Svedberg and K.O. Pedersen, The Ultracentrifuge, Oxford (1940).
6. H. Staudinger and W. Heuer, Ber. 63, 222 (1930).
7. M.L. Hunt, S. Newman, H.A. Scheraga and P.J. Flory, J. Chem. Phys. 60, 1278 (1956).
8. H.J. Phillips and C.F. Bjork, J. Polym. Sci. 6, 549 (1951).
9. R.S. Stein and P. Doty, J. Am. Chem. Soc. 68, 159 (1946).
10. R.M. Badger and R.H. Blaker, J. Phys. Chem. 53, 1056 (1949).
11. A.M. Holtzer, H. Benoit and P. Doty, J. Phys. Chem. 58, 624 (1954).
12. E.H. Immergut, B.G. Ranby and H. Mark, Ind. Eng. Chem. 45, 2483 (1953).
13. R. St.J. Manley, Arkiv For Kemi, 9, 519 (1956).
14. N. Gralen, Sedimentation and Diffusion measurements on Cellulose and Cellulose Derivatives, Inaugural Dissertation, Uppsala (1944).
15. I. Jullander, Studies on Nitrocellulose, Arkiv For Kemi, Minerologi Och Geologi, 21 A, 1 (1945).
16. O. Bryde and B. Ranby, Svensk Papperstidn. 50, 34 (1947).
17. H. Mosimann, Helv. Chim. Acta. 26, 61 (1943).
18. M.M. Huque, D.A.I. Goring and S.G. Mason, Can. J. Chem. 36, 952 (1958).
19. W.R. Krigbaum and L.H. Sperling, J. Phys. Chem. 64, 99 (1960).
20. T. Timell, Studies on Cellulose Reactions, Diss., Esselte AB, Stockholm (1950).
21. I. Croon and B. Lindberg, Svensk Papperstidn, 59, 794 (1956).

22. I. Croon and B. Lindberg, Svensk Papperstidn, 60, 843 (1957).

23. I. Croon and E. Flamm, Svensk Papperstidn, 61, 963 (1958).

24. I. Croon and C.B. Purves, Svensk Papperstidn, 62, 876 (1959).

25. C.J. Brown and A.A. Houghton, J. Soc. Chem. Ind. 60, 254 (1941).

26. F. Akkerman, D.T.F. Pals and J.J. Hermans, Rec. trav. Chim. 71, 56 (1952).

27. S. Basu and P.C. Das Gupta, J. Colloid Sci. 7, 53 (1952).

28. L.G. Allgen and S. Roswall, J. Polym. Sci. 12, 229 (1954).

29. D.F. MacLennan, Ph.D. Thesis, McGill University, 1954.

30. D.T.F. Pals and J.J. Hermans, Rec. trav. Chim. 71, 433 (1952).

31. J.J. Hermans and J.T.G. Overbeek, Rec. trav. Chim. 67, 762 (1948).

32. N.S. Schneider and P. Doty, J. Phys. Chem. 58, 762 (1954).

33. P.J. Flory, J. Chem. Phys. 21, 162 (1953).

34. H.J.L. Trap and J.J. Hermans, J. Phys. Chem. 58, 757 (1954).

35. A. Katchalsky and S. Lifson, J. Polym. Sci. 11, 409 (1953).

36. H. Fujita and T. Homma, J. Polym. Sci. 15, 277 (1955).

37. R. Longsworth and J.J. Hermans, 26, 47 (1957).

38. P.J. Napjus and J.J. Hermans, J. Colloid Sci. 14, 252 (1949).

39. J.G. Kirkwood and J. Riseman, J. Chem. Phys. 16, 565 (1948).

40. P. Debye and A.M. Bueche, J. Chem. Phys. 16, 563 (1948).

41. T. Timell and D.A.I. Goring, J. Phys. Chem. 64, 1426 (1960).

42. H. Abe and W. Prins, Makromolek, Chem. 42, 216 (1961).

43. D.A.I. Goring and A. Rezanowich, J. Colloid Sci. 15, 477 (1960).

44. A. Tiselius, Kolloid-Z. 59, 306 (1932).

45. K.O. Pedersen, J. Phys. Chem. 62, 1282 (1958).

46. M. Wales and K.E. Van Holde, J. Polym. Sci. 14, 81 (1954).

47. L. Boltzmann, Ann. Physik. 53, 959 (1894).

P A R T I

HYDRODYNAMIC STUDIES ON SODIUM CARBOXYMETHYL CELLULOSE IN AQUEOUS SOLUTIONS

ABSTRACT

Sodium carboxymethyl cellulose was fractionated and the fractions characterized by light scattering, viscometry, sedimentation and diffusion in 0.1 M NaCl. Viscosity and sedimentation measurements were extended to lower ionic strengths by the isoionic dilution technique. Light scattering molecular weights were from 3 to 9 times higher than the values computed by the hydrodynamic equations of Svedberg or Mandelkern and Flory. It appeared that the light scattering method yielded anomalously high M_w values because of a small proportion of colloidal material persisting in solution in spite of the rigorous ultraclarification procedure adopted. Interpretation of the results was therefore based on the sedimentation-diffusion molecular weights which ranged from 45,000 to 350,000.

The exponents determined from the logarithmic dependence of $[\eta]$ on $M_{s,D}$ were 0.95 and 1.40 respectively in 0.1 M and 0.001 M NaCl. This indicated an extended, non-gaussian configuration at low ionic strength due to expansion of the polyelectrolyte molecule. The corresponding exponents for the molecular weight dependence of s_o were 0.35 and 0.11 at 0.1 M and 0.001 M NaCl respectively.

Tests of the Kirkwood-Riseman and Debye-Bueche theories were made by substituting the parameters $[\eta]$, $M_{s,D}$ and the frictional constant, F_o in cubic equations derived from the approximate relationships recently proposed by Marrinan and Hermans. In this way, the monomer frictional constant, ζ could be calculated from data for each fraction. From both theories values of ζ were considerably lower than an approximate figure of 4×10^{-9} g. sec.$^{-1}$ deduced from the diffusion coefficient of sucrose at 25°C. However, at low molecular weights in 0.1 M NaCl and at all molecular weights in 0.001 M NaCl, ζ approached most closely the expected value indicating that the theories hold best for a highly extended configuration.

INTRODUCTION

In comparison with cellulose esters few studies have been made of the solution properties of cellulose ethers. The molecular weights of carefully fractionated samples of water soluble methylcellulose were determined by Signer and co-workers (1,2) and by Polson (3) from sedimentation equilibrium, viscosity and diffusion. Osmotic pressure and viscosity measurements on methylcelluloses have also been made by Staudinger and co-workers (4). Jullander (5) described certain of the solution properties of ethyl hydroxyethyl cellulose and more recently Manley (6) has reported a detailed study of this derivative by a variety of physico-chemical methods.

During recent years work on carboxymethyl cellulose (hereafter designated CMC) has emphasized the configurational behavior of the molecule at different ionic strengths (7-9). Pals and Hermans (7) showed that the polyelectrolyte expansion of CMC could be interpreted in terms of the Hermans-Overbeek theory (10). On the other hand, Schneider and Doty (8) found, in their studies on an unfractionated sample of CMC, that the observed polyelectrolyte expansion was a third of that predicted on the basis of the Hermans-Overbeek theory. The present study is, in part, an attempt to resolve this discrepancy.

The wider scope of the work concerns a systematic investigation of the hydrodynamic behavior of CMC at high and at low ionic strength. The purpose was to test the theories of Kirkwood and Riseman (11) (K.R.) and Debye and Bueche (12) (D.B.) when applied to a stiff chain polyelectrolyte

at different degrees of coiling. Such investigations are rare for polyelectrolytes of any kind and have never been reported for carboxymethyl cellulose.

The investigation followed the usual pattern adopted for high polymers. The CMC was fractionated and the fractions were characterized in 0.1 M NaCl by viscometry, sedimentation and diffusion. By means of the isoionic dilution techniques (7,8,13,14), viscosity and sedimentation measurements were extended to lower ionic strengths. Extensive light scattering measurements were also made but, in spite of rigorous purification procedures, gross irregularities were noted in the molecular weights obtained. Interpretation has therefore been based on molecular weights obtained by substitution of sedimentation and diffusion coefficients in the Svedberg equation.

Recently Marrinan and Hermans (15) have reported approximations of the Kirkwood-Riseman (11) and Debye-Bueche (12) equations which considerably facilitate application of the theory. Using these expressions it has been possible to test the theories by calculating for each particular fraction the frictional constant of the monomer unit for comparison with an approximate value deduced from the diffusion constant of sucrose (16).

EXPERIMENTAL AND RESULTS

Materials

Three samples of CMC, designated Hercules cellulose gum 7HP, 7MP and 7LP supplied to us by the courtesy of Hercules Powder Co., Wilmington, Delaware, were used for fractionation. Ethanol was distilled. Chemicals were Reagent Grade and laboratory distilled water was used in making up the solutions.

Fractionation

Attempts at fractionation with barium chloride, earlier used in the case of alkali lignins (17), were not successful. The barium ion precipitated the CMC as heavy globular flocs. Immediate and irreversible insolubility was produced which was probably due to a cationic cross-linking of the cellulose chains by means of the carboxymethyl groups. No trend in viscosity could be found for fractions thus obtained.

Fractional precipitation with ethanol (7) gave satisfactory fractions with a range of viscosities in spite of the fact that the precipitates were more diffucult to separate due to their gelatinous nature. In a typical experiment, five fractions were separated by dropwise addition of ethanol to a 1% solution of the polymer in 50% ethanol/water mixture containing 0.05% sodium chloride. Ethanol was added to arbitrary turbidity and

stirring was continued over a period of 12-16 hours in a bath maintained at 25 ± 0.05°C. The precipitates were separated by centrifugation at 20,000 r.p.m. for one hour. After dissolving the gel-like mass in water, the solutions obtained were dialyzed against distilled water to remove traces of sodium chloride, neutralized to pH 8.25 and then freezedried. Physico-chemical measurements were restricted exclusively to the fully neutralized sodium salts of CMC. The pH of neutrality, 8.25 was determined by potentiometric titration.

Integral distribution curves showed that the fractionation was fairly reproducible. This method originally standardized for CMC 7MP, was applied to 7HP and 7LP with appropriate changes in the quantity of the precipitant. The fractions so obtained were blended on the basis of their viscosity to give a series of eight fractions which were used for further study. Their characteristics are recorded in Table I.

Neutralization equivalent

The procedure used was to convert the sodium salt of CMC into the acid form by passage through a bed of Amberlite MB1. The number of equivalents of alkali required to neutralize unit weight of the polymer was determined by potentiometric titration. Evaporation of aliquots after neutralization gave the concentration of the solutions. The degree of substitution (i.e. the number of carboxymethyl groups per glucose residue) is given for all the fractions in Table I. A slight increase in the degree of substitution (D.S.) from high to low viscosity CMC was observed. From

TABLE I

Intrinsic Viscosity and Degrees of Substitution and Polymerization for Blended CMC Fractions

Fraction	$[\eta]$ dl. g.$^{-1}$		D.S.	D.P.*
	I_E = 0.1 M	I_E = 0.001 M		
H1	12.30	68.20	0.66	1138
H2	12.20	35.00	0.62	1017
H3	7.60	26.75	0.63	628
M1	6.95	18.75	0.72	534
M2	5.82	15.70	0.72	359
L1	5.16	9.30	0.70	329
L2	2.57	3.95	0.74	155
L3	1.57	3.40	0.73	149

* D.P. values were obtained on the basis of the D.S. and M_{SD} values.

the previous work of Timell (18) this trend could be attributed to greater degradation and subsequent substitution in the accessible portions of cellulose, thus producing a higher D.S. in the low molecular weight fractions.

Viscosity

A four-bulb Ubbelohde viscometer of the Schurz-Immergut type (19) with a large reservoir was used for viscosity measurements. Reduced viscosities were computed at various dilutions in the manner of Huque et al (20) at a standard shear rate of 500 $sec.^{-1}$ following the convention of Newman et al (21) and others (22).

Intrinsic viscosities of all the fractions were measured at 0.1 M and 0.001 M aqueous sodium chloride and are given in Table I. Fractions H1, M1 and L3 were selected for a more complete viscometric study over a range of ionic strengths from 0.1 to 0.00001 M.

At ionic strengths below 0.01 M isoionic dilution (8,13) was necessary; however, when 100% ionization of CMC was assumed, the reduced viscosity-concentration graphs were not linear. This effect was probably due to the binding of $Na^{\oplus}$ by the polyelectrolyte thereby leaving only a fraction of the ions hydrodynamically free in solution. Linear reduced viscosity graphs were obtained by the technique of Terayama and Wall (13,14). The polyelectrolyte solution was diluted with aqueous sodium chloride whose concentration was selected by trial and error (Fig. 1) to give a linear plot of η_{sp}/c vs. c. By this method the degree of ionization of H1, M1 and L3

Fig. 1

$\eta_{sp/c}$ vs. c for fraction M1. Curve A for dilution with deionized water; Curves B,C, D,E for isoionic dilution, assuming ionizations of 40%, 60%, 75% and 85% respectively

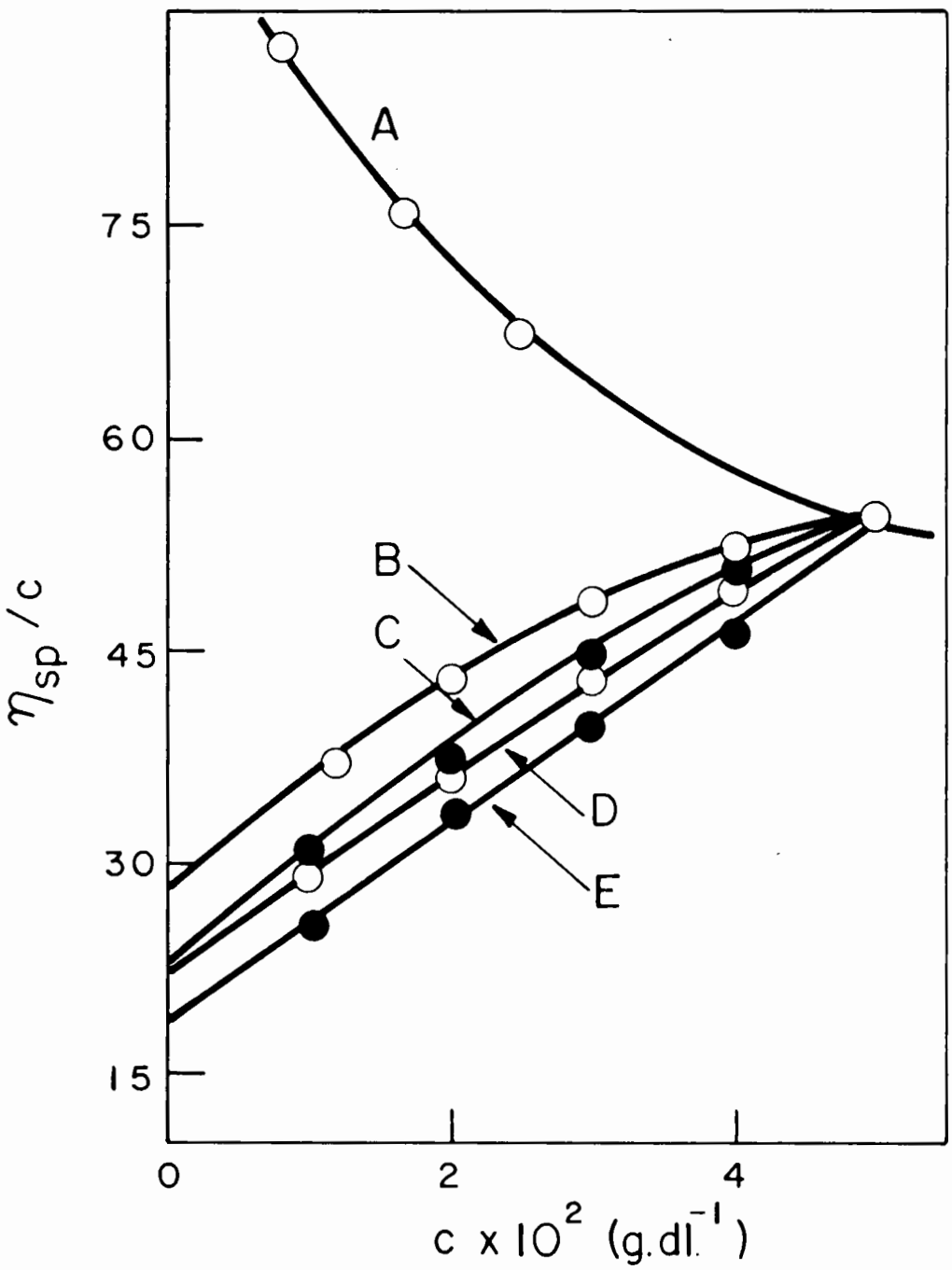
A
B
C
D
E
75
60
45
30
15
0
2
4
η_{sp}/c
$c \times 10^2$ (g.dl^{-1})

was obtained as 70, 85 and 100% respectively, a trend that would be expected on the basis of increase of counterion binding with chainlength. Intermediate values of the degree of ionization were assigned for the other fractions studied at an ionic strength of 0.001 M. Linear reduced viscosity graphs of the type shown in Fig. 2 were obtained and the $[\eta]$ values recorded in Table II were derived. Unusually high values of Huggins coefficient, k' (23) were found at low ionic strength. The significance of this effect is discussed in a later section (24).

The intrinsic viscosity at zero shear rate was determined for several fractions by the extrapolation method of Huque et al (20). Only at high molecular weight and low ionic strength, $[\eta]_{500}$ was smaller than $[\eta]_o$ by 20%. In most other cases this difference was smaller than 5%. A similar insensitivity to shear rate was noted previously for nitrocellulose fractions in acetone (20). Shear dependence of this order was considered small in comparison with other possible errors and because of the uncertainty of the extrapolation procedure, $[\eta]$ at a shear rate of 500 $sec.^{-1}$ was used throughout the present work.

Light Scattering

Light scattering measurements were made at a wavelength of 5461 Å with a Brice-Phoenix (25) photometer, calibrated as previously described with Ludox (26) colloidal silica. For clarification of the solutions in situ, light scattering cells amenable to ultracentrifugation, as described by Dandliker and Kraut (27,28), were used. Micellar debris caused striations

Fig. 2

$\eta_{sp/c}$ vs. c for fraction M1 at various ionic strengths

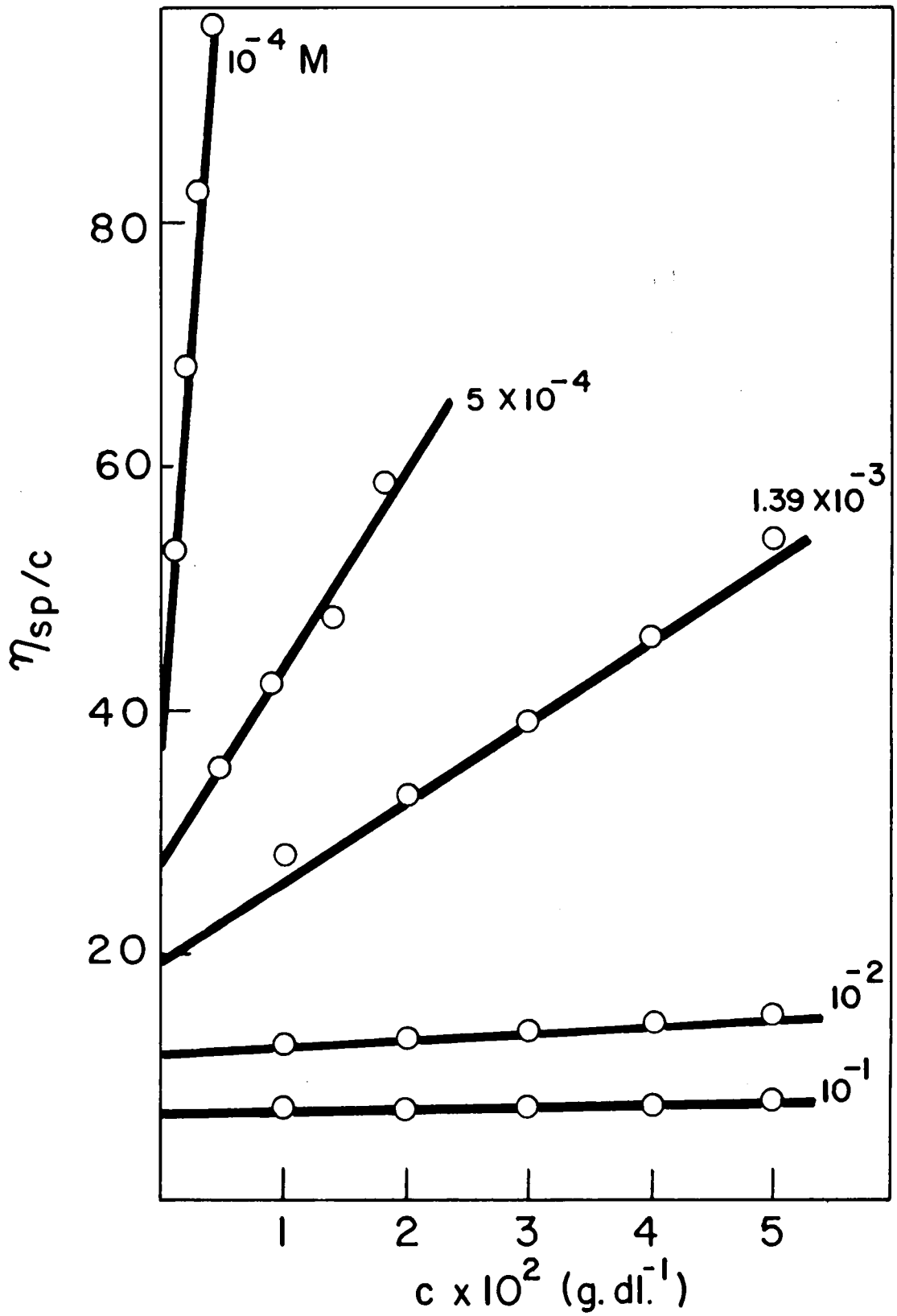
10^{-4} M
5×10^{-4}
1.39×10^{-3}
10^{-2}
10^{-1}
80
60
40
20
η_{sp}/c
1
2
3
4
5
c x 10^2 (g. dl.$^{-1}$)

TABLE II

Viscosity Data for H1, M1 and L3

at Different Ionic Strengths

Ionic Strength	$[\eta]$ dl. $g.^{-1}$		
	H1	M1	L3
0.1	12.3	6.95	1.57
0.01	28.8	11.7	2.32
0.00166	-	-	3.47
0.00139	-	18.8	-
0.00100	62.5	-	-
0.00064	68.2	-	-
0.00050	-	27.7	3.93
0.00010	91.8	39.0	-
0.00005	105.0	48.8	-
0.00003	-	51.3	-
0.00001	160.0	-	-

even in these cells and a new cell was therefore devised and used in all subsequent experiments (29). Both floating and sedimenting debris were effectively trapped by a narrow tubing at the top and a capillary at the bottom of the cell and striations were almost completely eliminated.

The solvent was 0.1 M aqueous sodium chloride and was clarified by filtration through a 10 mμ Millipore filter. The CMC was first dissolved in 0.1 M sodium chloride and then subjected to a preliminary ultracentrifugation at 140,000 g (40,000 r.p.m.) for 2 hours (29). The clear solution was decanted and diluted to give six different concentrations, ranging from zero to 0.25 $g.dl.^{-1}$. These solutions were shaken overnight (12-16 hours), syringed into the light scattering cells and centrifuged at 35,000 g for 1 hour. The cells were then transferred directly to the photometer and scattering intensities were measured at different angles (30 - 135°) relative to the incident beam.

The increment of refractive index, dn/dc of CMC in 0.1 M NaCl was measured by means of a Brice-Phoenix refractometer for λ = 5461 Å at 25°C. An average dn/dc value of 0.147 (± 0.0007) $ml.\ g.^{-1}$ was obtained for eight fractions and no trend with molecular weight was observed. This value is comparable with 0.154 $ml.\ g.^{-1}$ reported by Schneider and Doty (8) for λ = 4360 Å and with 0.136 $ml.\ g.^{-1}$ obtained by Trap and Hermans (30) for λ = 4360 Å. Manley (6) found a value of 0.147 $ml.\ g.^{-1}$ for ethyl hydroxyethyl cellulose in water.

Concentrations were determined by evaporation of aliquots and correcting for sodium chloride where necessary.

The data were plotted by the method of Zimm (31) and the molecular

weight was computed in the standard manner from the reciprocal of $(Kc/R_\theta)_{\substack{c=0 \\ \theta=0}}$ An example of the Zimm plot is shown in Fig. 3 and M_w values are given in Table III. In any one sample the reproducibility in the molecular weights was good (32). In the case of M 1 the solutions were subjected to different degrees of centrifugation for times between 2-12 hours at speeds up to 140,000 g. In four determinations the agreement in molecular weights obtained was $\pm$ 6.6%, showing that minor changes in the technique did not affect the molecular weights obtained.

Sedimentation

Sedimentation measurements were made in a Spinco Model E ultracentrifuge. The temperature was 26 ($\pm$ 0.5)^{0}C. Phase plate optics were used and the Schlieren angle was either 45^0 or 50^0. All runs were made at 260,000 g in a single sector cell. Usually 12 exposures at 4, 8 or 16 min. intervals were taken. Fractions were usually run at a number of concentrations between 0.005 — 0.05 g dl. $^{-1}$ at ionic strengths of 0.1, 0.01 and 0.001 M. Dilutions were made keeping the counterion concentration constant as in viscometry.

Single peaks were observed. The maximum-ordinate sedimentation constant, S_m was obtained in the standard manner (33) from the slope of linear plots of $\log_{10} X_m$ vs. t, where X_m is the distance of the maximum ordinate from the centre of the rotor and t is the time. The origin was not used as a point in order to eliminate the error due to the interval of time at which the peak remains at the meniscus (34,35). To allow for sedimentation during acceleration, one third the acceleration time (36)

Fig. 3

Zimm Plot for fraction H2

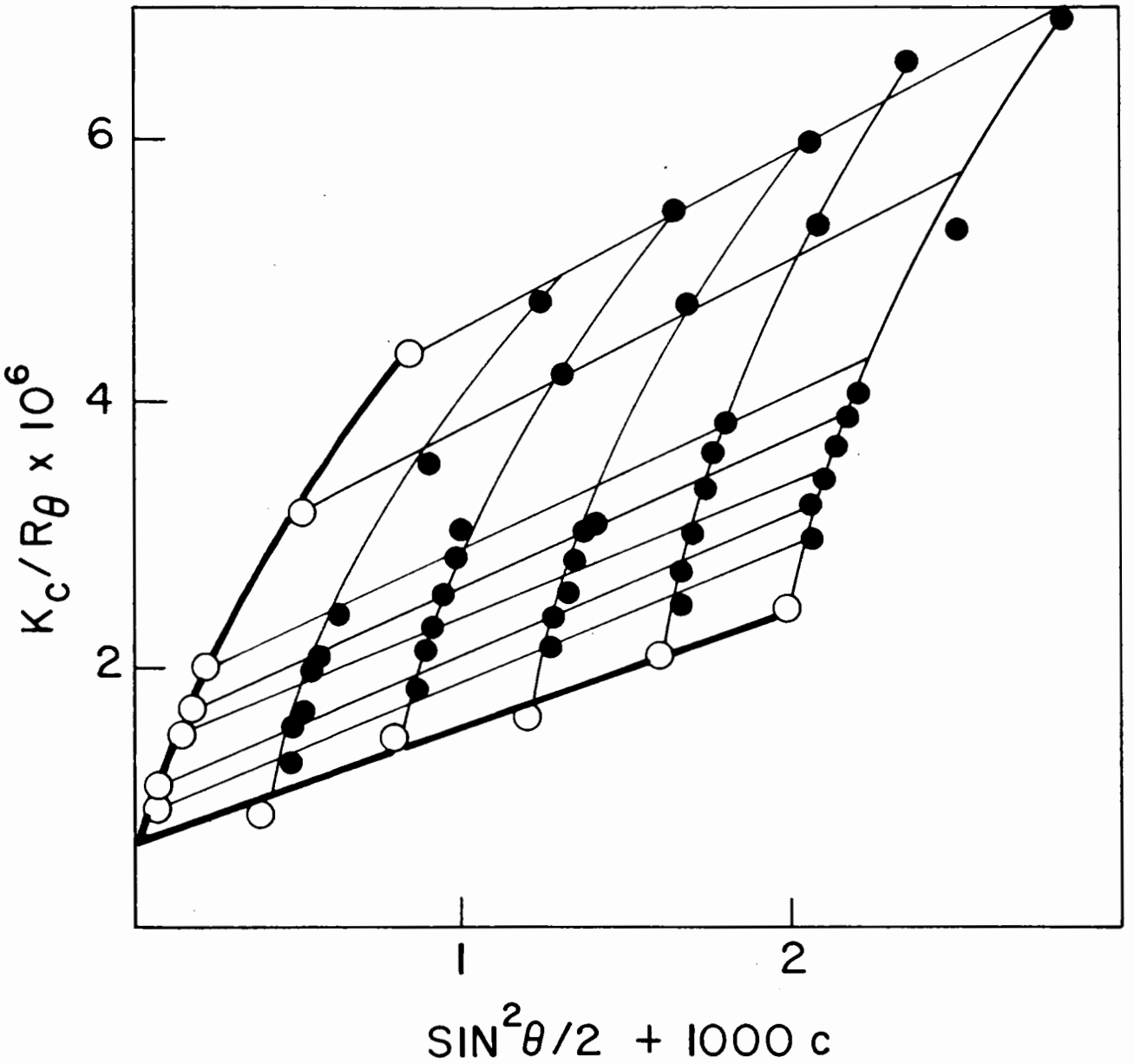
6
4
2
$K_c/R_\theta \times 10^6$
1
2
$SIN^2\theta/2 + 1000\,c$

TABLE III

Molecular Weights of the Fractions

Fraction	$M_{LS} \times 10^{-5}$	$M_{sq} \times 10^{-5}$	$M_{sD} \times 10^{-5}$	M_{LS}/M_{sD}
H1	15.87	3.25	2.46	4.6
H2	14.82	3.22	2.80	5.3
H3	5.88	1.92	1.94	3.0
M1	12.80	1.57	1.63	7.9
M2	4.35	0.998	0.942	4.6
L1	8.00	0.937	0.906	8.8
L2	2.11	0.530	0.460	4.6
L3	1.95	0.397	0.447	4.4

was added to the time at speed in computing s_m. Values of $(s_m)_{c=o}$ were obtained by extrapolation of $1/s_m$ to zero concentration as shown in Fig. 4. $(s_m)_{c=o}$ was adjusted by the standard method (33,36) to give s_o which was then the sedimentation constant at zero concentration and 25°C.

At low ionic strengths, graphs of $1/s_m$ vs. c had a marked upward curvature and extrapolation was not possible. However, as indicated in Fig. 4 the s_m vs. c graphs at 10^{-3} M approached linearity and therefore were used for determination of s_o by extrapolation. The s_o values are recorded in Table IV. A fuller account of the concentration dependence of sedimentation is given in a later section (37).

Partial Specific Volume

Densities of solutions of the fractions in 0.1 M sodium chloride were measured at 25 ± 0.01°C in the concentration range of 0.2 - 1.0%. The pycnometer used was a density bottle of 25 cc. capacity with a well-fitting ground glass cap. The partial specific volume, ($\bar{v}$) was calculated by Kraemer's formula (33). The average value was 0.565 ± 0.005 at 25°C.

Diffusion Constants

Diffusion constants were measured in 0.1 M NaCl by means of a Zeiss Diffusion Interferometer using a quartz micro diffusion cell. The interferograms were observed visually and recorded photographically after lapse of definite time, t. From the Raleigh fringe pattern and dn/dc, the interferograms could be directly interpreted as c vs. x graphs, where x denotes

Fig. 4

s vs. c and $1/s$ vs. c for fraction L3 at low and high ionic strength respectively

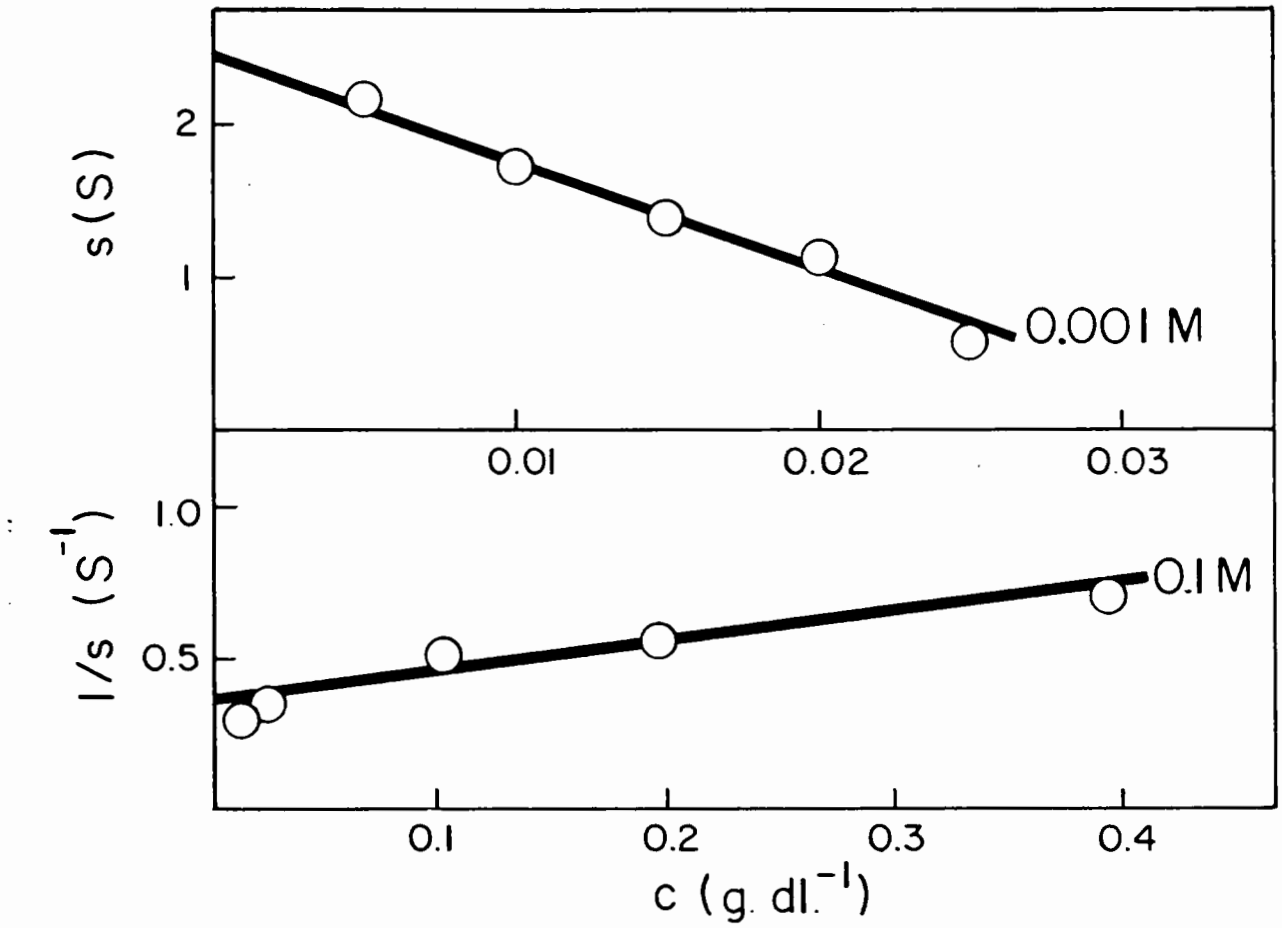
s(S)
2
1
0.001 M
0.01
0.02
0.03
1/s (S⁻¹)
1.0
0.5
0.1 M
0.1
0.2
0.3
0.4
c (g. dl.⁻¹)

TABLE IV

Sedimentation and Diffusion Data at 25°C

Fraction	$s_o \times 10^{13}$			$D_o \times 10^7$	$F_o \times 10^7$	
	at 0.1 M	0.01 M	0.001 M	0.1 M	0.1 M	0.001 M
H1	5.77	4.53	2.96	0.95	4.32	8.44
H2	5.70	-	2.85	1.16	3.54	7.08
H3	4.67	-	2.62	1.37	2.99	5.35
M1	4.26	3.11	2.65	1.49	2.76	4.45
M2	3.35	-	2.58	2.03	2.03	2.64
L1	3.29	-	2.50	2.07	1.98	2.62
L2	2.88	-	2.30	3.57	1.15	1.44
L3	2.80	2.70	2.40	3.58	1.15	1.35

the distance in the diffusion path from the initial boundary. The temperature of the diffusion compartment was maintained at 22.5 ± 0.1°C. There was no trace of convection, probably because of the small dimensions (1 mm. x 4 mm.) of the diffusion column.

Boltzmann's relation (38)

$$D = -\frac{d\lambda}{dc} \int_0^c \lambda \, dc \qquad \ldots(1)$$

in which $\lambda = x/\sqrt{t}$, was used for computing the diffusion constants. Linear plots of x vs. $\sqrt{t}$ were obtained as in Fig. 5, showing that the system conformed to the Boltzmann relation. An example of the sigmoidal relationship of C vs. λ is given in Fig. 6. The diffusion constant was then calculated at any concentration by substituting the graphically determined slope, $d\lambda/dc$ and area $\int_0^c \lambda \, dc$ in Eq. (3). The diffusion constant at zero concentration, $(D_m)_{c=o}$ was obtained by extrapolation of D values as shown in Fig. 7. Values of the diffusion constant corrected to 25°C were obtained from

$$D_o = (D_m)_{c=o}\left(\frac{298}{0.89\times10^{-2}}\right) \cdot \frac{\eta_T}{T} \qquad \ldots(2)$$

where $D_o = (D_m)_{\substack{T=25^\circ \\ c=o}}$ and T and η_T are absolute temperature and viscosity of the solvent under the conditions of the experiment. Values of D_o are listed in Table IV.

The method was tested on one sample by making diffusion measurements at a series of concentrations.

Values of D_A and D_m were then obtained by

Fig. 5

Boltzmann plot for diffusion of fraction L3

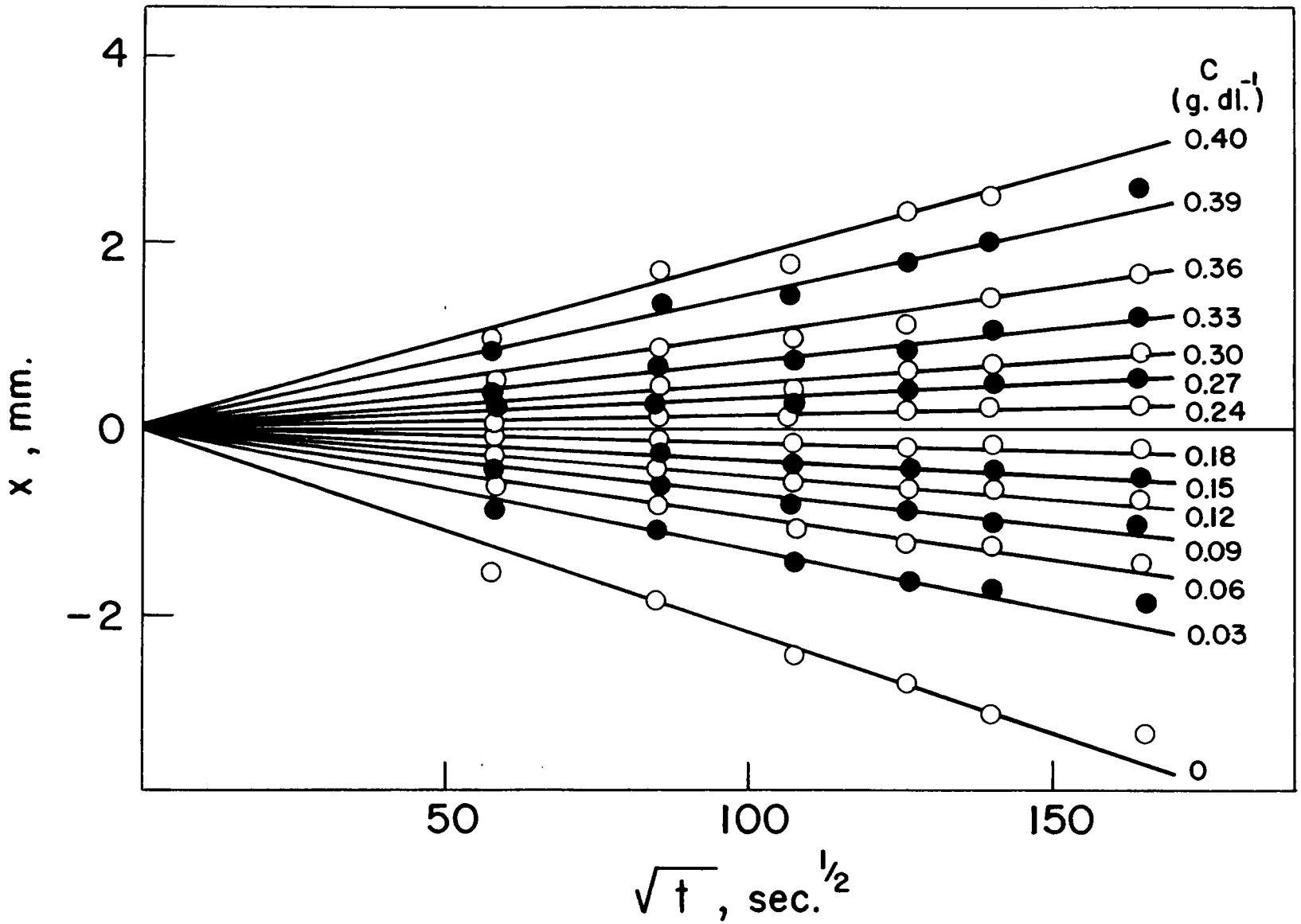
4
2
0
−2
x , mm.
50
100
150
√t , sec.^1/2
C (g. dl.^-1)
0.40
0.39
0.36
0.33
0.30
0.27
0.24
0.18
0.15
0.12
0.09
0.06
0.03
0

Fig. 6

Plot of c vs. $x/\sqrt{t}$ for diffusion of fraction L3

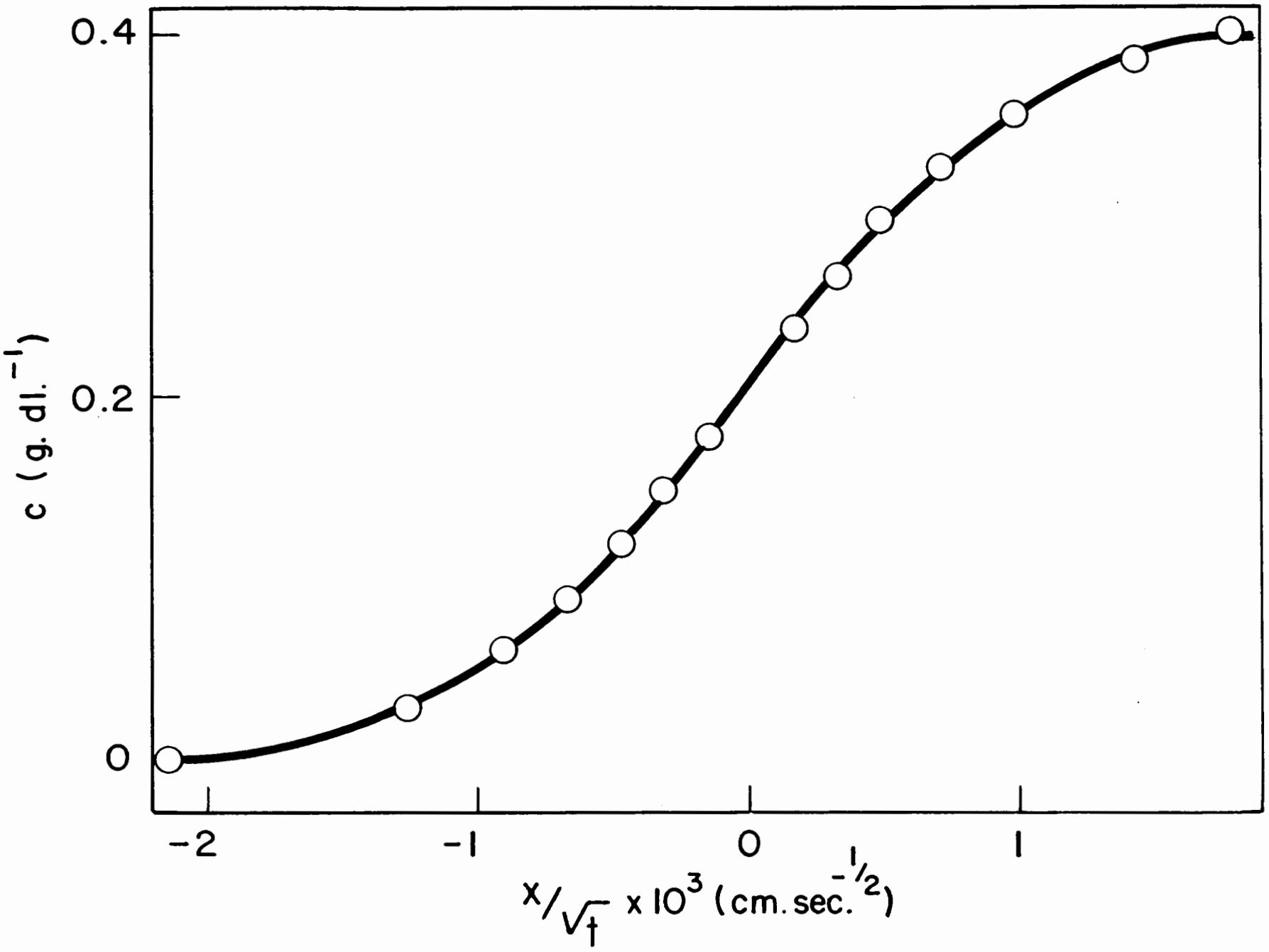
0.4
0.2
0
c (g. dl.$^{-1}$)
-2
-1
0
1
$x/\sqrt{t}$ x 10^3 (cm. sec.$^{-1/2}$)

$$D_A = C_o^2 / 4\pi t H^2 \qquad \ldots(3)$$

$$D_m = m_2 / 2 C_o t \qquad \ldots(4)$$

where C_o is the lateral displacement of vertical bands due to the concentration of solution, H is the tangent maximum of the curve and m_2 is the second moment given by $\int_{-\infty}^{\infty} x^2 \frac{dn}{dx} dx$. Details of obtaining D_m and D_A values are given in a separate appendix (40).

As shown in Fig. 7, D_A was somewhat lower than the corresponding D_m. Such a trend has been noted by other workers (6,39) and is to be expected for polydisperse samples. However, the second moment values of the diffusion constant were found to agree reasonably well with D_m determined by the Boltzmann technique, thus confirming the reliability of the method. A further test was made in which D_m for sucrose at 25°C was found to be 4.4×10^{-6} cm.^{2} sec.$^{-1}$ compared with the value of 4.8×10^{-6} cm.^{2} sec.$^{-1}$ given by Gosting and Morris (16). In view of the small dimensions of the cell and corresponding decrease in the precision of the measurement, such an absolute accuracy was considered adequate in the present work.

Calculation of M_{sD} and $M_{s\eta}$

The molecular weight from sedimentation and diffusion was determined from the Svedberg equation

$$M_{sD} = \frac{RT\, s_o}{(1 - \bar{v}\rho)\, D_o} \qquad \ldots(5)$$

in which ρ is the density of the solvent.

Fig. 7

D vs. c for fraction M1

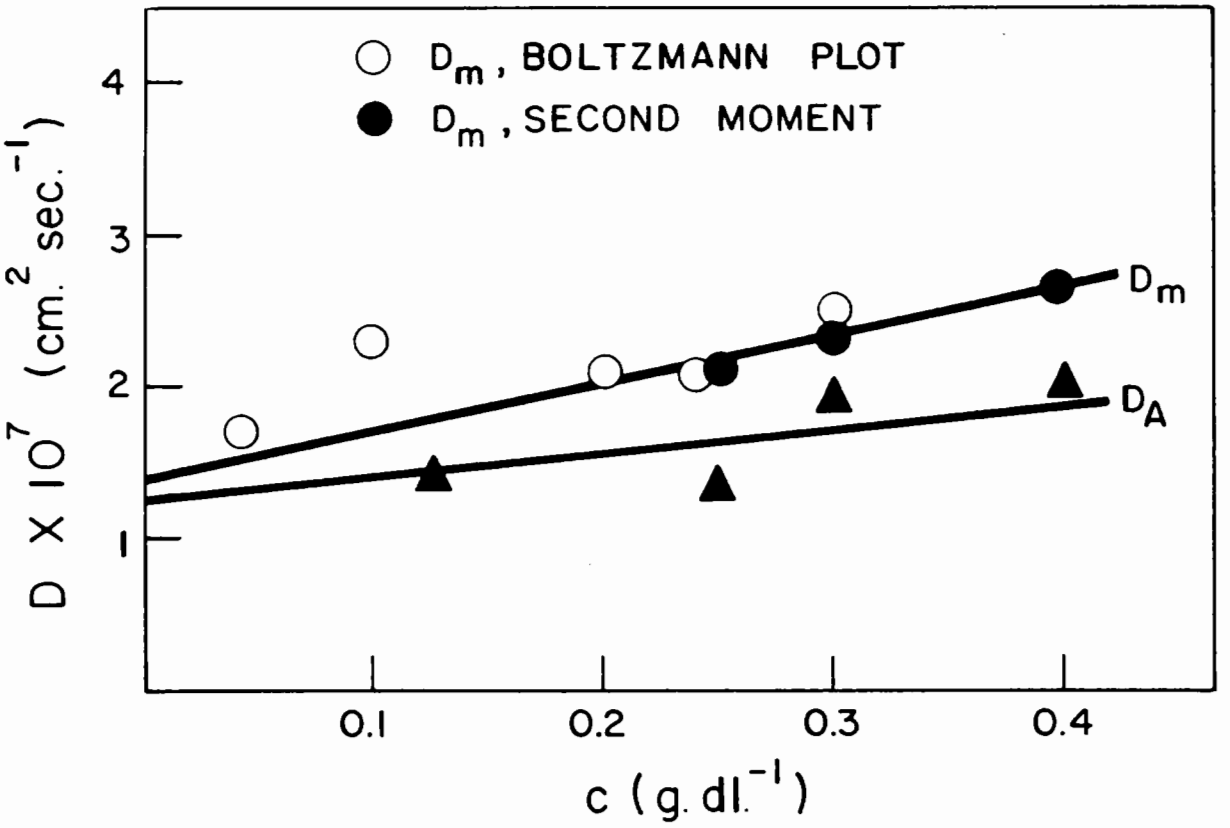
D_m, BOLTZMANN PLOT
D_m, SECOND MOMENT
D_m
D_A
D X 10^7 ($cm.^2 sec.^{-1}$)
4
3
2
1
0.1
0.2
0.3
0.4
c ($g. dl.^{-1}$)

Similarly $M_{s\eta}$, the sedimentation-viscosity molecular weight was derived from the Mandelkern-Flory equation (41)

$$s_o[\eta]^{1/3}/M^{2/3} = (\phi^{1/3}P^{-1})\ (1 - \bar{v}\rho)\ \eta_o N \qquad \ldots(6)$$

with Manley's (6) value of 3.08×10^6 for $\phi^{1/3}P^{-1}$. The molecular weight results are given in Table III.

To facilitate comparison of M_{sD} with light scattering molecular weights, the ratio of M_{LS}/M_{sD} is included in Table III. Further consideration of Eq. (6) is reserved for the discussion.

DISCUSSION

Comparison of the light scattering molecular weights with those computed from the hydrodynamic parameters reveals a marked discrepancy. While $M_{s\eta}$ values agree within $\pm$ 6.6% with the M_{sD} values, it is evident from Table III that the light scattering molecular weights exceed M_{sD} values by a factor of 3-9. An equally serious objection against the light scattering values is the erratic molecular weight trend when compared with the regularity in the other parameters, $[\eta]$, s_o and D_o.

These discrepancies were probably due to the presence of small amounts of high molecular aggregates in solution. In the preparation of alkali cellulose and its subsequent conversion to CMC, an uneven distribution of substituents would occur, (42-44) because accessible regions in the amorphous portions of cellulose would react more rapidly than the interior of highly crystalline regions. Upon dispersing in water, fragments of this unreacted cellulose would not go into true solution but could exist as colloidal aggregates in a wide range of particle sizes. In spite of the rigorous methods of clarification prior to light scattering, a small percentage of these aggregates still persisted in the solutions giving the high values of M_{LS}. The effect would be expected to be most pronounced in the first fraction of each series. From Table III, the mean value of M_{LS}/M_{sD} for H1, M1 and L1 was 7.1 which exceeded the average value for the remaining fractions by 61%.

There can be no doubt that the presence of small proportions of colloidal material is the prime cause of anomalies in the light scattering

of biological macromolecules (20,26,29,45). Manley (6) has observed fibre fragments of various sizes and states of swelling in the photomicrographs of the gel component of ethyl hydroxyethyl cellulose. Manley points out that these aggregates were possibly responsible for the anomalously high light scattering molecular weights which he obtained. In a recent paper on polyanhydroglucose addition polymers, Abe and Prins (46) have noted ratios up to 15 for M_{LS}/M_w where M_w was determined by an Archibald sedimentation method. They attribute the discrepancy to small proportion of microgel produced in the formation of the polymer. A similar effect has been recently reported for carboxymethyl cellulose by Schurz (47).

Striations caused, by the presence of aggregates, were first observed by Huque et al (20,28) and later in the case of several xylans by Goring and Timell (29). Striations were also seen in the present study but were practically eliminated by rigorous ultraclarification. The striation effect, however, must be regarded as a gross symptom of the presence of colloidal debris and therefore disappearance of striations might not necessarily mean total removal of aggregates from the solution.

Let us now consider what effect a small proportion of heavy aggregates would have in sedimentation, diffusion and viscometry. In sedimentation it would be expected that the aggregates would sediment quickly and therefore would not affect the movement of the main boundary. No second component was observed in the Schlieren diagrams, except for H1 where a small second peak was seen to move quickly down the cell wall

ahead of the main peak. The diffusion constants were weight averages and therefore would not be appreciably dependent on the low D values of the small proportion of aggregated material. In the case of the intrinsic viscosity, the aggregates would behave as compact spheres. Their contribution to the intrinsic viscosity would therefore be negligible and small proportion would not affect the concentration. Hence s_o, D_o and $[\eta]$ values would be expected to be influenced only slightly by the presence of colloidal debris.

In view of the above it was decided to restrict further discussion to M_{SD} and the hydrodynamic parameters. It is realized that this is somewhat arbitrary. But, until more detailed work on the light scattering technique can resolve the anomaly, it seems that the M_{LS} values in the CMC - water system must be regarded as being unrealistic.

Polyelectrolyte Expansion

Before considering the polyelectrolyte expansion of CMC, two important assumptions will be made in discussing the results. The first is that the primary electroviscous effects are negligibly small. The presence of a cationic layer of $Na^{(+)}$ ions is presumed to have no effect *per se* on $[\eta]$, s_o and D_o. All changes in the intrinsic parameters are taken to reflect changes in the configuration or size of the coil. This assumption has been discussed by other workers (8) and recent calculations based on Booth's (48) equations have shown the effect to be negligible in the case of viscometry (14).

The second assumption is that the molecular weight distribution in each fraction is reasonably narrow and similar for all the fractions. Clearly, this can not be strictly correct particularly in view of the variations in ratios of M_{LS}/M_{sD} shown in Table III. However, the assumption can be justified by the fact that fractions were selected from fractionations performed on three different samples of high, medium and low molecular weights. Thus any fluctuations in $[\eta]$, s_o and D_o produced by variations in molecular weight distributions would be expected to be random over the series and would not give a false trend with molecular weight. In any case further interpretation will be limited to relatively big effects and clear-cut differences which would be expected to transcend irregularities from fraction to fraction due to changes in the degree of polydispersity.

The configurational changes of the CMC molecule are perhaps most clearly shown by the variations in the molecular weight dependence of the hydrodynamic parameters. The graphical relationships between $[\eta]$, s_o, D_o and F_o vs. M are shown in Figs. 8-10 and the exponents are given at different ionic strengths in Table V.

At 0.1 M the value of the exponent $\underline{a}$, in the Mark-Howinck (49-50) equation was 0.91 which is about the same magnitude ($\underline{a} \sim 1$), as observed for other cellulose derivatives (20,51-56). The exponent of unity is the highest obtainable for a random coil (57) and indicates the asymptotic limit of complete free-draining. Similarly the exponents in the sedimentation, diffusion and frictional constant equations (Table V) confirm the free-draining configuration in 0.1 M NaCl.

Fig. 8

Log $[\eta]$ vs. log M_{SD} at different ionic strengths

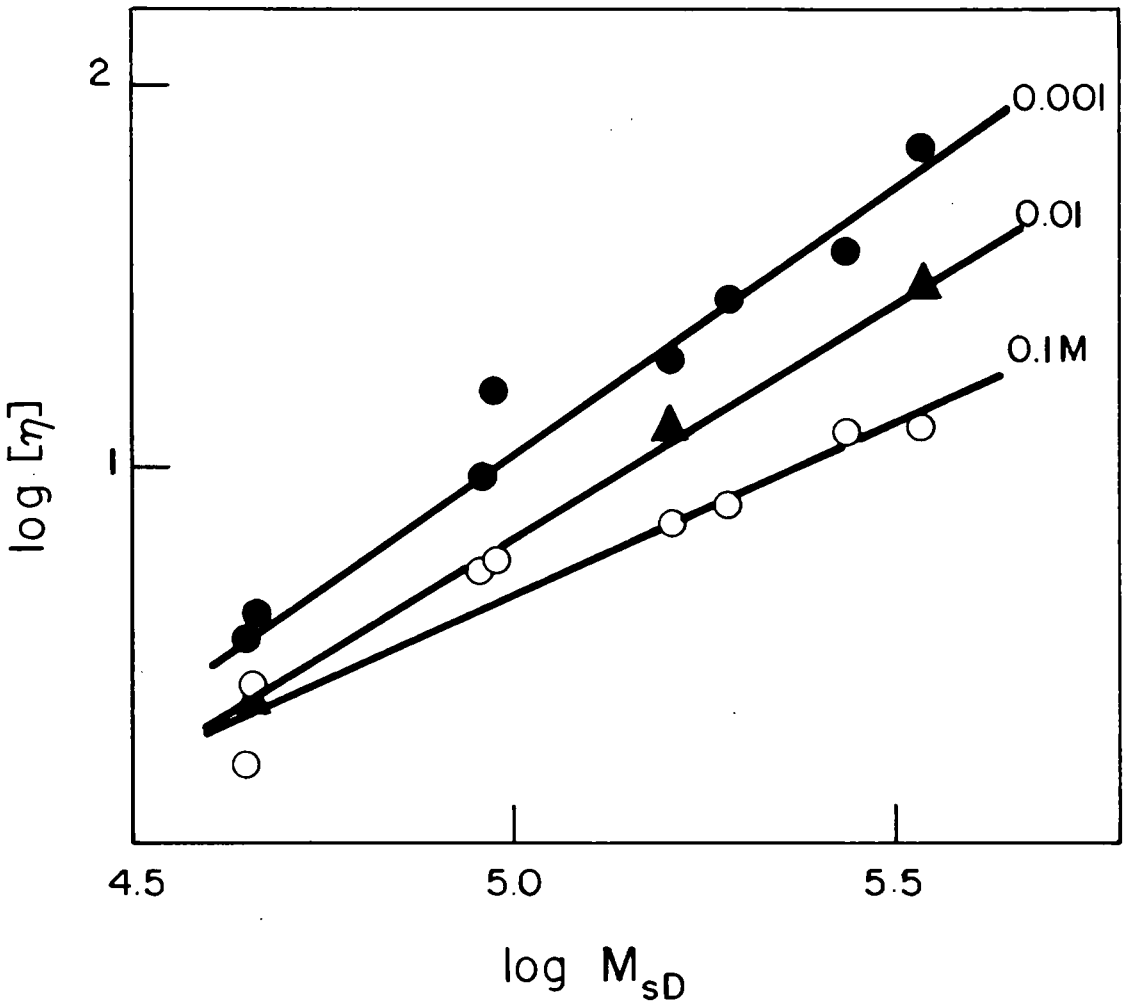
2
1
log [η]
0.001
0.01
0.1M
4.5
5.0
5.5
log M_sD

Fig. 9

Log s_o vs. log M_{SD} at different ionic strengths

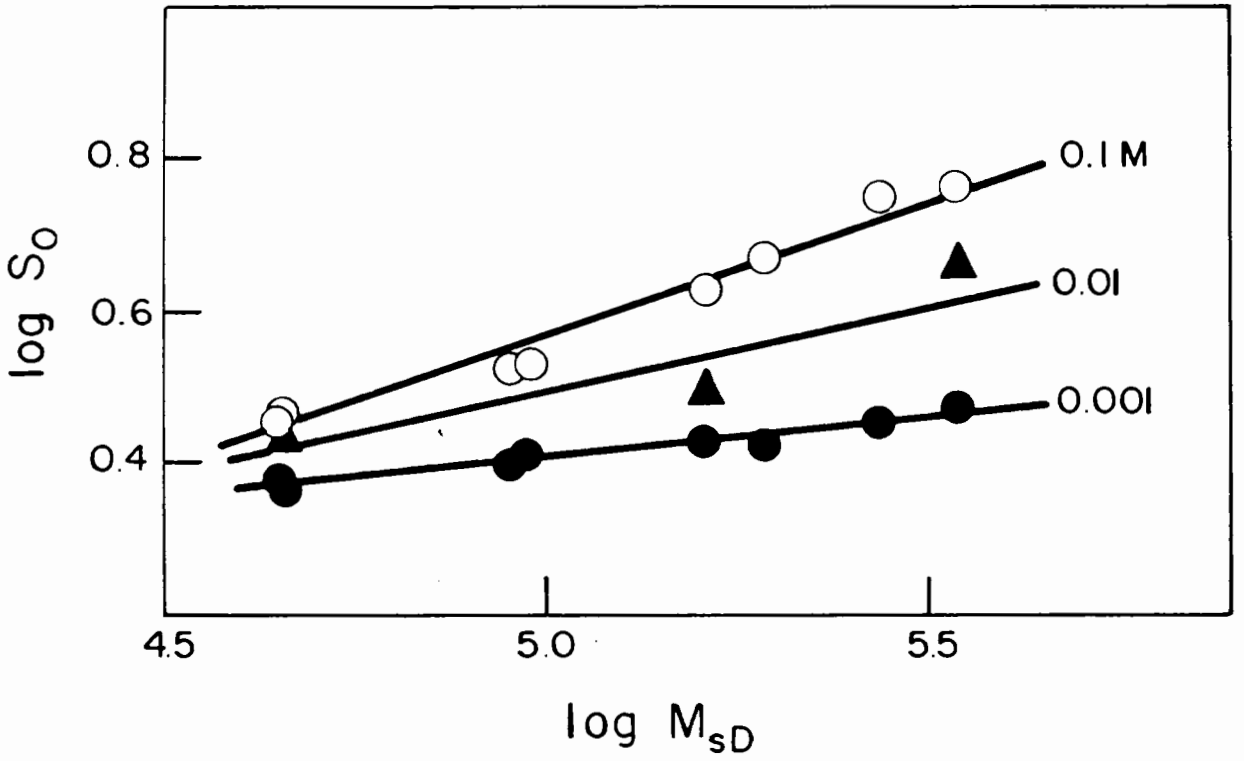
0.8
0.6
0.4
log S_O
0.1 M
0.01
0.001
4.5
5.0
5.5
log M_{sD}

Fig. 10

Log F_o and log D_o vs. log M_{SD}

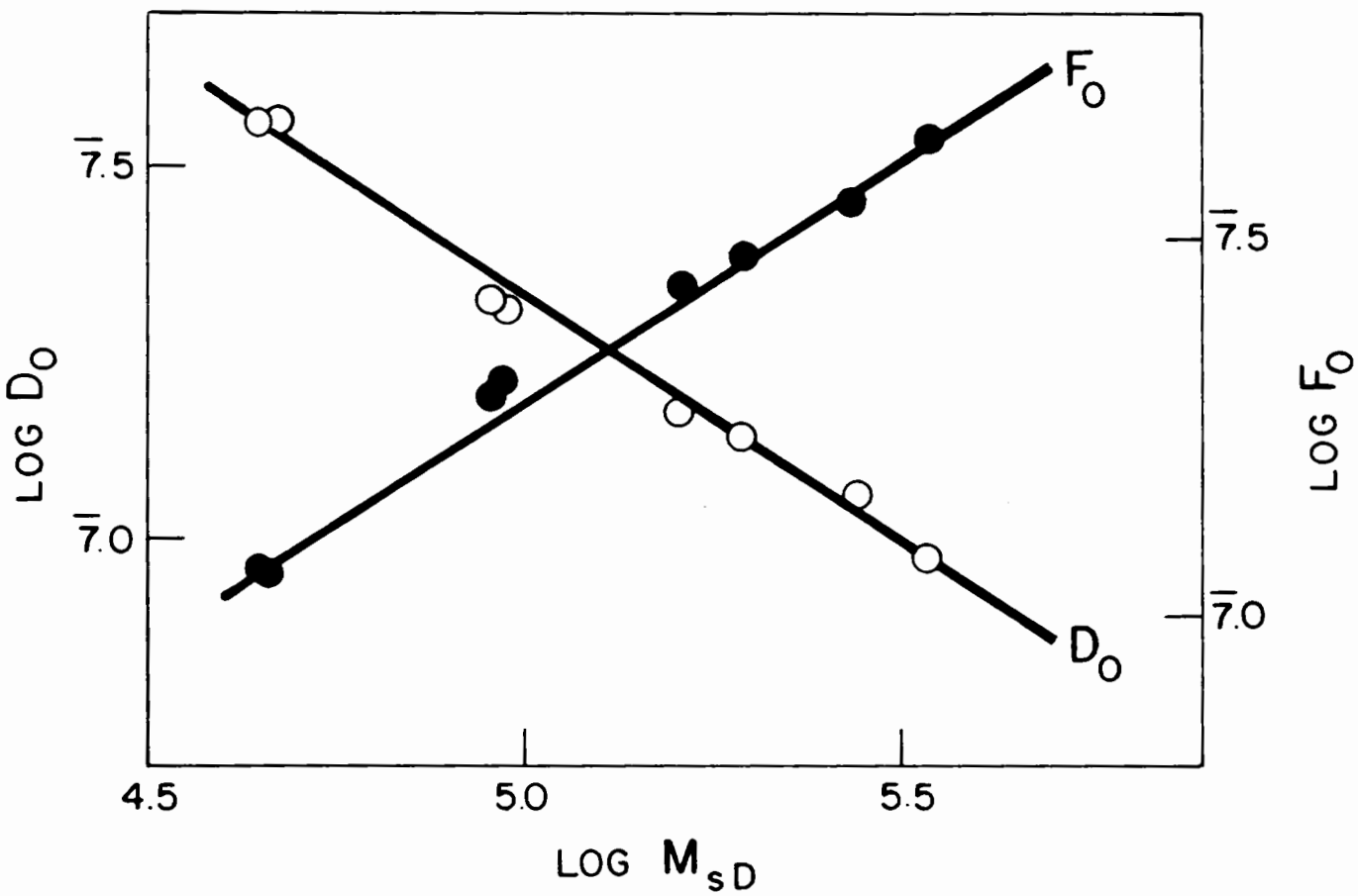
F_O
D_O
$\overline{7}.5$
$\overline{7}.0$
LOG D_O
LOG F_O
4.5
5.0
5.5
LOG M_{sD}

TABLE V

Dependence of $[\eta]$, s_o, D_o and F_o on M_{sD}

Parameter	Ionic Strength (I_E)	Equation
Viscosity	0.1	$[\eta] = 1.23 \times 10^{-4} M^{0.91}$
	0.01	$[\eta] = 6.46 \times 10^{-6} M^{1.20}$
	0.001	$[\eta] = 1.00 \times 10^{-6} M^{1.40}$
Sedimentation	0.1	$s_o = 6.56 \times 10^{-2} M^{0.35}$
	0.01	$s_o = 2.21 \times 10^{-1} M^{0.23}$
	0.001	$s_o = 7.20 \times 10^{-1} M^{0.11}$
Diffusion	0.1	$D_o = 6.31 \times 10^{-4} M^{-0.65}$
F_o	0.1	$F_o = 7.16 \times 10^{-12} M^{0.65}$

For long rods, the viscosity and sedimentation exponents approach 2 and zero respectively (6,57). Thus the increase of the viscosity exponent to 1.4 at 0.001 M indicates a transition to an extended rod-like form at low ionic strength. Similar ionic strength dependence of $\underline{a}$ has been reported by other workers. Debye et al (58) found that $\underline{a}$ increased from 0.98 to 1.46 in the case of cellulose xanthate and ascribed this to the rod-coil transformation. Masson and Caines (59) observed a similar increase at low ionic strengths for carrageenin. In a study of a series of fractions of sodium lignin sulfonates, Gardon and Mason (60) observed $\underline{a}$ to increase from 0.47 in 2 M NaCl to 1 in distilled water and postulated a change in configuration from a compact coil to a more free-draining form at low ionic strength.

The decrease of the exponent, b' in the sedimentation equation to 0.11 at I_E = 0.001 M provides further support for the change to a rod-like configuration. The experimentally determined value of $\underline{a}$ and b' at I_E = 0.001 M (Table V) approach but do not equal the theoretical values of 2 and zero expected for a stiff rod. Although the molecule becomes extended it can not be fully stretched in 0.001 M NaCl but must exist in some intermediate, asymmetric configuration approximated by a prolate ellipsoid.

The polyelectrolyte expansion could be estimated at considerably lower ionic strengths by means of the isoionic viscosities shown in Table II for H1, M1 and L3. The data may be treated in terms of the volume expansion factor, α which is given for cellulose derivatives (7,8) by

$$\alpha^2 = [\eta]_{I_E} / [\eta]_{I_E} = \infty$$

where $[\eta]_{I_E = \infty}$ is intrinsic viscosity at infinite ionic strength.

In Figs. 11 and 12 the results are plotted according to the theoretically linear relationship of Hermans and Overbeek (10) and of Flory (61,62). Although the curves are approximately linear between 0.1 M and 0.001 M, all show pronounced downward curvature at lower ionic strengths. It seems that the qualitative agreement with the above theories found for CMC by other workers (8,9) can not be extended to lower ionic strengths. A similar but smaller curvature has been reported for CMC by Pals and Hermans (7). It is also interesting to note that non-linear graphs of the type shown in Figs. 11 and 12 have been reported for lignin sulfonate microgels by Rezanowich and Goring (14).

As mentioned previously the changes in the viscosity and sedimentation exponents suggest that at 0.001 M the CMC molecule has adopted an asymmetric, non-gaussian configuration. Thus the decrease in $[\eta]$ below I_E = 0.001 M must arise from the increase in the axial ratio of the hydrodynamically equivalent prolate ellipsoid rather than the swelling of a roughly spherical Gaussian coil. The theories of Hermans and Overbeek (10) and of Flory (61,62) would not be expected to hold in this range since they are based on the statistics of the random coil model.

It is interesting to note that the curves of M1 and L3 appear to flatten while for H1 the expansion is increasing even at the lowest value of I_E. This indicates that for M1 and L3 the molecules in solution may have been almost fully stretched under the conditions of lowest ionic strength used.

A calculation of the initial linear variation of α^2 vs. $3/\sqrt{I_E}$ was made after the manner of Schneider and Doty (8) by

$$1 + \alpha^2 = 1.55 + 0.53 \frac{a}{\underline{K}} \qquad \ldots(7)$$

$$\text{and} \quad a^2 = (36/5\, r_o^2)^{3/2} (3\, \underline{Z}^2\, e^2/2 \epsilon k T)$$

in which $\underline{Z}$ represents the number of charges per polyion, ϵ is the dielectric constant, and $\underline{K}$ is the reciprocal of the Debye radius ($\underline{K} = \sqrt{I_E}/3$ in $\mathring{A}$ for a mono-monovalent electrolyte). The mean square end to end distance, r_o^2 was $Z\, b^2$ where Z is the D.P. of the polymer and b, the effective bond length according to Kirkwood and Riseman (11).

Values of $\frac{\alpha^2 \sqrt{I_E}}{3}$ were 2.5, 2.8 and 2.6 times the slope determined experimentally for H1, M1 and L3 respectively. This result supports the finding of Schneider and Doty that the Hermans-Overbeek theory over-estimates the polyelectrolyte expansion. Schneider and Doty found a threefold discrepancy between α calculated by Eq. (7) and measured experimentally whereas the present results give a difference of only 1.6. The reason may well be that the light scattering molecular weight of 400,000 used by Schneider and Doty (8) in Eq. (7) was too high because of the presence of aggregated material. From Fig. 8, the M_{sD} corresponding to the $[\eta]$ value of their CMC was 180,000. An experimentally determined M_{sD} on their CMC would probably be yet lower because of the increased $[\eta]$ expected from their D.S. of 1.1 compared with the average value of 0.69 (Table I) in the present study. The lower molecular weight is equivalent to lower $\underline{Z}$ which when substituted in Eq. (7) would reduce $\frac{\alpha^2 \sqrt{I_E}}{3}$ to a value considerably nearer to that found experimentally.

Fig. 11

Hermans plot of α^2 vs. $\sqrt[3]{I_E}$ for H1, M1 and L3

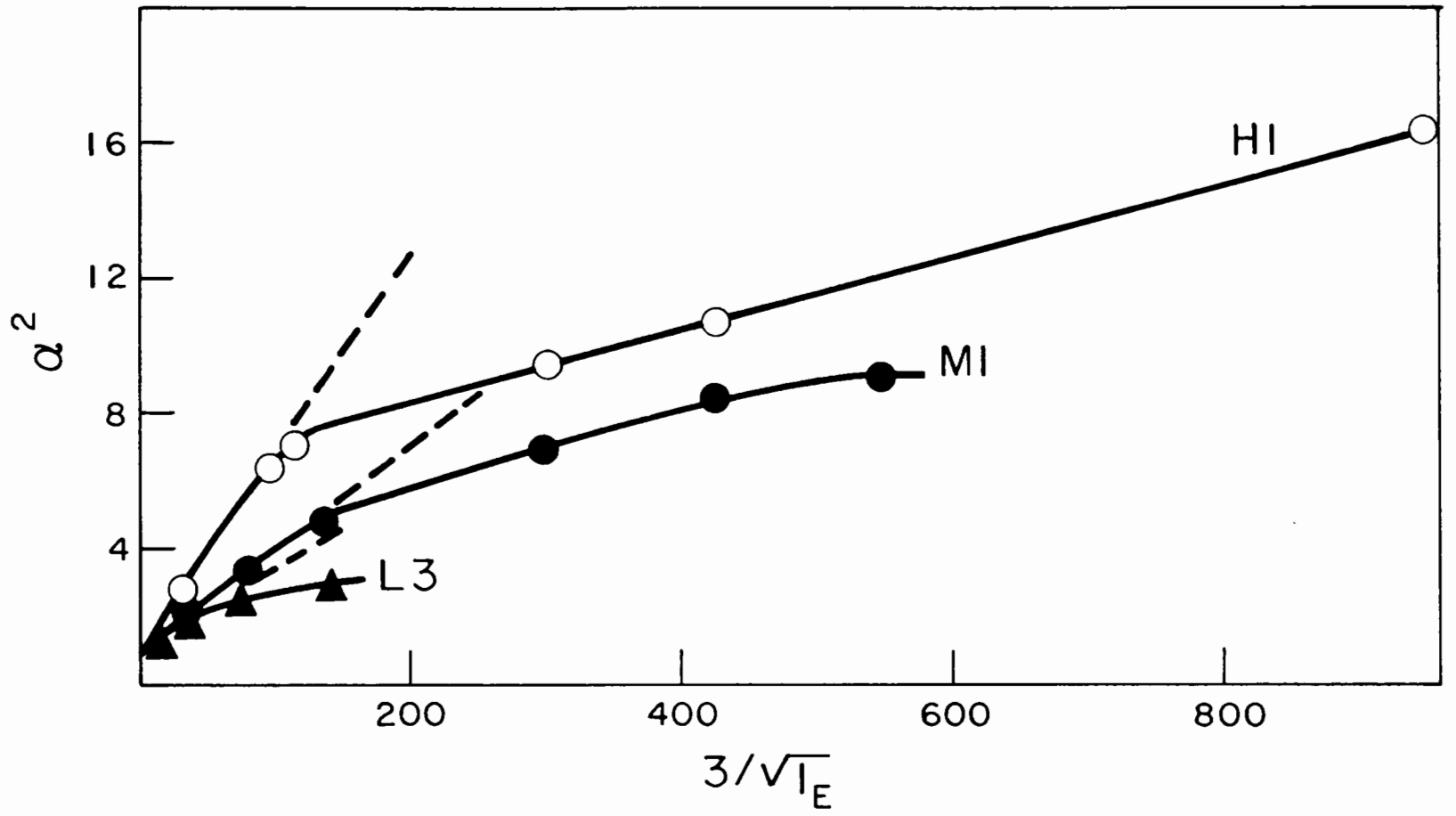
16
12
8
4
α^2
HI
MI
L3
200
400
600
800
$3/\sqrt{I_E}$

Fig. 12

$(\alpha^5 - \alpha^3)$ vs. $1/I_E$ for fractions H1, M1 and L3

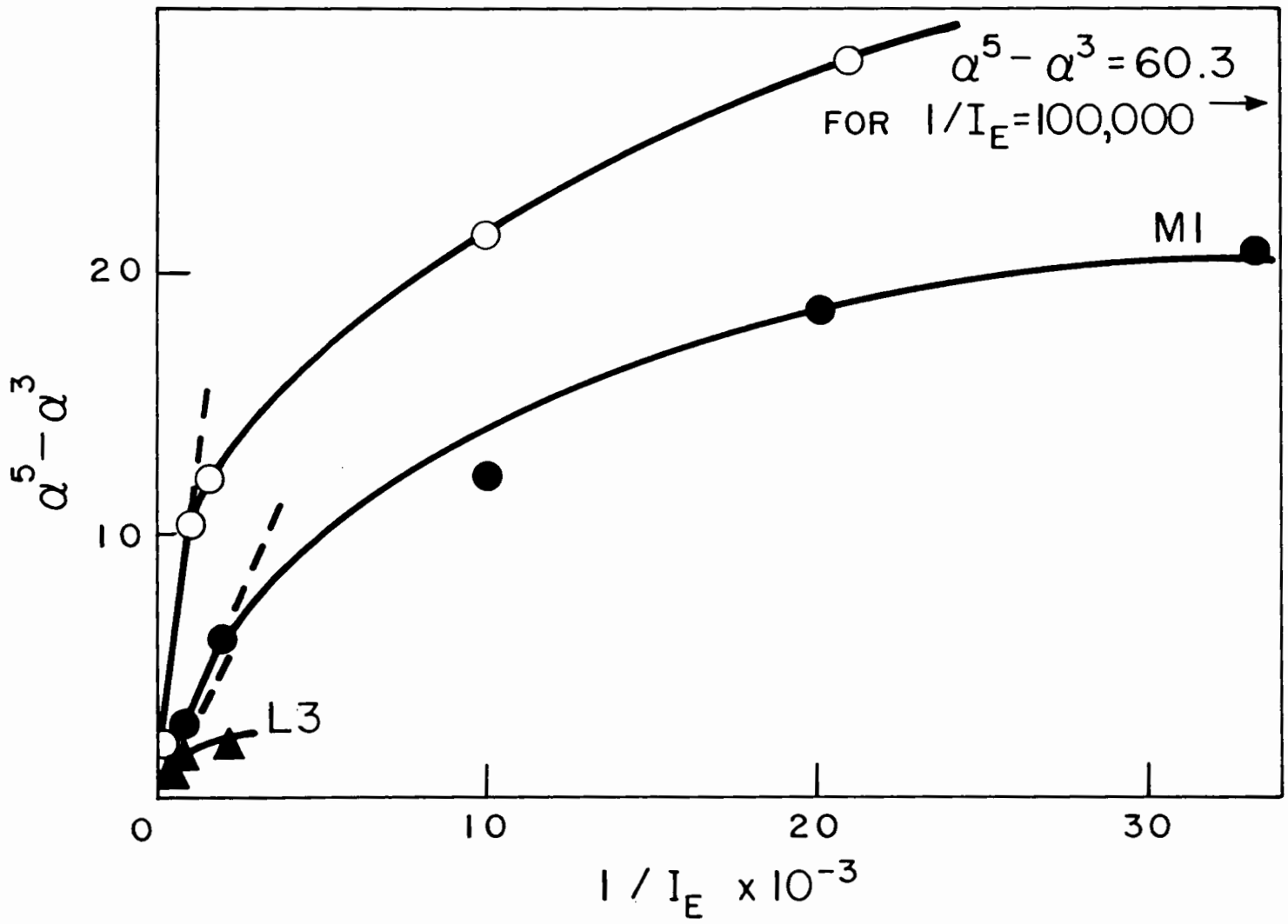
$\alpha^5 - \alpha^3 = 60.3$
FOR $1/I_E = 100{,}000$
M1
L3
20
10
0
10
20
30
$\alpha^5 - \alpha^3$
$1/I_E \times 10^{-3}$

An interesting indication of configurational change can be obtained by computing the effective bond length, b from the equation of Kirkwood and Riseman (11).

$$b^3 = \frac{2435\, M_o}{(6\pi^3)^{1/2} N} \lim_{Z \to} \frac{[\eta]}{Z^{1/2}} \qquad \ldots(8)$$

where M_o is the monomer molecular weight and N is Avagadro's number. $\lim \frac{[\eta]}{Z^{1/2}}$ can be computed from the extrapolation of $[\eta]/Z^{1/2}$ to infinite molecular weight. Values of b at 0.1, 0.01 and 0.001 M were computed from the plots shown in Fig. 13 and are given in Table VI.

For an unbranched polymer chain the mean square end to end distance is related to D.P. by the relation

$$Z\, b^2 = \overline{R^2} = Z\, b_o^2 \left(\frac{1 + \cos\theta}{1 - \cos\theta}\right) \left(\frac{1 + \cos\phi'}{1 - \cos\phi'}\right) \qquad \ldots(9)$$

where b_o is the bond length of the glucose unit (equal to 5.15 Å), θ' is the supplement of the valence angle (equal to 70° for cellulose derivatives) and $\cos\phi'$ is the mean value of the cosine of the angle between successive bond planes. Using the values of b obtained from the K.R. theory, $\cos\phi'$ was computed by substitution in Eq. (9) and is given in Table VI.

The Porod-Kratky persistence length, q reduces for large M to

$$r_o^2/r_{max} = 2\, q \qquad \ldots(10)$$

where r_{max} is the length of the stretched chain. The value of q for fraction H1 was 131 Å, comparable with Huque's value (20) of 115 Å and 117 Å found by Hunt et al (48) for cellulose trinitrate in acetone. A persistence

Fig. 13

K.R. Plot of $[\eta]/Z^{\frac{1}{2}}$ vs. $Z^{-\frac{1}{2}}$

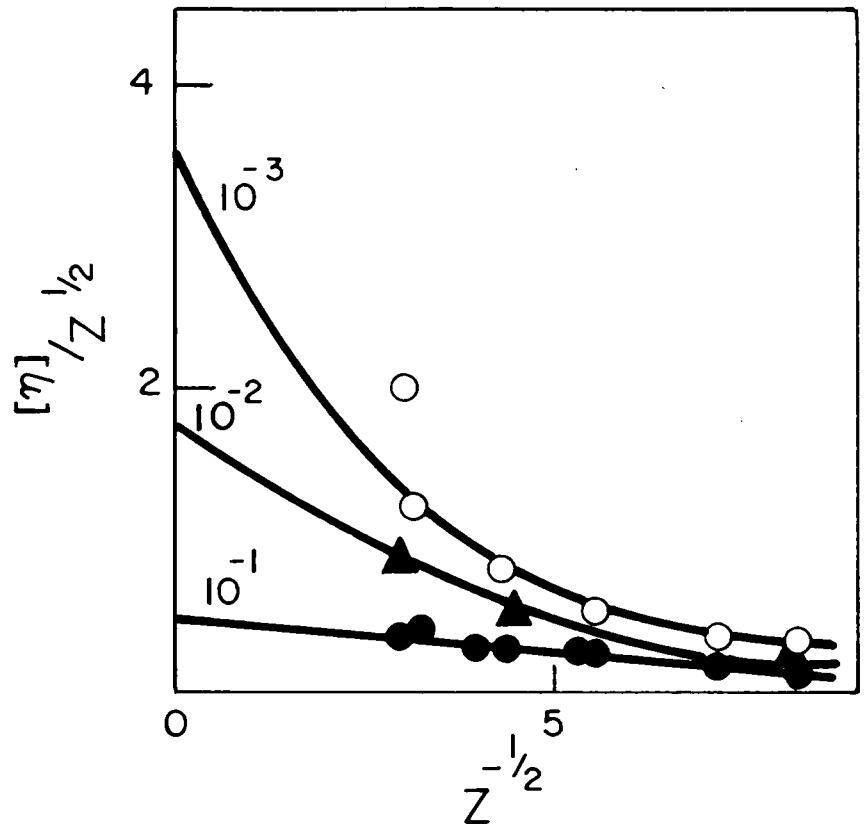
4
2
0
5
10^{-3}
10^{-2}
10^{-1}
$[\eta]/Z^{1/2}$
$Z^{-1/2}$

Fig. 14

Plot of Z/F_o vs. $Z^{\frac{1}{2}}$

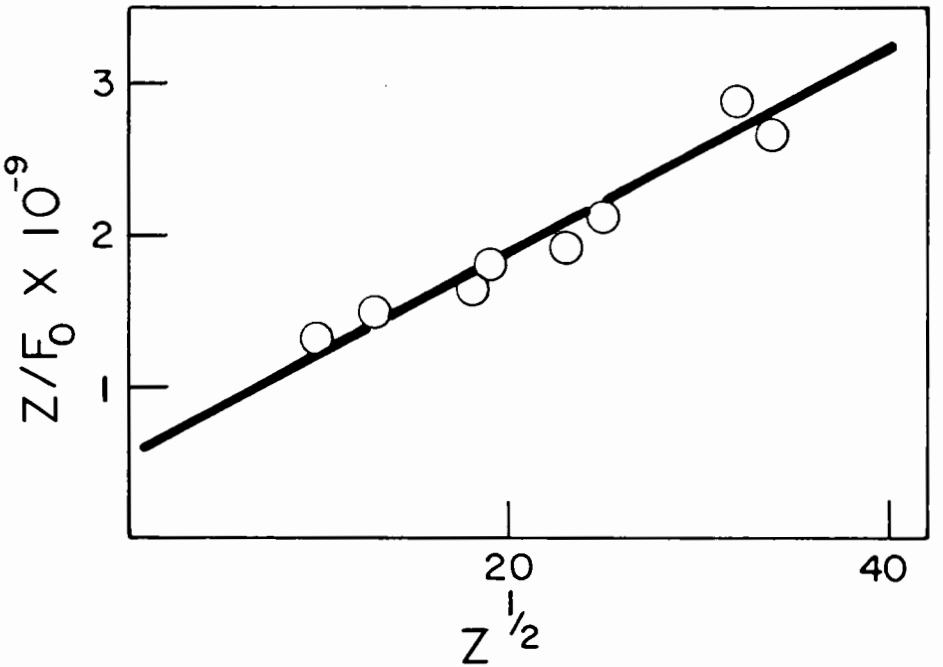
3
2
1
$Z/F_0 \times 10^{-9}$
20
40
$Z^{-1/2}$

length could also be calculated by substituting the appropriate value of r^2 in Eq. (10). q increases at lower ionic strengths. From Table VI it is seen that the effective bond length at 0.1 M agrees well with other values reported for cellulose derivatives (6,7,8). At lower ionic strength b and q increase significantly while cos ϕ' approaches unity. While it is unlikely that parameters such as b and cos ϕ' retain their strict significance for a non-gaussian configuration, none-the-less the changes in Table VI illustrate the stiffening of the chain with decrease in ionic strength.

It was interesting to note that the viscometrically determined binding of counter ions was governed more by the molecular weight than the ionic strength. The change of the degree of ionization from 70% for H1 to 100% for L3 might be expected because of the increased tendency of the molecule to coil at higher molecular weight (20). In contrast a given degree of ionization gave linear η_{sp}/c plots over a wide range of ionic strengths, as noted by Terayama and Wall (13). It is possible that the viscometric method of determining degree of ionization may not be sensitive enough to detect differences expected from configurational changes with ionic strength (65-69).

Hydrodynamic Theories

Several investigations have shown that cellulose derivatives do not comply with the empirical relationships proposed by Flory and co-workers (70,71) for the hydrodynamic behaviour of random coil polymers. Values of $(\phi^{1/3} P^{-1})$ were computed by substituting M_{SD} in Eq. (6) and are given in

TABLE VI

Values of b, cos ϕ' and Persistence Length (q)

at Different Ionic Strengths (I_E)

I_E	b (Å)	cos ϕ'	q (Å)
0.1	36.6	0.930	131
0.01	55.3	0.965	384
0.001	68.8	0.977	837

Table VII. As pointed out by Krigbaum and Sperling (72) the constants are characteristically high. The average value of $\phi^{1/3}{}_P{}^{-1}$ in 0.1 M was 3.55×10^6 compared with the value of 3.08×10^6 obtained by Manley (6) for ethyl hydroxyethyl cellulose and 2.6×10^6 found for many synthetic polymers (41). Two interesting limiting theoretical cases are 2.1×10^6 for Einstein spheres and 3.6×10^6 for a prolate ellipsoid of axial ratio 300 (73). In this respect the cellulose molecule appears to conform more closely to the behaviour of an elongated ellipsoid rather than a random coil.

No trend with molecular weight can be claimed for the results in Table VII. The average values of 3.55×10^6 in 0.1 M and 3.24×10^6 in 0.001 M may be regarded as being equal within experimental error. This supports the use of the Mandelkern-Flory equation for determination of M_s of extended macromolecules even when Gaussian statistics do not strictly apply.

Values of $\phi^{1/3}{}_P{}^{-1}$ were also calculated from M_{LS} substituted in Eq. (6). As shown in Table VII these values were well below the theoretical minimum of 2.1×10^6 expected for a hard sphere. A further demonstration of the unrepresentative nature of the light scattering results in this particular system is thus provided.

As mentioned previously, a random coil configuration is a prerequisite for the exact interpretation of the hydrodynamic properties in terms of the current polymer theories (11,12,70,71). In the present system, the Gaussian coil model was applicable only to the high molecular weight fractions at I_E = 0.1 M. At lower ionic strength the molecule was probably

TABLE VII

$\phi^{1/3}{}_{P^{-1}}$ at High and Low Ionic Strength

Fraction	$M_{sD} \times 10^{-5}$	0.1 M		0.001 M
		$\phi^{1/3}{}_{P^{-1}} \times 10^{-6}$ (from M_{sD})	$\phi^{1/3}{}_{P^{-1}} \times 10^{-6}$ (from H_{LS})	$\phi^{1/3}{}_{P^{-1}} \times 10^{-6}$ (from M_{sD})
H1	3.462	3.36	1.27	2.99
H2	2.798	3.84	1.29	2.73
H3	1.938	3.49	1.70	2.93
M1	1.632	3.41	0.873	2.95
M2	0.942	3.65	1.34	3.90
L1	0.906	3.58	0.855	3.26
L2	0.460	3.85	1.42	3.55
L3	0.447	3.24	1.24	3.63
		Av = 3.55	Av = 1.38	Av = 3.24

asymmetric. In view of the rod-coil transitions with increase in M found for cellulose trinitrates (20,51,54), it is likely that a rod-like configuration existed for the low molecular weight fractions in an ionic strength of 0.1 M. In spite of this it was considered of interest to apply to the data the hydrodynamic theories of Debye and Bueche (12) and Kirkwood and Riseman (11) in order to test the effect of a changing configuration on the molecular parameters derived in these theories.

In both theories the frictional behavior of the complete coil is given quantitatively in terms of the frictional constant of a monomer unit, ζ and other molecular parameters. In some early paper (7,8) the values obtained for ζ have been up to an order of magnitude lower than expected from Stokes law and the dimensions of the monomer unit. The discrepancy has been ascribed (7) to the inapplicability of Stokes law to a particle moving in a medium and of comparable size to the molecules of the medium. On the other hand, Edward (74) has shown that the Stoke's equation probably applies to molecules of radius 3-6Å. Recently, the diffusion coefficent of sucrose in water (16) has been determined at 25°C to be 4.8×10^{-6} cm.^{2} sec.$^{-1}$ which corresponds to an F_o ($= \frac{kT}{D_o}$) value of 8.56×10^{-9} g. sec.$^{-1}$. It seems likely that one half this value (i.e. 4×10^{-9} g. sec.$^{-1}$) would be a reasonable approximation to the frictional constant of a carboxymethyl glucose unit in a CMC chain. Thus the D.B. and K.R. theories could be tested by comparing ζ obtained from the appropriate hydrodynamic equations with the value of 4×10^{-9} g. sec.$^{-1}$.

Attempts were made to use the methods originally suggested by the authors (11,12). Due to the uncertainty involved in the exponents and

extrapolations, such testing of the theories from the data in the present study was not satisfactory. Recently Marrinan and Hermans (75) gave simplified forms of D.B. and K.R. equations to facilitate their application to polydisperse systems. In the following, the Marrinan and Hermans approximations are used to derive single-variable cubic equations which allow calculation of D.B. and K.R. parameters for each fraction individually. The ambiguity of the extrapolation procedure is thereby eliminated.

In the D.B. treatment

$$[\eta] = (4\pi/3)\left(N R_S^3/M\right)\phi(\sigma) \qquad \ldots(11)$$

in which R_S is the radius of the hydrodynamic sphere and can be written

$$R_S = F_o \Big/ 6\pi\eta_o \psi(\sigma) \qquad \ldots(12)$$

In Eqs. (11) and (12), $\phi(\sigma)$ and $\psi(\sigma)$ are appropriate factors of the shielding ratio, σ.

Marrinan and Hermans approximate $\phi(\sigma)$ and $\psi(\sigma)$ by

$$\phi(\sigma) = \left(\sigma^2/10\right)\left(1 + 0.0486\,\sigma^2\right) \qquad \ldots(13)$$

$$\psi(\sigma) = \left(2\sigma^2/9\right)\left(1 + 0.243\,\sigma^2\right)^{-1} \qquad \ldots(14)$$

$$\left.\begin{aligned}[\eta] &= \frac{N F_c^3}{162 \pi^2 M \eta_0^3} \cdot \frac{\phi(\sigma)}{[\psi(\sigma)]^3} \\ &= A \frac{F_c^3}{M} \cdot \frac{\phi(\sigma)}{[\psi(\sigma)]^3}\end{aligned}\right\} \quad \ldots(15)$$

where $A = N/162\,\pi^2 \eta_0^3$

Eq. (15) can be rearranged to

$$\frac{\phi(\sigma)}{[\psi(\sigma)]^3} = \frac{M[\eta]}{A F_c^3} = B \quad \ldots(16)$$

using Eq. (13) and (14)

$$\frac{\phi(\sigma)}{[\psi(\sigma)]^3} = \frac{729\Theta^3 + 532\Theta^2 + 129\Theta + 10.5}{80\Theta + 3.888} \quad \ldots(17)$$

where $\Theta = \frac{1}{\sigma^2}$

Substituting the result of Eq. (17) in Eq. (16),

$$729\,\Theta^3 + 532\,\Theta^2 + (129 - 80\,B)\,\Theta + (10.5 - 3.88\,B) = 0 \quad \ldots(18)$$

Eq. (18) can be used to compute σ and by substitution of the value of $\psi(\sigma)$ from the tables of Debye and Bueche in Eq. (12) R_s is obtained. Hence the frictional constant for monomer can be computed for each molecular weight from the relation

$$\sigma^2 = 3Z\zeta / 4\pi R_s \eta_0 \quad \ldots(19)$$

The values of σ , R_s and ζ shown in Table VIII are discussed later.

In the K.R. theory

$$[\eta] = \frac{NZ}{36\eta_0 M_0} \cdot \zeta h^3 F(\lambda_0 Z^{1/2}) \qquad \ldots(20)$$

$$\lambda_0 Z^{1/2} = \zeta Z^{1/2} / (6\pi^3)^{1/2} \eta_0 b \qquad \ldots(21)$$

$$F_c = Z\zeta / 1 + 8/3\ \lambda_0 Z^{1/2} \qquad \ldots(22)$$

Marrinan and Hermans approximated

$$F(\lambda_0 Z^{1/2}) = 1/1 + 0.78\ \lambda_0 Z^{1/2} \qquad \ldots(23)$$

Combining Eqs. (20–23)

$$\zeta b^3 / b + 0.78\ A\zeta = B = \frac{36\eta_0 M_0 [\eta]}{NZ} \qquad \ldots(24)$$

where

$$Z^{1/2} / (6\pi^3)^{1/2} \eta_0 = A \qquad \ldots(25)$$

also

$$F_c / Z = b\zeta / b + 2.67\ A\zeta = C \qquad \ldots(26)$$

Hence $\zeta = Cb / (b - 2.67\ AC)$ ...(27)

Substituting the value of ζ of Eq. (27) in Eq. (24)

$$B = Cb^3 / (b - 1.89\ AC) \quad ...(28)$$

or $$Cb^3 - Bb + 1.89\ ABC = 0 \quad ...(29)$$

By solving the cubic equation, the effective bond length, b can be computed, from which the frictional constant of the monomer may be obtained for each molecular weight from Eq. (27). Values of b and ζ at two ionic strengths are given in Table VIII.

Let us first consider the ζ values in Table VIII. It is apparent that ζ is not constant but ranges from 0.5×10^{-9} g. sec.$^{-1}$ to 3×10^{-9} g. sec.$^{-1}$. In all cases ζ was less than the approximate value of 4×10^{-9} g. sec.$^{-1}$ based on the diffusion coefficient of sucrose. A similar discrepancy has been noted by others (8,11,12,51).

Included in Table VIII is an apparent frictional constant, ζ_a computed as the ratio $F_o/$[illegible]. For complete free-draining and in absence of hydrodynamic shielding ζ_a should be rigorously equivalent to ζ. Under all conditions ζ_a was less than the corresponding ζ value from the D.B. and K.R. equations. Thus the theories correct to some extent for the hydrodynamic interaction within the molecule. The trend of the data in Table VIII shows that ζ from the K.R. theory approaches more nearly to

TABLE VIII

Values of σ , R_s, b and ζ at High and Low Ionic Strength

Fraction	$\zeta_a = F_o/Z_{x10^9}$		D.B. and M.H.						K.R. and M.H.			
			I_E = 0.1 M			I_E = 0.001 M			0.1 M		0.001 M	
	0.1 M	0.001 M	σ	R Å	ζ x10^9	σ	R Å	ζ x10^9	b Å	ζ x10^9	b Å	ζ x10^9
H1	0.380	0.742	1.20	1134	0.54	1.41	1802	1.17	68	0.735	80	2.35
H2	0.348	0.696	1.05	1104	0.45	1.60	1289	1.21	57	0.605	65	2.70
H3	0.477	0.851	1.18	786	0.65	1.52	1023	1.41	52	0.959	62	2.85
M1	0.517	0.834	1.19	724	0.72	1.45	892	1.32	50	1.082	58	3.06
M2	0.564	0.735	1.11	586	0.75	1.04	841	0.95	52	1.026	57	1.58
L1	0.603	0.795	1.16	541	0.83	1.28	621	1.16	50	1.158	56	1.83
L2	0.687	0.863	1.04	371	0.76	1.15	389	1.15	44	1.812	50	1.83
L3	0.775	0.904	1.27	282	1.28	1.15	314	1.15	36	1.821	37	2.60

sucrose diffusion value of 4 X 10^{-9} g. sec.$^{-1}$ than the D.B. data for ζ. A similar improvement has been noted by Manley(6).

A further interesting trend is that ζ approaches most nearly the correct value when the molecule is in its most extended state and therefore is not like a gaussian coil. At 0.1 M ζ increases from high to low molecular weight i.e. from a coiled to a rod-like configuration. At I_E = 0.001 M, no change of ζ with molecular weight can be detected but the values of ζ are higher than found at 0.1 M and approach most closely the expected 4 X 10^{-9} g. sec.$^{-1}$. Extrapolation of ζ to M_{sD} = 0 at 0.1 M gives 1.1 X 10^{-9} g. sec.$^{-1}$ and 2.0 X 10^{-9} g. sec.$^{-1}$ for D.B. and K.R. theories respectively. These figures are respectively near the mean ζ of 1.19 X 10^{-9} g. sec.$^{-1}$ and 2.35 X 10^{-9} g. sec.$^{-1}$ in 0.001 M.

As expected the effective hydrodynamic radius, R_s of the D.B. theory (Table VIII) increases with increase of molecular weight and decrease of ionic strength. The shielding ratio of the D.B. theory is constant in 0.1 M but decreases with M in 0.001 M. Similarly the effective bond length, b of the K.R. theory decreases with M to extrapolate to values comparable with those found by the conventional K.R. extrapolation in Fig. 13 and Table VI.

The failure of the theories to yield correct values of ζ is probably due to the inadequacy of the models on which they are based. In both, the molecule is considered to be an aggregate of resisting points. In the K.R. theory the points are in a random coil arrangement while the D.B. theory is based on a spherical model with a uniform distribution of resisting units.

Distortion of the molecule in shear or gravitational fields is neglected. That such effects can have marked influence on configuration is indicated by the studies of Rumscheidt and Mason (76) on the deformation of fluid droplets in shear fields. A further important factor could be internal circulation of the type observed by Mason and co-workers (77,78) for fluid drops. Such circulation may cause independent fluid movement in the interior of the molecule which would compensate for the frictional losses in the outlying parts of the chain. Modifications of the D.B. and K.R. theories to allow for the above important effects may lead to better agreement of the theory with the experiment.

REFERENCES

1. R. Signer and J. Liechti, Helv. Chim. Acta 21, 530 (1938).
2. R. Signer and P. Tavel, Helv. Chim. Acta 21, 535 (1938).
3. A. Polson, Koll-Z. 83, 172 (1938).
4. H. Staudinger and F. Reinecke, Ann. 47, 535 (1938).
5. I. Jullander, Svensk Papperstidn. 55, 197 (1952).
6. R. St.J. Manley, Arkiv For Kemi 9, 519 (1956).
7. D.T.F. Pals and J.J. Hermans, Rec. trav. Chim. 71, 433 (1952).
8. S. Schneider and P. Doty, J. Phys. Chem. 58, 762 (1954).
9. H. Fujita and T. Homma, J. Polym. Sci. 15, 277 (1955).
10. J. J. Hermans and J.T.G. Overbeek, Rec. trav. Chim. 67, 762 (1948).
11. J.G. Kirkwood and J.J. Riseman, J. Chem. Phys. 16, 565 (1948).
12. P. Debye and A.M. Bueche, J. Chem. Phys. 16, 573 (1948).
13. H. Terayama and F.T. Wall, J. Polym. Sci. 16, 357 (1955).
14. A. Rezanowich and D.A.I. Goring, J. Colloid Sci. 15, 452 (1960).
15. H.J. Marrinan and J.J. Hermans, Paper presented at Am. Chem. Soc. meeting, Cleveland, Ohio. April, 1960.
16. L.J. Gosting and M.S. Morris, J. Am. Chem. Soc. 71, 1998 (1949).
17. P.R. Gupta and D.A.I. Goring, Can. J. Chem. 38, 248 (1960).
18. T.E. Timell, Svensk Papperstidn. 56, 311 (1953).
19. J. Schurz and E.H. Immergut, J. Polym. Sci. 9, 281 (1952).
20. M.M. Huque, D.A.I. Goring and S.G. Mason, Can. J. Chem. 36, 952 (1958).
21. S. Newman, L. Loeb and C.M. Conrad, J. Polym. Sci. 10, 463 (1953).
22. T.E. Timell, Svensk Papperstidn. 57, 777 (1954).
23. M.L. Huggins, J. Am. Chem. Soc. 64, 2716 (1942).

24. Part II of this thesis.

25. B.A. Brice, M. Halwer and R. Speiser, J. Gpt. Soc. Am. 40, 768 (1950).

26. D.A.I. Goring, M. Senez, B. Melansen and M.M. Huque, J. Coll. Sci. 12, 412 (1957).

27. W.B. Dandliker and J. Kraut, J. Am. Chem. Soc. 78, 2380 (1956).

28. M.M. Huque, J. Jaworzyn and D.A.I. Goring, J. Polym. Sci. 39, 9 (1959).

29. D.A.I. Goring and T.E. Timell, J. Phys. Chem. 64, 1426 (1960).

30. H.J.L. Trap and J.J. Hermans, J. Phys. Chem. 58, 757 (1954).

31. B.H. Zimm, J. Chem. Phys. 16, 1093, 1099 (1948).

32. Appendix on Light scattering in this thesis

33. T. Svedberg and K.O. Pedersen, The Ultracentrifuge, Oxford, 1940.

34. H. Fujita and V.J. MacCosham, J. Chem. Phys. 30, 291 (1959).

35. P.R. Gupta, R.F. Robertson and D.A.I. Goring, Can. J. Chem. 38, 260 (1960).

36. H.K. Schachman, Ultracentrifugation in Biochemistry, Academic Press, 1959.

37. Part III of this thesis

38. L. Boltzmann, Ann. Physik. 53, 959 (1894).

39. N. Gralen, Inaugural Dissertation, Uppsala (1944).

40. Appendix on diffusion of this thesis

41. L. Mandelkern and P.J. Flory, J. Chem. Phys. 20, 212 (1952).

42. I. Croon and C.B. Purves, Svensk Papperstidn. 61, 963 (1959).

43. I. Croon and B. Lindberg, Seensk Papperstidn. 59, 794 (1956).
60, 82 (1957).

44. I. Croon, Svensk Papperstidn. 63, 247 (1960).

45. D.A.I. Goring and P. Johnson, J. Chem. Soc. 33 (1952).

46. H. Abe and W. Prins, Makromolek. Chem. 42, 216 (1961).

47. V.J. Schurz, Das Papier 14, 518 (1960).

48. F. Booth, Proc. Roy. Soc. (London) A 203, 533 (1950).

49. H. Mark, Der feste Korper, Leipzig. 103 (1938).

50. Howinck, J. Parkt. Chem. 157, 15 (1940).

51. M.L. Hunt, S. Newman, H.A. Scheraga and P.J. Flory, J. Phys. Chem. 60, 1278 (1956).

52. R.S. Stein and P. Doty, J. Am. Chem. Soc. 68, 159 (1946).

53. R.M. Badger and R.H. Blaker, J. Phys. Chem. 53, 1056 (1949).

54. A.M. Holtzer, H. Benoit and P. Doty, J. Phys. Chem. 58, 624 (1959).

55. E.H. Immergut, B.G. Ranby and H.F. Mark, Ind. Engg. Chem. 45, 2483 (1953).

56. H.J. Phillips and C.F. Bjork, J. Polym. Sci. 6, 549 (1951).

57. P.J. Flory, Principles of Polymer Chemistry, Cornell Univ. Press (1953).

58. C.W. Tait, R.J. Vetter, J.M. Swanson and P. Debye, J. Polym. Sci. 7, 303 (1951).

59. C.R. Masson and G.W. Caines, Can. J. Chem. 32, 51 (1954).

60. J.L. Gardon and S.G. Mason, Chem. And Engg. Data series 3, 115 (1958).

61. P.J. Flory, J. Chem. Phys. 21, 162 (1953).

62. P.J. Flory and J.E. Osterheld, J. Phys. Chem. 58, 653 (1954).

63. G. Porod, Monatsh. 80, 251 (1949).

64. O. Kratky and G. Porod, Rec. trav. Chim. 68, 1106 (1949).

65. R.M. Fuoss and U.P. Strauss, J. Polym. Sci. 3, 246 (1948).

66. J.R. Huizenga, P.F. Grieger and F.T. Wall, J. Am. Chem. Soc. 72, 2636, 4228 (1950).

67. R.M. Fuoss, J. Polym. Sci. 12, 185 (1959).

68. F.E. Harris and S.A. Rice, J. Phys. Chem. 58, 725, 733 (1954).

69. V.P. Strauss, J. Am. Chem. Soc. 81, 5292-5302 (1959).

70. P.J. Flory and T.G. Fox, J. Polym. Sci. 5, 745 (1950).

71. P.J. Flory and T.G. Fox, J. Am. Chem. Soc. 73, 1904, 1915 (1951).

72. W.R. Krigbaum and L.H. Sperling, J. Phys. Chem. 64, 99 (1960).

73. H.A. Scheraga and L. Mandelkern, J. Am. Chem. Soc. 75, 179 (1953).

74. J.T. Edward, J. Polym. Sci. 25, 483 (1957).

75. H.J. Marrinan and J.J. Hermans, Paper presented at Am. Chem. Soc. meeting, Cleveland, Ohio. April, 1960.

76. F. Rumscheidt and S.G. Mason, J. Colloid Sci. In Press.

77. M.A. Nawab and S.G. Mason, J. Phys. Chem. 62, 1248 (1958).

78. F. Rumscheidt and S.G. Mason, J. Colloid Sci. In Press.

P A R T II

CONCENTRATION DEPENDENCE OF VISCOSITY OF SODIUM CARBOXYMETHYL CELLULOSE SOLUTIONS

ABSTRACT

The Huggins coefficient, k' was measured for eight fractions of sodium carboxymethyl cellulose by an iso-ionic dilution technique and was observed to increase markedly with decrease of ionic strength. It was shown that the large increases of k' were due to the increased secondary electroviscous effects rather than to changes in configuration. The concept of a collision doublet proposed by Goring and Rezanowich was extended to CMC. An expression for the surface charge density, Q was derived by considering the equilibrium between the hydrodynamic compressive force and the electrostatic repulsive force in the rotating doublet. A comparison was made between the values of Q and a quantity, Q_a obtained by dividing the number of charges on the polyion by the area of the surface assuming spherical symmetry of the molecule.

INTRODUCTION

The change in the reduced viscosity with concentration of dilute solutions of high polymers has been expressed by the relationship (1)

$$\eta_{sp/c} = [\eta] + k'[\eta]^2 c \qquad \ldots(1)$$

where k', the Huggins constant depends on the nature of the polymer-solvent interactions in solution. For non-ionic polymers k' has been generally found to vary between 0.3 and 0.5 (2-5). However, in the case of polyelectrolytes higher k' values have been reported for a number of systems (6-9).

Recently, Goring and Rezanowich (9) observed for fractions of lignin sulfonate a large increase in k' with decrease in the ionic strength. This behavior was interpreted in terms of the secondary electroviscous effect. The treatment by Goring and Rezanowich (19) is based on the particle collision behavior as reported in detail by Mason and Co-workers (10-14). The constant, k' is assumed to arise from the rotation of the doublet formed by the collision of spherical particles in the streamlines of the sheared solution. When the particles carry charges, the double layers interact during collision and the collision radius increases. A higher value of k' results.

A relation was deduced between k' and half the distance of closest approach, δ

$$\left(\frac{r_\eta + \delta}{r_\eta}\right)^6 = \frac{k'}{k'_o} \qquad \ldots(2)$$

where r_η is the radius of the equivalent sphere obtained by substituting $[\eta]$ in the Einstein viscosity equation and k'_o is the value of k' under conditions of high ionic strength when δ is zero. From Eq. (2), δ was computed over a range of ionic strengths. Goring and Rezanowich (9) found the ratio of δ to the Debye width of the double layer constant over a wide range of the ionic strengths, I_E.

In the above theory two forces are acting on the charged spheres. A hydrostatic compressive force tends to push the spheres into contact while the electrical repulsive force pushes them apart. The two charged spheres are separated by a distance which is set by the equilibrium between the two forces. In the present section a theoretical extension of the original proposal is deduced from this condition of equilibrium.

It was considered of interest to test the validity of the theory now proposed by its application to the results of the current studies on the molecular size and hydrodynamic properties of sodium carboxymethyl cellulose (CMC) (15). Intrinsic viscosities and k' values were available for a series of fractions, over a range of ionic strengths and molecular weights. A quantitative interpretation of the k' values obtained will be given here in terms of the concept outlined above.

THEORETICAL

A diagramatic representation of the rotating doublet is given in Fig. 1. The electrostatic repulsive force, F_E may be obtained from an approximate equation of Verwey and Overbeek (16) for the repulsive energy, V_R of two charged spheres separated by a distance 2δ. Written in present symbols the Verwey-Overbeek equation is

$$V_R = \frac{r_\eta^2 \epsilon \psi_o^2}{2} \cdot \frac{e^{-2\underline{K}\delta}}{(r_\eta + \delta)} \qquad \ldots(3)$$

where ϵ = Dielectric constant of the medium

ψ_c = Surface Potential

$\frac{1}{\underline{K}}$ = Debye width of double layer

The electrostatic repulsive force, F_E is given by

$$F_E = \frac{1}{2} \frac{d V_R}{d \delta} \qquad \ldots(4)$$

$$= \frac{\epsilon r_\eta^2 \psi_c^2}{4} d\left[(r_\eta + \delta)\, e^{-2\underline{K}\delta}\right]^{-1} \Big/ d\delta \qquad \ldots(5)$$

$$= -\frac{\epsilon r_\eta^2 \psi_c^2}{4} \frac{1}{e^{2\underline{K}\delta}} \left[\frac{2\underline{K}}{(r_\eta + \delta)} + \frac{1}{(r_\eta + \delta)^2}\right] \qquad \ldots(6)$$

Fig. 1

Collision of spheres with interacting double layers in a shear field

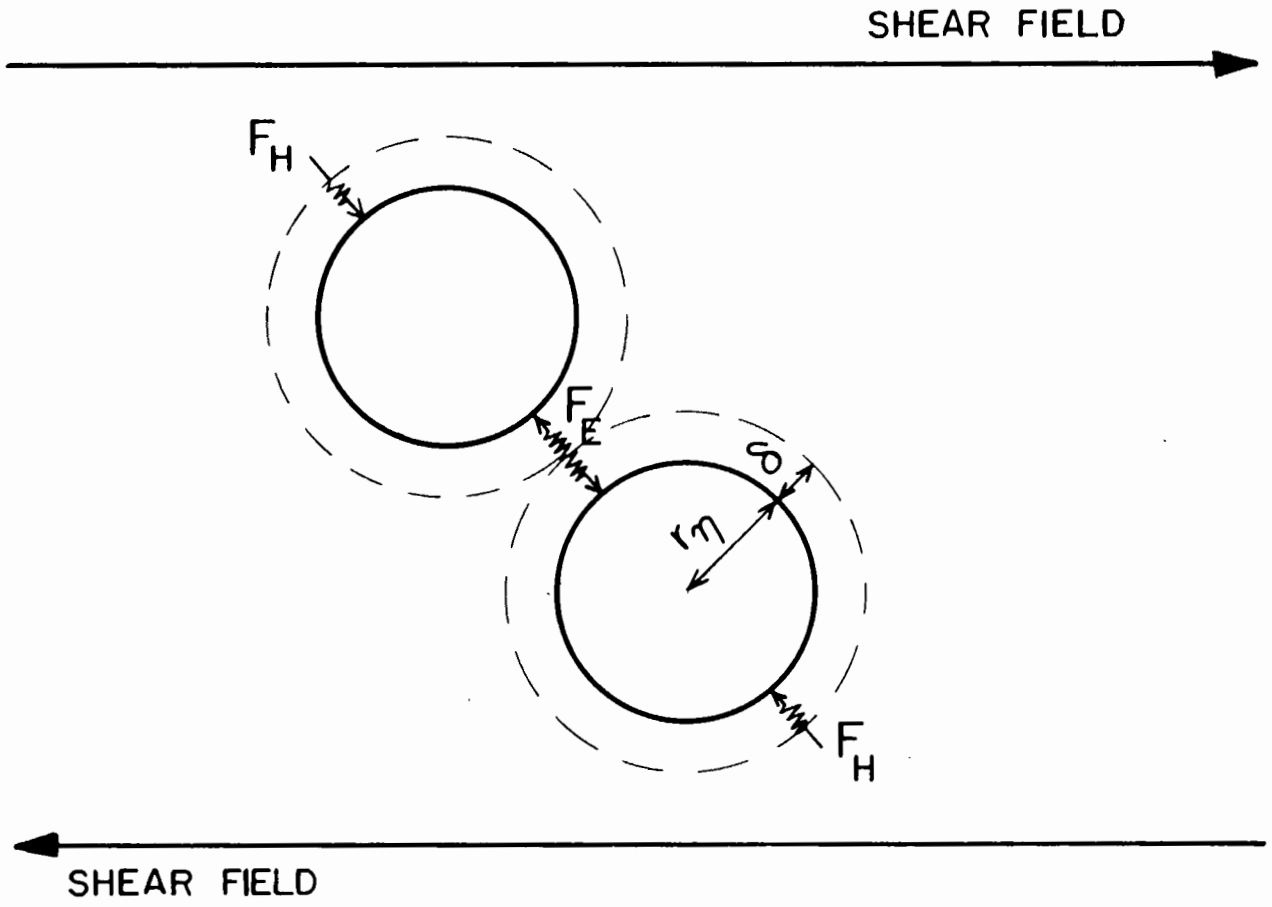
SHEAR FIELD
F_H
F_E
δ
r_n
F_H
SHEAR FIELD

According to Mason (17), the hydrodynamic compressive force, F_H is

$$F_H = \frac{2\pi \eta_0 G (r_\eta + \delta)^2}{\alpha} \sin 2\phi^* \qquad \ldots(7)$$

where α is a function of the axial ratio of the prolate ellipsoid equivalent hydrodynamically to the doublet, ϕ^* is the angle its major axis makes perpendicular to the direction of the streamlines, η_0 is the viscosity of the solvent and G is the shear rate.

Approximating all directions between 0 and $\pi/2$ for ϕ^* being equally likely, the average value of Sin $2\phi^*$ becomes $2/\pi$. Mason (17) has shown that the factor, α reduces to a value of 2.32 when the ellipsoid equivalent hydrodynamically to the doublet has an axial ratio of 2. Assuming an axial ratio of 2 and substituting $2/\pi$ for Sin $2\phi^*$, Eq. (7) becomes

$$F_H = \frac{4 \eta_0 G (r_\eta + \delta)^2}{2.32} \qquad \ldots(8)$$

Equating the compressive and repulsive forces for equilibrium

$$\frac{4 \eta_0 G (r_\eta + \delta)^2}{2.32} = \frac{\epsilon r_\eta^2 \psi_c^2}{4} \frac{1}{e^{2K\delta}} \left[\frac{2K(r_\eta + \delta) + 1}{(r_\eta + \delta)^2} \right] \qquad \ldots(9)$$

Rearranging Eq. (9), we get

$$\frac{e^{2K\delta} (r_\eta + \delta)^4}{r_\eta^2 \left[2K (r_\eta + \delta) + 1 \right]} = \frac{2.32 \epsilon \psi_c^2}{16 \eta_0 G} \qquad \ldots(10)$$

Substituting for ψ_0 in terms of $\underline{K}$, (18)

$$\psi_0 = \frac{4\pi Q}{\epsilon \underline{K}} \qquad \ldots(11)$$

where Q is the surface charge density, Eq. (10) may be written

$$\frac{\underline{K}^2 e^{2\underline{K}\delta} (r_\eta + \delta)^4}{r_\eta^2 \left[2\underline{K} (r_\eta + \delta) + 1 \right]} = \frac{2 \cdot 32 \pi^2 Q^2}{\eta_0 G \epsilon} \qquad \ldots(12)$$

Assuming $r_\eta >> \frac{1}{\underline{K}}$

$$2\underline{K} (r_\eta + \delta) + 1 \simeq 2\underline{K} (r_\eta + \delta) \qquad \ldots(13)$$

Then Eq. (12) becomes

$$\underline{K} e^{2\underline{K}\delta} \frac{(r_\eta + \delta)^3}{r_\eta^2} = \frac{4 \cdot 64 \pi^2 Q^2}{\eta_0 G \epsilon} \qquad \ldots(14)$$

Eq. (14) can now be used to compute the effective charge per unit area of the surface of the molecule.

EXPERIMENTAL

Viscosities were measured in aqueous sodium chloride by means of a capillary viscometer of Schurz-Immergut type, (19) with four bulbs and a reservoir to permit measurement at different shear rates and concentrations. An isoionic dilution technique (15) was employed to obtain linear graphs of reduced viscosity vs. concentration. All measurements were made at 25 $\pm$ 0.01°C and $\eta_{sp/c}$ vs. C graphs computed for G = 500 sec.$^{-1}$. The materials used, preparation of the fractions, as well as details of viscometry have been described in an earlier section of this thesis (15).

DISCUSSION OF RESULTS

Values of $[\eta]$ and k' derived for the fractions at different ionic strengths are given in Tables I and II. There is a marked increase of the Huggins coefficient with decrease in ionic strength. The k' value of 29.0 for fraction L3 at $I_E = 5 \times 10^{-4}$ M is the highest so far reported for CMC. Pals and Hermans (6) reported k' values for CMC ranging between 0.5 - 10.0 whereas the values of Fujita and Homma (7) were between 0.4 - 4.0. Increase of k' linearly with the reciprocal of the ionic strength has been observed in the past (6,20). Data from the present work, plotted in Fig. 2, confirm the linear relationship for I_E values from 0.1 - 0.0004 M. At lower I_E, k' falls below the straight lines shown in Fig. 2 for fractions M1 and H1.

At 0.1 M, the k' values varied erratically from fraction to fraction

Fig. 2

k' vs. reciprocal ionic strengths for H1, M1 and L3

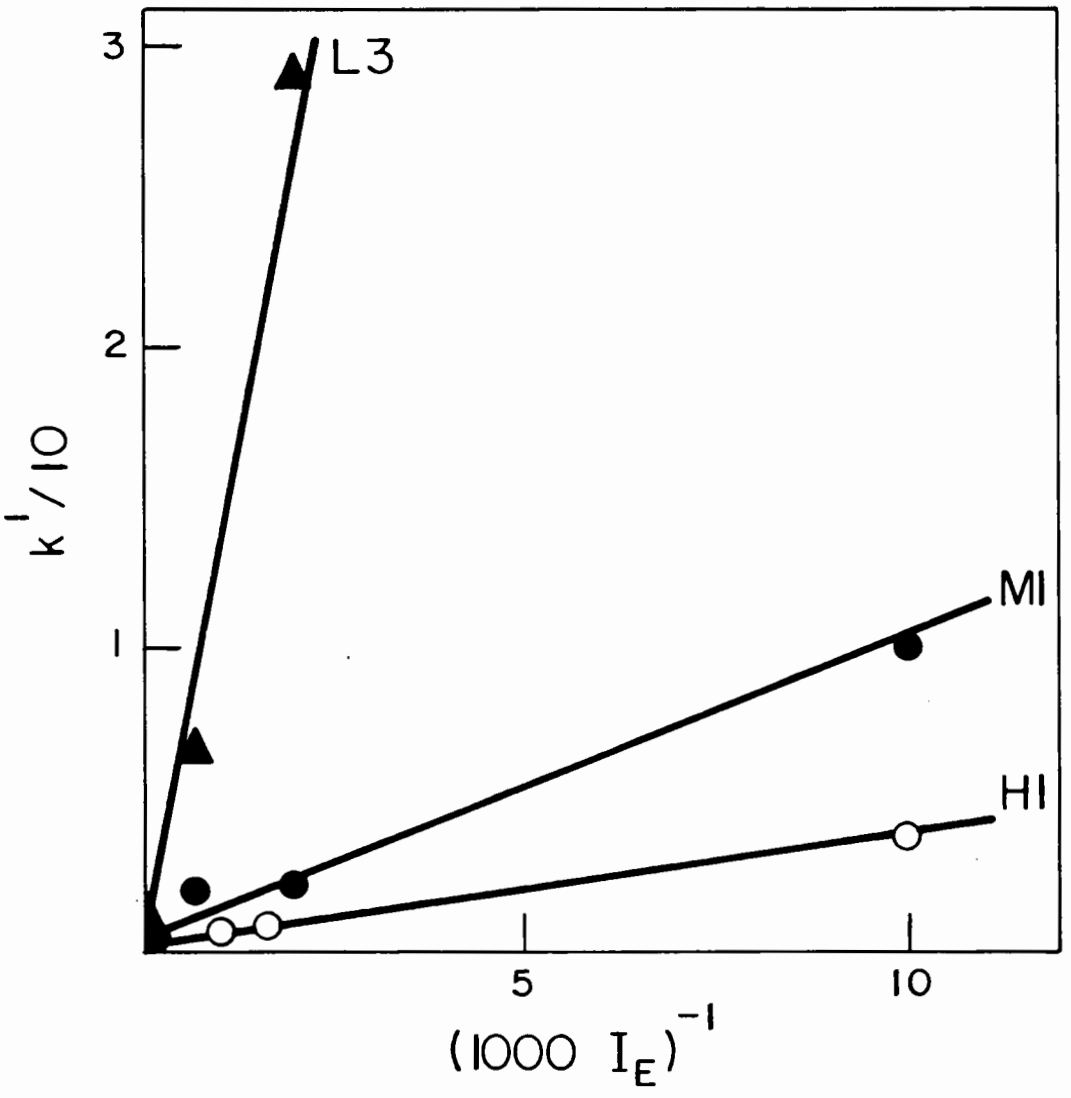
3
2
1
k'/10
L3
MI
HI
5
10
(1000 I_E)$^{-1}$

and did not exhibit any special trend with molecular weight (Table II). For many synthetic polymer systems, k' has been shown to be independent of molecular weight (2). The cause of the random variation of k' found here for CMC is uncertain but it might be attributed in part to the disturbing effect of molecular aggregation in some of the fractions (15). Marked variation in the k' values from fraction to fraction has also been observed for alkali lignin (21) and dextrans (22). At an ionic strength of 0.001 M, k' is larger than at 0.1 M and shows an increasing trend with the decrease of molecular weight, as shown in Table II.

Two possible reasons may now be considered for the trends in k' shown in Tables I and II. They are (a) the effect of configurational changes (b) the effect of double layer interaction.

From changes in several hydrodynamic parameters it was concluded in an earlier section (15) that the molecules possess an extended rod-like configuration at low ionic strengths. It also seemed possible that the CMC molecule could undergo a transition from coiled to a rod-like configuration with decrease in molecular weight analogous to the rod-coil transition obtained for cellulose trinitrate (23,24). Eirich and Riseman (25) attributed k' values greater than 2 to rod-like bodies. Thus the increase of k' with decrease in I_E and M_{sD} shown in Tables I and II could be partly due to an increased rod-like tendency in the configuration of the polyelectrolyte. However, this influence is probably small. For cellulose trinitrate, Hunt et al (26) found k' decrease with decrease in molecular weight in spite of a change to a rod-like configuration. Also

TABLE I

Data for $[\eta]$, r_η, k' and δ for Fractions H1, M1 and L3 at Various Ionic Strengths

Fraction	I_E (moles Na^+/)	$[\eta]$ (dl. $g.^{-1}$)	r_η (Å)	k'	δ (Å)
H1	0.1	12.3	740	0.51	7
	0.01	28.8	1140	0.51	34
	0.001	62.7	1680	0.65	76
M_{sD} = 346,200	0.00064	68.2	1750	1.1	240
	0.00010	91.8	2040	3.7	737
	0.00005	105.0	2180	8.2	1290
	0.00001	160.0	2690	8.9	1660
M1	0.1	6.95	460	0.45	4
	0.01	11.7	629	0.46	8
	0.00139	19.5	826	1.9	237
M_{sD} = 163,200	0.00050	27.7	1040	2.2	326
	0.00010	39.0	1190	10.5	842
	0.00005	48.8	1330	10.6	946
	0.00003	51.3	1370	12.8	1040
L3	0.1	1.57	241	0.55	10
	0.01	2.32	311	1.1	52
M_{sD} = 44,700	0.00166	3.47	380	6.5	216
	0.00050	3.93	404	29.0	408

TABLE II

Data for $[\eta]$, r_η and k' for Fractions at High and Low Ionic Strength

Fraction	M_{sD} x10^{-5}	0.1 M			0.001 M			
		$[\eta]$ (dl. g.$^{-1}$)	r_η (Å)	k'	$[\eta]$ (dl.g.$^{-1}$)	r_η (Å)	k'	δ Å
H1	3.462	12.3	740	0.51	62.5	1680	0.65	74
H2	2.798	12.2	629	0.28	35.0	1060	1.1	140
H3	1.938	7.98	494	0.50	26.8	905	1.5	179
M1	1.632	6.95	460	0.45	18.8	900	1.9	228
M2	0.942	5.80	374	0.19	15.7	615	4.3	265
L1	0.906	5.16	358	0.33	9.3	480	6.1	248
L2	0.460	2.57	246	0.36	3.95	-		-
L3	0.447	1.57	241	0.55	3.50	390	6.5	210

in the present study there was no trend of k' with M_{SD} at I_E = 0.1 M It is therefore likely that the large increases of k' in Tables I and II with decrease in I_E are due to the greater significance of the double layer thickness at low ionic strengths. Similarly the ratio of the double layer thickness at 0.001 M to the effective molecular radius increases with decrease in molecular weight and thus produces the increasing trend of k' with decrease in M_{SD} shown in Table II. Absence of the trend at 0.1 M is anticipated because of the decrease of the double layer thickness by an order of magnitude.

In consideration of the above, the molecule will be assumed to possess spherical symmetry in order to apply the analysis given in the Theoretical Section. It is realized that this assumption is an oversimplification and it is expected that at very low I_E or molecular weight the treatment will break down because of the considerable extension of the polyelectrolyte.

Proceeding, the molecule is considered equivalent to a sphere of radius, r_η . In the case of CMC, r_η at infinite ionic strength, $(r_\eta)_{I_E=\infty}$ was calculated from the relationship

$$(r_\eta)^2_{I_E=\infty} = \frac{5}{18} Z b^2 \qquad \ldots(15)$$

where Z is the degree of polymerization and b is the effective bond length in the K.R. theory (27). Values of r_η at other ionic strengths were obtained from (6,20),

$$\left(r^2_{\eta}\right)_{I_E} = \frac{[\eta]_{I_E}}{[\eta]_{I_E=\infty}} \cdot \left(r^2_{\eta}\right)_{I_E=\infty} \qquad \ldots(16)$$

$$= \alpha^2 \cdot \left(r^2_{\eta}\right)_{I_E=\infty}$$

$[\eta]_{I_E=\infty}$ in Eq. (16) needed to calculate r_{η} at different ionic strengths was estimated from plots of $[\eta]$ vs. $1/I_E$ and was 9.8, 5.7 and 1.38 dl.g.$^{-1}$ for H1, M1 and L3 respectively. Values of δ were obtained from Eq. (6). For the calculation of δ values at different ionic strengths in Table I, k'_o values of 0.5, 0.43 and 0.44 for H1, M1 and L3 respectively were used and were obtained from k' vs. $1/I_E$ graphs shown in Fig. 2. A constant k'_o value of 0.5 at I_E = 0.1 M was used to compute δ values of the fractions at 10^{-3} M in Table II.

As shown in Table I, δ increased with decrease in I_E. The composite graph of δ vs. $1/\underline{K}$ (Fig. 3) was approximately linear with a slope of 2.4. The magnitude of the slope which is a function of variables such as charge density and configuration of the particles may be characteristic for the cellulosic polyelectrolytes. For lignin sulfonates (9) a linear relationship between δ and $1/\underline{K}$ was noted with $\delta\ \underline{K} = 1.5$.

The approximate co-linearity of the δ vs. $1/\underline{K}$ plots for H1, M1 and L3 marked a smaller but significant decrease of δ with increase in molecular weight as shown in Fig. 4 for I_E = 0.001 M. Evidently, in the collision doublets formed by the larger molecules the distance of separation was less than in the case of small molecule doublets.

It is now of interest to apply the theoretical approach to CMC and by the use of Eq. (14) calculate Q, the charge per unit area of the surface of the molecule. These values are compared with a quantity, Q_a obtained from the expression

Fig. 3

δ vs. the Debye radius for H1, M1 and L3

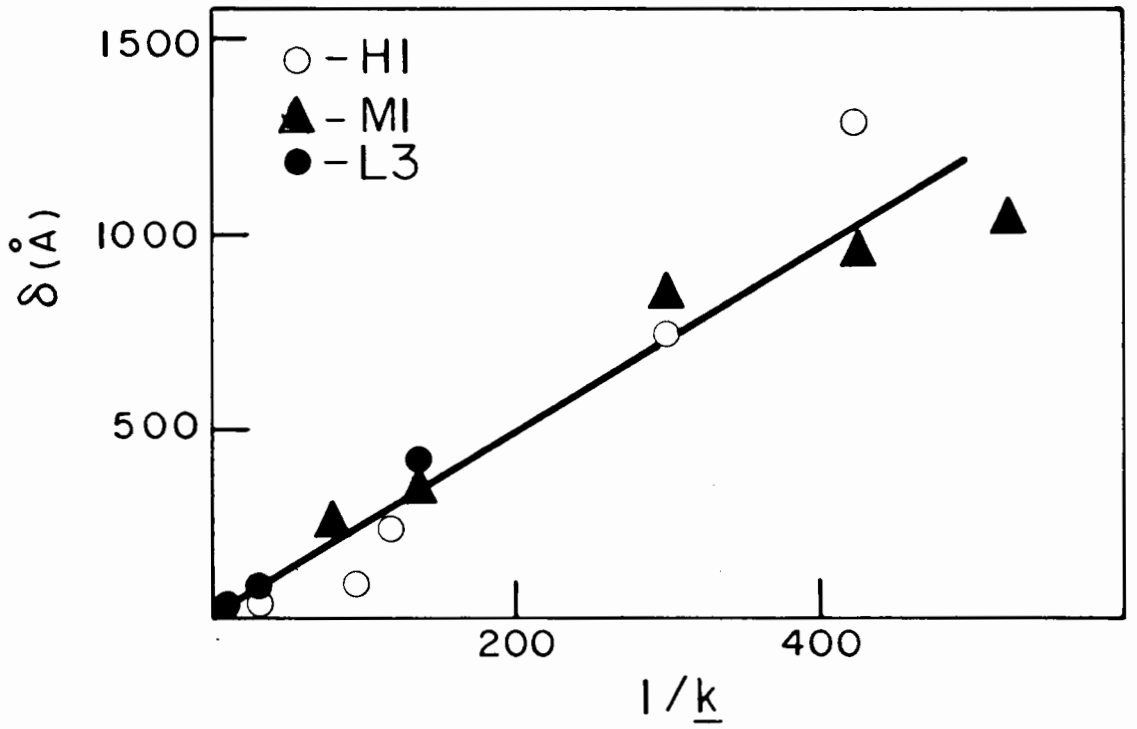
1500
1000
500
δ(Å)
○ - HI
▲ - MI
● - L3
200
400
1/k

Fig. 4

δ vs. M_{SD} at I_E = 0.001 M

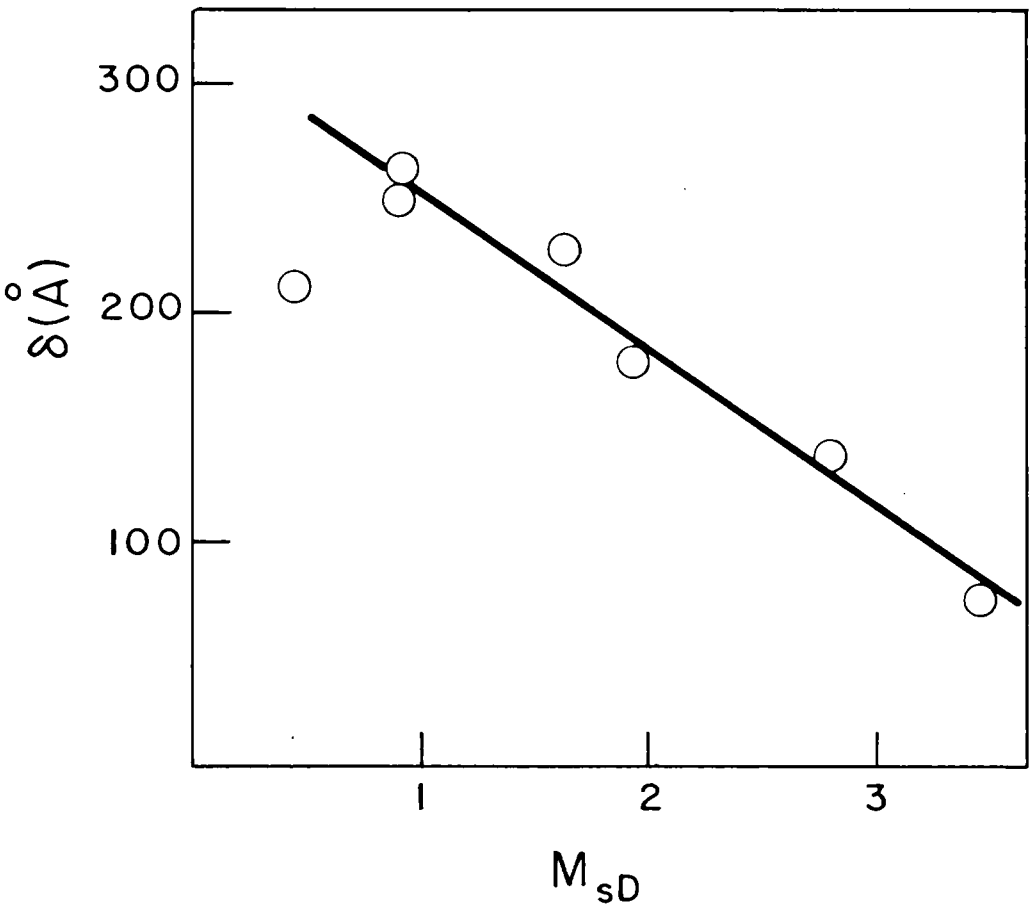
300
200
100
δ(Å)
1
2
3
M_{sD}

$$Q_a = \frac{Z}{4\pi r_\eta^2} \qquad \ldots(17)$$

where $\underline{Z}$ is the number of charges carried by a polyion and $4\pi r_\eta^2$ is the surface area assuming that the particles are spheres of radius, r_η. Thus Q_a will be the surface charge density if all the ionizable groups are located on the surface of the polyion. Values of Q and Q_a calculated from Eqs. (14) and (17) are recorded in Tables III and IV.

In spite of the irregularities in the trends in Table III, it is clear that Q increases with the decrease in ionic strength, except for the lowest values of I_E. This trend would be expected due to the contraction of the molecular coil at high ionic strengths. The charge density on the surface decreases with increased coiling because a greater part of the charge is shielded within the coil and is not effective in promoting the repulsion shown in Fig. 1. On the other hand, the regular decrease of Q_a with ionic strength arises because in Eq. (17) $\underline{Z}$ is constant while r_η increases with decrease in I_E. At high I_E, Q_a must represent an overestimate of the surface charge because of the coiled configuration of the polyelectrolyte. As I_E decreases, the CMC molecule becomes more extended and Q_a then more nearly approaches the surface charge density, Q. Thus the approximate convergence of Q and Q_a to equality at I_E = 0.0005 M can be expected from these qualitative considerations. The decrease of Q again at yet lower values of I_E may be due to a breakdown of the theory when the chain becomes fully stretched.

Table IV demonstrates a trend in Q from high to low molecular weight

TABLE III

Surface Charge Density for H1, M1 and L3

at Different Ionic Strengths

Fraction	I_E	$(r_\eta + \delta)$ (Å)	$\frac{(r_\eta + \delta)}{r_\eta}$	$Q_{x10^{-10}}$ (e.s.u./cm.^{2})	$Q_{a\ x10^{-10}}$ (e.s.u./cm.^{2})
H1	0.1	747	1.13	11	109
	0.01	1170	1.15	12	46
	0.001	1760	1.17	6	21
	0.00064	1990	1.27	21	19
	0.00010	2780	1.52	28	14
	0.00005	3470	1.78	55	13
	0.00001	4350	1.81	36	8
M1	0.1	464	1.13	7	121
	0.01	637	1.13	4	77
	0.00139	1060	1.44	52	45
	0.0005	1370	1.47	28	29
	0.0001	2030	1.91	43	22
	0.00005	2280	1.91	21	17
	0.00003	2410	1.96	14	16
L3	0.1	251	1.16	9	135
	0.01	363	1.31	13	91
	0.00166	596	1.75	49	61
	0.00050	812	2.24	60	54

TABLE IV

Surface Charge Density for the Fractions at 0.001 M

Fraction	M_{sD} x10^{-5}	$(r_\eta + \delta)$ (Å)	$\frac{(r_\eta + \delta)}{r_\eta}$	Q x10^{-10} (e.s.u./cm.^{2})	Q_a x10^{-10} (e.s.u./cm.^{2})
H1	3.462	1760	1.17	6	21
H2	2.798	1200	1.26	10	44
H3	1.938	1080	1.34	16	39
M1	1.632	1130	1.40	28	38
M2	0.942	880	1.60	41	48
L1	0.906	728	1.69	33	69
L3	0.447	600	1.72	21	58

similar to those shown in Table III from high to low ionic strength. It is seen that Q is least at high molecular weight and increases with the decrease in M_{sD}. An exception is seen for the lowest molecular weights corresponding to the decrease in Q at the lowest ionic strengths in Table III. As noted in a previous section (15), coil to rod transitions with decrease in molecular weight probably occur with the present range of CMC fraction similar to the configurational changes noted for cellulose trinitrate (20,23,25). Thus, the trend of Q in TableIV supports again the picture that the polyelectrolyte in its most coiled state yields the lowest values of Q. It is interesting to note in Table II that Q_a is always larger than Q, because at 10^{-3} M the molecule is still coiled enough for Q_a to be an overestimate of the effective surface charge.

Finally, it must be mentioned that the explanations offered for the trends in Q are qualitative. However, the agreement of Q and Q_a at $I_E = 0.005$ suggests that the proposed hydrodynamic doublet theory yields a surface charge density of the correct order of magnitude in spite of the simplifying assumptions required. Further tests are recommended with model charge bearing particles.

REFERENCES

1. M.L. Huggins, J. Am. Chem. Soc. 64, 2716 (1942).
2. P.J. Flory, Principles of Polymer Chemistry, Cornell U.P. (1953).
3. J. Kooy and J.J. Hermans, J. Polym. Sci. 16, 417 (1955).
4. L.H. Cragg and C.C. Bigelow, J. Polym. Sci. 16, 177 (1955).
5. M.H. Jones, Can. J. Chem. 34, 1027 (1956).
6. D.T.F. Pals and J.J. Hermans, Rec. trav. Chim. 71, 433 (1952).
7. H. Fujita and T. Homma, J. Polym. Sci. 15, 277 (1955).
8. H. Terayama and F.T. Wall, J. Polym. Sci. 16, 357 (1955).
9. D.A.I. Goring and A. Rezanowich, J. Colloid Sci. 15, 472 (1960).
10. B.J. Trevelyan and S.G. Mason, J. Colloid Sci. 6, 354 (1951).
11. R. St.J. Manley and S.G. Mason, J. Colloid Sci. 7, 354 (1952).
12. R. St.J. Manley and S.G. Mason, Can. J. Chem. 33, 763 (1955).
13. R. St.J. Manley and S.G. Mason, Proc. Roy. Soc. (London) A, 238, 117 (1956).
14. W. Bartok and S.G. Mason, J. Colloid Sci. 13, 293 (1958).
15. Part I of this thesis.
16. E.J.W. Verwey and J. Th. G. Overbeek, Theory of the Stability of Lyophobic Colloids, Elsevier p 152 (1948).
17. S.G. Mason, to be published.
18. S. Glasstone, Textbook of Physical Chemistry, Von Nostrand, p 1222 (1958).
19. J. Schurz and E.H. Immergut, J. Polym. Sci. 9, 281 (1952).
20. N.S. Schneider and P. Doty, J. Phys. Chem. 58, 762 (1954).
21. P.R. Gupta and D.A.I. Goring, Can. J. Chem. 38, 248 (1960).
22. F.R. Senti et al. J. Polym. Sci. 17, 527 (1955).
23. M.M. Huque, D.A.I. Goring and S.G. Mason, Can. J. Chem. 36, 952 (1958).

24. A.M. Holtzer, H. Benoit and P. Doty, J. Phys. Chem. 58, 624 (1954).

25. F. Eirich and J. Riseman, J. Polym. Sci. 4, 417 (1949).

26. M.L. Hunt, S. Newman, H.A. Scheraga and P.J. Flory, J. Phys. Chem. 60, 1278 (1956).

27. J.G. Kirkwood and J. Riseman, J. Chem. Phys. 16, 565 (1948).

P A R T III

CHARGE AND CONFIGURATIONAL EFFECTS IN THE CONCENTRATION DEPENDENCE OF SEDIMENTATION OF SODIUM CARBOXYMETHYL CELLULOSE

ABSTRACT

The dependence of the sedimentation constant on concentration was studied at 0.1 M, 0.01 M and 0.001 M for 8 fractions of sodium carboxymethyl cellulose. The graphs of $1/s_m$ vs. conc. showed unusually predominant upward curvature at low ionic strengths. This anomaly was not eliminated when the sedimentation constants were corrected for charge effects by the method of Tiselius.

Values of the initial slope constant, k_s in the concentration dependence equation

$$s_m = (s_m)_{c=o} (1 + k_s c)^{-1}$$

ranged from 0.79 dl.g.$^{-1}$ to 54.8 dl.g.$^{-1}$ between 0.1 M and 0.001 M. It was observed that the correction to the k_s values for the primary charge effect on the basis of the Tiselius equation was generally negligible except for low molecular weight fractions at low ionic strengths. Thus the concentration dependence effects observed in the sedimentation of CMC at ionic strengths of 0.001 M or greater were due more to configurational changes of the molecule rather than to the primary charge effect.

Values of $k_s/[\eta]$ were reasonably constant with averages of 1.14 ± 0.27 and 1.23 ± 0.41 at 0.1 M and 0.001 M respectively. These were lower than theoretical 1.66 deduced by Wales and Van Holde for vinyl polymers. If the value of 3.4×10^6 for $(\phi^{1/3} P^{-1})$ is used in the equation of Wales and Van Holde, $k_s/[\eta]$ becomes 0.7, which gives some theoretical justification for the lower $k_s/[\eta]$ values obtained in the present work.

INTRODUCTION

The dependence on concentration of the sedimentation constant in dilute solutions of polyelectrolytes is influenced by two effects:-

a) The effect of charge which decreases the sedimentation constant due to the electric field produced in the cell of the ultracentrifuge.

b) Configurational changes which alter the effective volume of the molecule in solution.

The decrease in the sedimentation velocity due to the electric field generated by the sedimenting charged particles was first observed by Smoluchowski (1). Theoretical treatment of the sedimentation of charged particles was undertaken by Tiselius (2) and by Booth (3) who derived equations to estimate the magnitude of this effect. The equation of Tiselius is

$$s_m = s_m' \left(1 - \frac{F \Lambda_o}{k \times 10^3} \cdot m_o c\right) \qquad \ldots(1)$$

where s_m is the sedimentation constant of the charged particle and s_m' is the sedimentation constant in the absence of charge effects; $F\Lambda_o$ is the equivalent conductance; k and $m_o c$ are specific conductance of the solution and molar concentration of the macro-ion respectively. Tiselius found that the experimental data obtained for phykoerythrin conformed to Eq. (1).

Pedersen (4), during his studies on the sedimentation rate of egg albumin, observed that two types of charge effect, the primary and the secondary, may be distinguished. The former which is the larger arises from

the differential sedimentation of the macro-ion and its 'Gegenion'. The macro-ion sediments more quickly than the small counter ions, builds up a charge at the base of the cell and causes a decrease in sedimentation rate by back electrophoresis of the sedimenting macro-ions. The secondary charge effect is due to the difference in the sedimentation rate of the positive and negative ions in the supporting electrolyte. Pedersen found that the primary charge effect in sedimentation was inversely related to the conductivity and directly related to the concentration of protein solutions, as predicted by Eq. (1).

In the sedimentation of polyelectrolytes, complications due to the charge effects were observed. However, the main interest in the charge effect in sedimentation has been confined to investigations on proteins (4,8,11). Recently, Pedersen (11) studied the effect of neutral salts as well as pH and ionic strength in the sedimentation of bovine serum albumin and observed that the concentration dependence of sedimentation was greater than that predicted by the Tiselius theory of the primary charge effect.

Turning now to uncharged macromolecules, the concentration dependence of sedimentation has often been shown to fit the well-known empirical equation

$$s_m = (s_m)_{c=o} \quad (1 + k_s c)^{-1} \qquad \ldots(2)$$

where s_m is the sedimentation constant at any concentration, $(s_m)_{c=o}$ is the sedimentation constant at zero concentration, and k_s is a constant. Newman and Eirich (12) found that, in the case of polystyrene fractions, k_s varied between 0.73 and 5.0 dl.g.$^{-1}$ but $k_s/[\eta]$ was approximately constant equal to

1.4 - 1.6. Wales and Van Holde (13), on the basis of the Flory relationships (14) for the sedimentation constant and intrinsic viscosity (15) $[\eta]$, derived an expression

$$k_s/[\eta] = \Lambda \frac{N (\phi^{1/3}_P - 1)^{-3}}{16,200\ \pi^2} \quad \ldots(3)$$

where $(\phi^{1/3}_P - 1)$ is the universal polymer constant, described by Mandelkern et al (14), N is the Avagadro's number and Λ is a constant deduced by Burgers (16) to be equal to 55/8 for dilute suspensions of spheres. Assuming a value of 2.5×10^6 for $(\phi^{1/3}_P - 1)$, Wales and Van Holde (13) obtained

$$k_s = 1.66 [\eta] \quad \ldots(4)$$

which agreed with the experimental $k_s/[\eta]$ value of 1.6 ± 0.26 for a wide variety of vinyl polymers. However, in the case of cellulose acetate and nitrate from the work of Singer (17) and of Newman et al (18), $k_s/[\eta]$ values between 0.3 - 1.0 were obtained.

During the course of the present investigation of the hydrodynamic properties (19) of sodium carboxymethyl cellulose (CMC), sedimentation constants were measured in aqueous sodium chloride at high and low ionic strengths. This paper deals with certain interesting observations on the concentration dependence of the sedimentation constant. An interpretation is given based on the theories of the effects of charge and molecular volume given above.

EXPERIMENTAL AND RESULTS

Details of the sedimentation measurements have been described in an earlier section (19). The concentration range was 0.1 - 0.5 g.dl.$^{-1}$ at 0.1 M and 0.005 - 0.05 g.dl.$^{-1}$ at lower ionic strengths. A typical set of curves of $1/s_m$ vs. c at different ionic strengths is shown in Fig. 1. Values of $(s_m)_{c=o}$ were obtained at 0.1 M by extrapolation of such curves. At higher concentrations deviation from linearity with a small downward curvature was observed. This trend has also been noted for other macromolecular systems (18,20).

At lower ionic strengths the small negative deviation gave place to considerable upward curvature. The graph of $1/s_m$ vs. c for 0.001 M (Fig. 1) is non-linear in the opposite direction with respect to the plot at 0.1 M; and this trend increased with the decrease of molecular weight. As mentioned in a previous section, plots of s_m vs. c were approximately linear at 0.001 M and $(s_m)_{c=o}$ was computed by extrapolation of such graphs.

A quantitative estimate of the concentration dependence was obtained by computing k_s in Eq. (2) from the initial linear portion of the $1/s_m$ vs. c graph. Accurate measurements were possible at 0.1 M but at lower ionic strengths the pronounced curvature (Fig. 1) reduced the precision. No improvement was found when

$$s_m = (s_m)_{c=o} \cdot (1 + k_s c + k_s' c^2) \qquad \ldots(5)$$

Fig. 1

Graph of $1/s_m$ vs. c for ML at high and low ionic strength

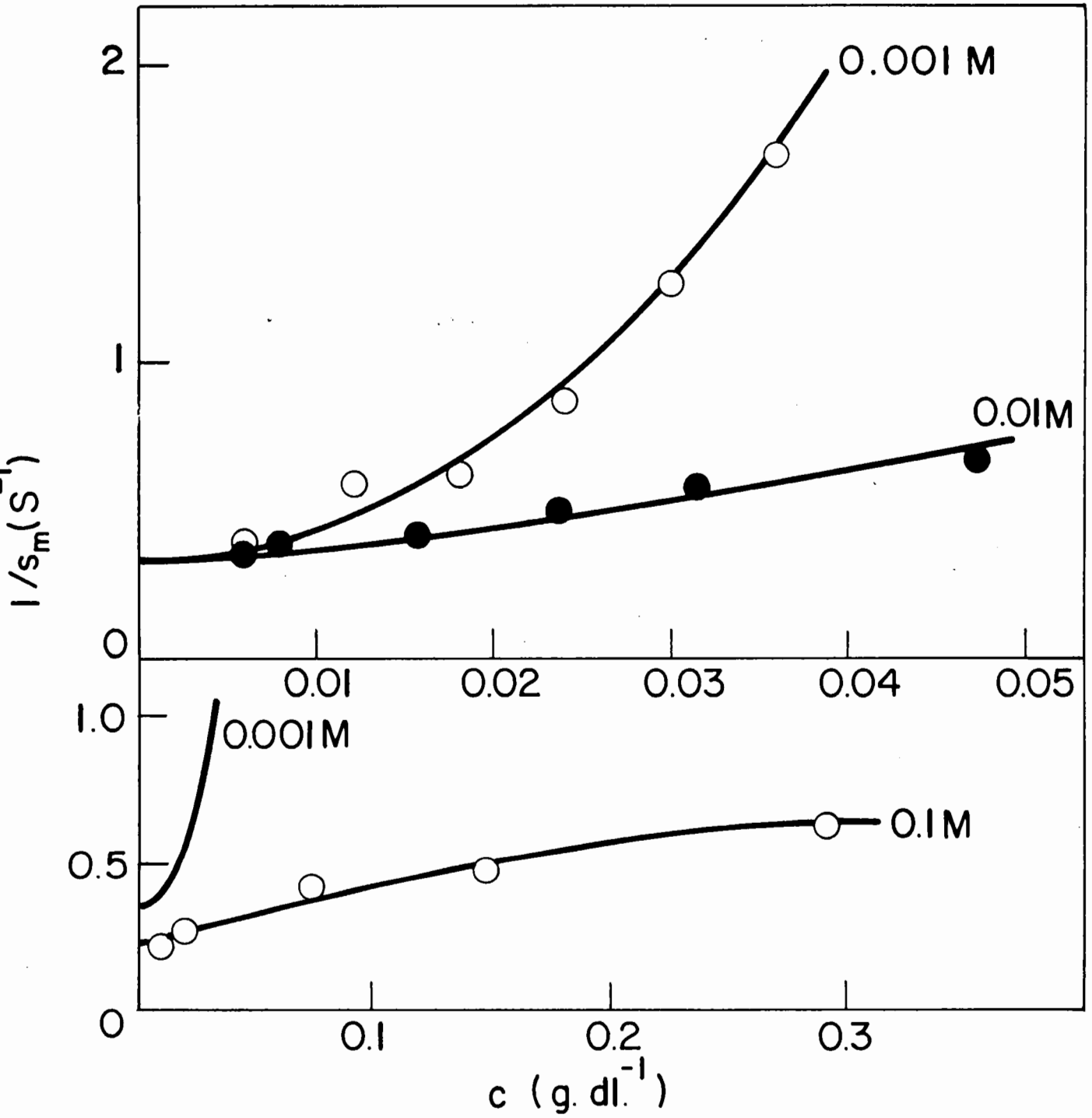
2
1
0
0.001 M
0.01M
$1/s_m(S^{-1})$
0.01
0.02
0.03
0.04
0.05
1.0
0.5
0
0.001M
0.1M
0.1
0.2
0.3
c (g. dl.$^{-1}$)

was used instead of Eq. (2), after the manner of Manley (20) and others(18). The values of k_s at ionic strengths of 0.01 and 0.001 must therefore be regarded as only approximate. Data for k_s are given in Table I. Also included are $(s_m)_{c=o}$ values corrected to 25°C (s_o) by the standard procedure (4).

DISCUSSION

The results in Fig. 1 show rather pronounced differences in the concentration dependence of the sedimentation constant with the change in ionic strength. This is manifest also by the marked increase of k_s at low ionic strength as shown in Table I. A decrease of k_s with molecular weight is also seen. Let us first consider how much of the variation can be attributed to increased charge effects due to changes in ionic strength.

Of the two charge effects considered by Pedersen (4), only the primary charge effect is of importance in the present work on CMC. The added electrolyte is sodium chloride and therefore the secondary charge effect is not significant because the sedimentation constants of the $Na^{(+)}$ and $Cl^{(-)}$ ions are approximately equal (6,11).

Eq. (1) predicts that the primary charge effect will cause a decrease of s_m with concentration over and above that due to the frictional component. This decrease varies inversely as the specific conductance of the solution. The effect would be expected to increase by two orders of magnitude between 0.1 and 0.001 M. Thus, the upward curvature of $1/s_m$ vs. c, as seen in Fig. 1 for I_E = 0.001 M, may be partly due to the increased primary charge effect with the decrease in ionic strength.

TABLE I

Values of k_s and $k_s/[\eta]$ at Different Ionic Strengths

Fraction		I_E = 0.1 M			0.01 M			0.001 M			
	$M_{sD} \times 10^{-5}$	$s_o \times 10^{13}$	k_s (dl.g.$^{-1}$)	$\frac{k_s}{[\eta]}$	$s_o \times 10^{13}$	k_s (dl.g.$^{-1}$)	$\frac{k_s}{[\eta]}$	$s_o \times 10^{13}$	k_s (dl.g.$^{-1}$)	k_s^c (dl.g.$^{-1}$)	$\frac{k_s^c}{[\eta]}$
H1	3.462	5.77	13.3	1.08	4.53	28.5	0.99	2.96	54.8	48.1	0.77
H2	2.798	5.70	10.8	0.89	-	-	-	2.85	51.3	44.6	1.27
H3	1.938	4.67	9.8	1.29	-	-	-	2.62	34.1	27.4	1.02
M1	1.632	4.26	7.2	1.04	3.11	18.7	1.59	2.65	25.2	18.5	0.99
M2	0.942	3.35	4.7	0.81	-	-	-	2.58	18.1	11.4	0.73
L1	0.906	3.29	4.3	0.79	-	-	-	2.50	16.3	9.6	1.03
L2	0.460	2.88	3.7	1.46	-	-	-	2.30	13.8	7.1	1.80
L3	0.447	2.80	2.8	1.78	2.70	8.1	3.49	2.40	14.4	7.7	2.20

According to Lauffer (9,10) a plot of $(1-s_m/s_m')$ vs. c should be linear, where s_m' is the sedimentation constant in the absence of charge effects. Termaine and Lauffer (10) observed such a linear relationship for southern bean mosaic virus. However, if s_m' and s_m are taken to be the sedimentation constants for the same CMC concentration at ionic strengths of 0.1 M and 0.001 M respectively, the graph is curved as shown in Fig. 2.

An attempt was made to correct the sedimentation constants at 10^{-3} M for charge effects on the basis of the Tiselius equation (2). Taking the value of 25 $ohms^{-1}$ $cm.^2$, for the equivalent conductance of CMC macro-ion, reported by Longsworth and Hermans (21) and the values of small ion conductances from the tables of Pedersen (11), the s_m values at 10^{-3} M were corrected in accordance with Eq. (1). As seen in Fig. 3 the graph of $1/s_m$ vs. c remained non-linear curving away from the c axis. This indicates that the effect of charge estimated by the Tiselius equation was not the only cause of the upward curvature at 0.001 M.

Fig. 3 also demonstrates that the effect of charge on k_s as predicted by Eq. (1) is small. A quantitative estimate can be made of this by writing Eq. (1) in the form

$$\frac{1}{s_m} = \frac{1}{s_m'} \cdot \left(1 + \frac{F\mu\, m_o c}{10^3\, k} + \cdots\right) \qquad \ldots(6)$$

If higher powers of c are neglected the coefficient of c in Eq. (6) represents the contribution of the primary charge effect to the experimentally determined values of k_s. If k is assumed to be the specific conductance of

Fig. 2

$(1 - s_m/s'_m)$ vs. concentration for M1

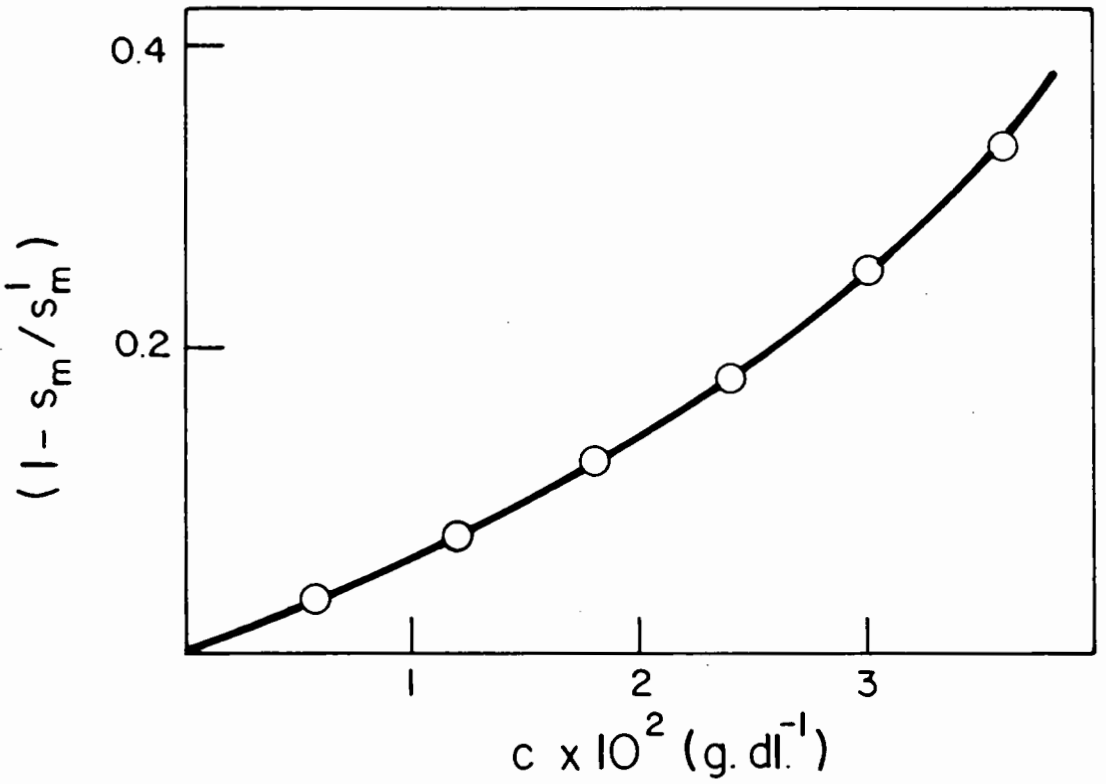
0.4
0.2
$(1 - s_m / s_m^1)$
1
2
3
$c \times 10^2$ (g. dl.$^{-1}$)

Fig. 3

Curve A - $1/s_m$ vs. c for M1

Curve B - $1/s_m$ vs. c for M1 after correction for primary charge effect

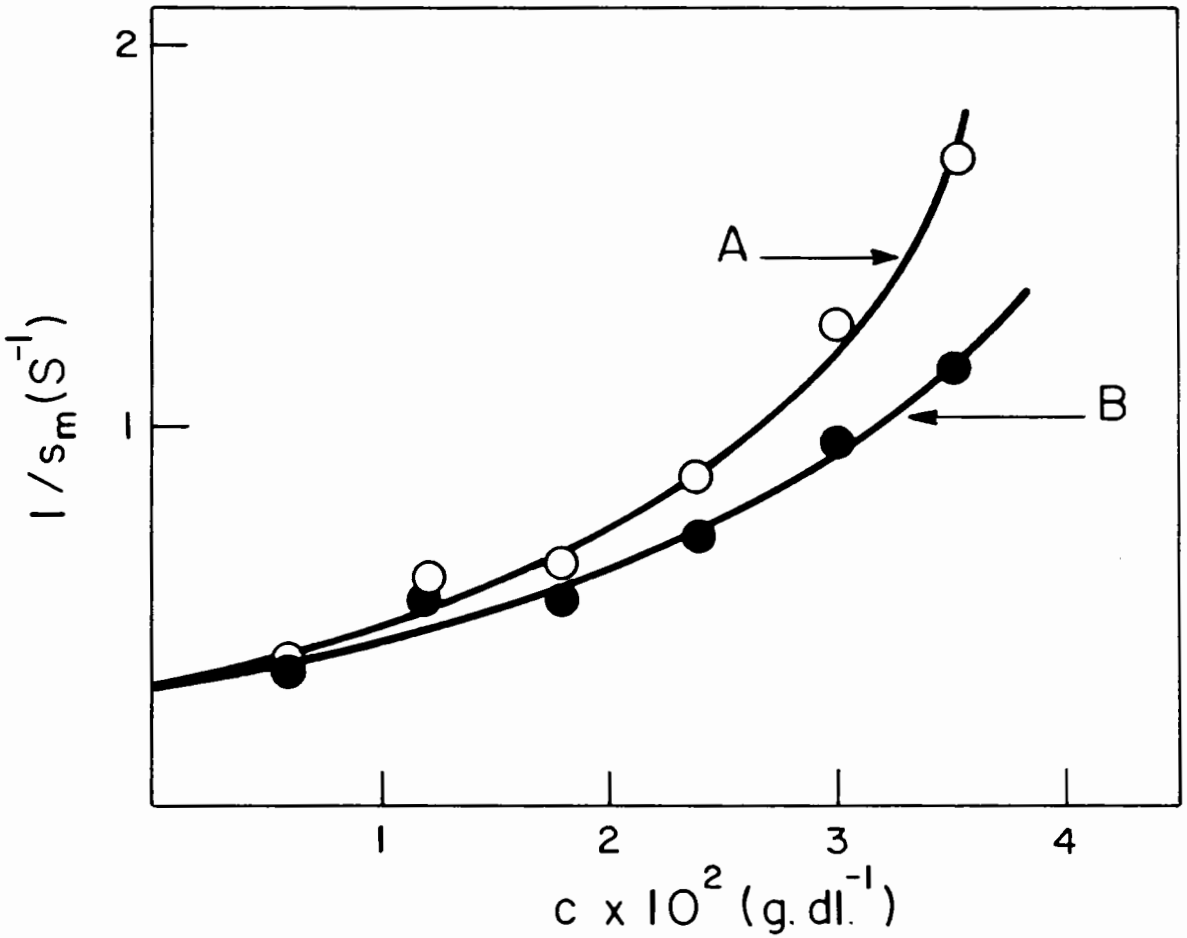
2
1
$1/s_m (S^{-1})$
A
B
1
2
3
4
$c \times 10^2 (g.dl.^{-1})$

the supporting electrolyte at zero concentration of CMC and a mean value of the monomer weight, m_o is taken, the coefficient of c in Eq. (6) becomes 0.08, 0.7 and 6.7 dl.g.$^{-1}$ for 0.1, 0.01 and 0.001 M respectively. These quantities when subtracted from k_s computed from $1/s_m$ vs. c graphs give a coefficient (k_s^c), corrected for the primary charge effect. Comparison with k_s values in Table I reveals that the correction is negligible for 0.1 M and 0.01 M and small for 0.001 M except for the low molecular weight fractions.

From the above it is clear that for sedimentation of CMC at 10^{-3} M and higher ionic strengths, the differences in the concentration dependence of sedimentation are due mainly to differences in the size and configuration of the molecule. Recently Pedersen (11) in his studies on bovine serum albumin found that the concentration dependence observed was larger than predicted by Eq. (1). The anomaly, according to Pedersen, was partly due to the expansion of the molecule. Termaine and Lauffer (10) also observed that the Tiselius equation underestimates the concentration dependence in the case of southern bean mosaic virus. Schachman (22) has noted a difference in sign of the coefficient of c^2 in Eq. (4) for polystyrene latex particles and deoxyribonucleic acid, presumably due to the changes in the shape of the particles.

In the manner of Wales and Van Holde (13) $k_s/[\eta]$ values were obtained at 0.1, 0.01 and 0.001 M and are shown in Table I; k_s corrected for charge effects, k_s^c was used at 0.001 M. In spite of the wide range of k_s values (0.79 to 54.8 dl.g.$^{-1}$), $k_s/[\eta]$ was relatively constant. This supports the findings of Wales and Van Holde for a series of vinyl polymers for which k_s varied from 0.23 - 8.29 dl.g.$^{-1}$, while $k_s/[\eta]$ was 1.6 ($\pm$ 0.26).

The slight increasing trend of k_s with decrease of molecular weight and ionic strength was not regarded as significant because of lack of precision in the data. The average values of $k_s/[\eta]$ at 0.1 M and 0.001 M were respectively 1.14 $\pm$ 0.27 and 1.23 $\pm$ 0.41 which were somewhat lower than the theoretical value of 1.66 deduced from Eq. (3). Evidently the greater free-draining property of the CMC molecule causes a lower dependence of the sedimentation coefficient on concentration. It is significant that the value of 3.4×10^6 for $(\phi^{1/3}P^{-1})$ obtained in an earlier section (19), when used in Eq. (3) results in $k_s/[\eta]$ value of 0.7. This lends some theoretical support for the lower average value of $k_s/[\eta]$ found in the present work on CMC.

REFERENCES

1. M.V. Smoluchowski, Gratz Handbuch der Elektrizitat und des Magnetismus (Leipzig, 1921, 2, 385.
2. A. Tiselius, Kolloid-Z, 59, 306 (1932).
3. F. Booth, J. Chem. Phys. 22, 1956 (1954).
4. K.O. Pedersen, The Ultracentrifuge, Oxford University Press, 1940.
5. J. Kraut, J. Polym. Sci. 14, 222 (1954).
6. G.J. Howard and D.O. Jordan, J. Polym. Sci. 12, 209 (1954).
7. B. Rosen, P. Kamath and F. Eirich, Discussions Faraday Soc. 11, 135 (1951).
8. P.A. Charlwood and A. Ens, Can. J. Chem. 35, 99 (1957).
9. M.A. Lauffer, J. Am. Chem. Soc. 66, 1195 (1944).
10. J.H. Termaine and Max A. Lauffer, J. Phys. Chem. 64, 568 (1960).
11. K.O. Pedersen, J. Phys. Chem. 62, 1282 (1958).
12. S. Newman and F. Eirich, J. Colloid Sci. 5, 541 (1950).
13. M. Wales and K.E. Van Holde, J. Polym. Sci. 14, 81 (1954).
14. L. Mandelkern, W.R. Krigbaum, H.A. Scheraga and P.J. Flory, J. Chem. Phys. 20, 1392 (1952).
15. P.J. Flory and T.G. Fox, J. Polym. Sci. 5, 745 (1950).
16. J.M. Burgers, Proc. Acad. Sci. Amsterdam, 45, 9 (1942).
17. S. Singer, J. Chem. Phys. 13, 341 (1947).
18. S. Newman, L. Loeb and C.M. Conrad, J. Polym. Sci. 10, 463 (1953).
19. Part I of this thesis.
20. R. St.J. Manley, Ark. Kemi 9, 519 (1956).
21. R. Longsworth and J.J. Hermans, J. Polym. Sci. 26, 47 (1957).
22. H.K. Schachman, Ultracentrifugation in Biochemistry, Academic Press, New York 91-102, 1959.

CONCLUDING REMARKS

The main conclusion to be drawn from the present work is that the coil to rod configurational transition which has been shown to occur from low to high molecular weight for the trinitrate also occurs from high to low ionic strength for carboxymethyl cellulose. This is supported by changes in the exponents and in the hydrodynamic parameters, as well as by the polyelectrolyte expansion determined viscometrically.

It is interesting to note that the hydrodynamic theories of Kirkwood and Riseman, and Debye and Bueche seem to interpret best the experimentally determined values of $[\eta]$, s_o and D_o when the molecule is in its most extended form i.e. at low molecular weight or low ionic strength. These theories, proposed to explain the hydrodynamic behavior of a randomly coiled macromolecule, fit the data well for an extended rod-like particle. Clearly some important hydrodynamic factor has been omitted and it is suggested that molecular deformation and internal circulation within the polymer coil are to be considered in this respect.

The concentration dependence of the reduced viscosity and the sedimentation coefficient are each influenced both by the electrostatic effect of the charge carried by the macromolecule and by the configurational changes of the chain. However, in the case of viscosity, the electrostatic effect appears to predominate while the concentration dependence of sedimentation is governed mostly by the configurational changes in the molecule at least for ionic strengths between 0.1 M and 0.001 M.

Finally, the investigation has added evidence for the existence of a persistent, wide-spread anomaly in the light scattering technique as applied to naturally occurring macromolecules. The anomaly was not clearly resolved, but the indications are that the present methods of preparing solutions for light scattering are not yet adequate to guarrantee the reliability of the molecular weights.

CLAIMS TO ORIGINAL RESEARCH

1. Carboxymethyl cellulose was fractionated and molecular weights of the fractions were obtained from sedimentation and diffusion, sedimentation and viscosity, and light scattering.

2. The counterion binding of carboxymethyl cellulose was measured viscometrically.

3. The exponents in the logarithmic relation between the intrinsic viscosity, sedimentation and diffusion constant vs. the molecular weight were determined at different ionic strengths and interpreted in terms of configurational changes in the molecule.

4. For a series of fractions, the hydrodynamic theories of Kirkwood and Riseman, and Debye and Bueche were interpreted in terms of Marrinan and Hermans approximations. Two plausible reasons for the failure of the theories were suggested.

5. A theoretical relationship was derived for surface charge density from the concentration dependence of the reduced viscosity and values of Huggins coefficient were explained on the basis of this relationship.

6. The concentration dependence of sedimentation of carboxymethyl cellulose was interpreted by the theories of Tiselius and of Wales and Van Holde.

7. A diffusion technique was developed to determine diffusion constants by working at a single concentration.

8. The increment of refractive index, dn/dc was measured on a series of fractions of carboxymethyl cellulose.

9. The partial specific volume of carboxymethyl cellulose was determined.

SUGGESTIONS FOR FURTHER WORK

1. The present light scattering investigations on sodium carboxymethyl cellulose as well as previous work on cellulose trinitrate and the xylans show that the occurrence of aggregation in these solutions is the major drawback to the use of the method. A detailed and sustained investigation on resolving this difficulty is needed. Unless this problem is solved, the application of the light scattering technique to these and similar systems should not be considered uniquely reliable but should be supported by some independent method of molecular weight determination.

2. It has been pointed out that the discrepancy in the monomer frictional constant calculated on the basis of the Kirkwood-Riseman and Debye-Bueche theories may be due to the neglect of the effect of deformation of the molecules in the shear field as well as internal circulation within the molecular domain. A theoretical investigation to modify the existing hydrodynamic theories to correct for these two factors is therefore recommended.

3. The relationship for surface charge density derived on the basis of the equilibrium between the compressive force and the electrostatic repulsive force may be further tested by extending the viscometric investigation to other model systems of charge bearing particles.

4. The results of counterion binding obtained viscometrically may be checked by conductance, electrophoresis and membrane transport

measurements to obtain more information about the change of counterion binding with chain length and ionic strength.

5. The Archibald sedimentation and osmotic pressure measurements may be applied to the low molecular fractions of carboxymethyl cellulose to obtain the molecular weights as well as to lead to a better understanding of the polydispersity in these samples.

6. A continuation of the present work on a fully substituted carboxymethyl cellulose should yield interesting results. The problem of aggregation would probably not arise because of the greater degree of hydrophilic character in the chain. Here the preliminary research would be concerned with achieving as high a D.S. as possible without excessive degradation of the molecule.

A P P E N D I C E S

These appendices supplement the experimental details given in Part I.

APPENDIX I

PURIFICATION AND FRACTIONATION

PURIFICATION AND FRACTIONATION

Carboxymethyl cellulose 7MP was used in the preliminary experiments.

Neutralization Equivalent

The pH of the neutralization of CMC was determined as follows. 100 mg. of 7MP sample dissolved in 100 ml. of water was passed through Amberlite MB1 and 50 ml. of the acid was titrated potentiometrically with 0.03835 N sodium hydroxide. The alkali was standardized with potassium hydrogen phthlate In Fig. 1, the pH of the CMC solution is plotted against the volume of alkali added. The pH of neutralization was 8.25 taken from inflection point of the curve. This pH of 8.25 was used as the neutralization point in all further work. From the volume of alkali added the neutralization equivalent i.e. the number of equivalents per gm. of the polymer was calculated as shown in the sample calculation.

Sample Calculation of Neutralization Equivalent and D.S. for H2

52mg. of H2 was dissolved in water and passed through Amberlite MB1 twice. The pH after ion-exchange was 3.54. This solution of the acid form of H2 required 5.55 ml. of 0.01341 N sodium hydroxide solution to neutralize to pH 8.25. The neutralized solution after evaporation contained 25.52 mgms. of H2.

$$\text{Equivalent weight of H2} = \frac{0.02552 \times 1000}{5.55 \times .01341} = \underline{342.9}$$

Fig. 1

Potentiometric titration of CMC 7MP

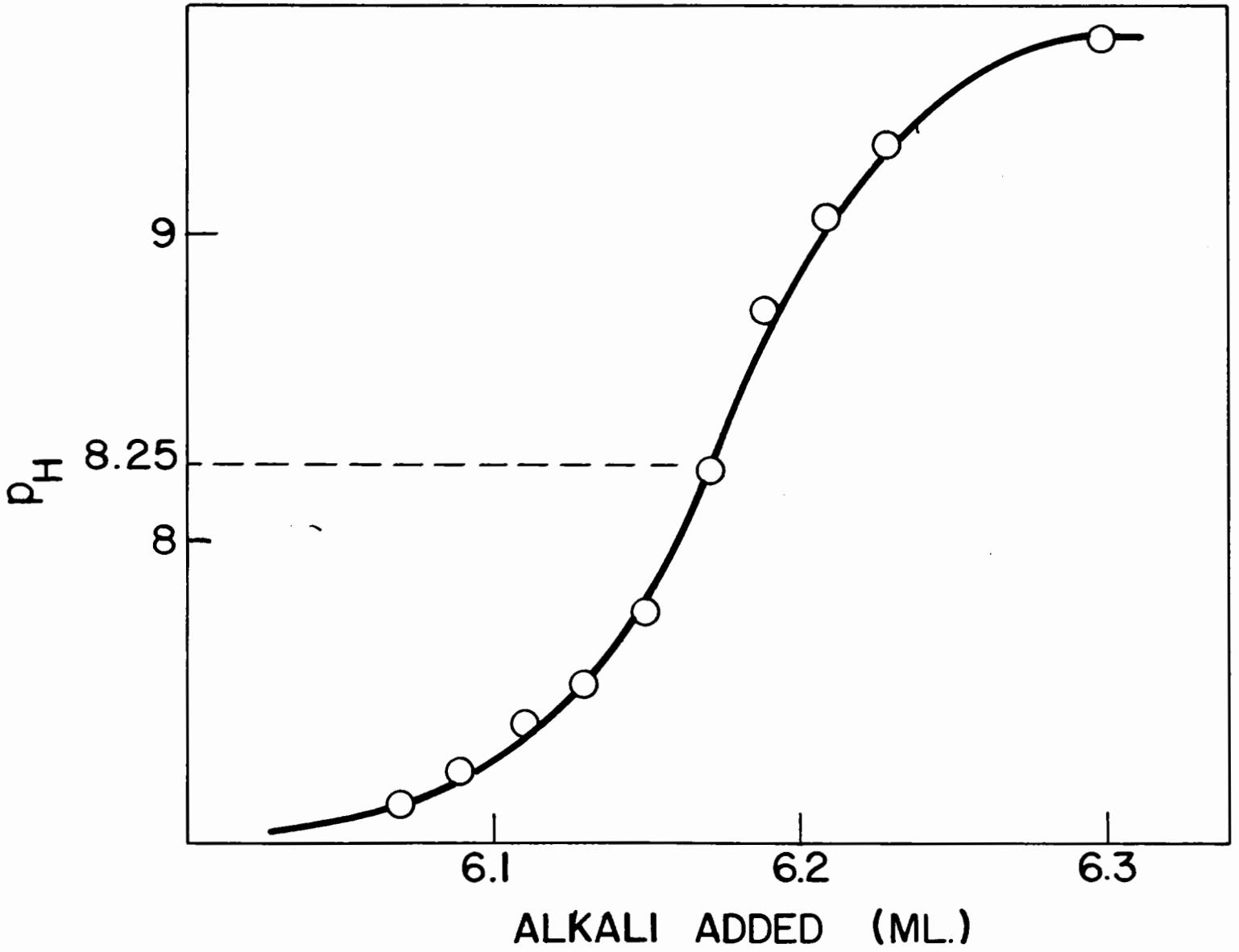
9
8.25
8
P_H
6.1
6.2
6.3
ALKALI ADDED (ML.)

$$\text{Neutralization equivalent} = \frac{1}{342.9} = 2.92 \times 10^{-3} \text{ eq.g.}^{-1}$$

$$\text{Equivalent weight} = \frac{162 + 80 \text{ D.S.}}{\text{D.S.}}$$

$$342.9 = \frac{162 + 80 \text{ D.S.}}{\text{D.S.}}$$

Degree of substitution (D.S.) of H2

$$= \underline{\underline{0.62}}$$

Purification

Initially a sample of CMC 7MP was purified by being passed as a dilute solution over an anionic resin (Dowex 1 x 10), then a cationic resin (Dowex 50 - x 12) and finally over a mixed bed resin (Amberlite MB1). The acid form of the polyelectrolyte was then neutralized and freezedried.

Samples 7HP and 7LP were tested for their purity by conductivity experiments with the purified 7MP sample as a standard. The specific conductances of 7HP and 7LP were 1.03×10^{-4} ohms^{-1} cm.$^{-1}$ and 1.21×10^{-4} ohms^{-1} cm.$^{-1}$ compared with 1.02×10^{-4} ohms^{-1} cm.$^{-1}$ for 7MP which showed the absence of small ion impurities in them. Hence samples 7HP and 7LP were used for fractionation without further purification.

In the fractionation experiments, 10 gms. of CMC was dissolved in 1000 ml. of 50% ethanol/water mixture, containing 0.05% of sodium chloride. The fractions were precipitated by dropwise addition of ethanol, as described in part I. The last fraction in each sample was recovered by evaporation of

the solvent. The fractions were purified by dialysis and were then freeze-dried. Due to the gelatinous nature of the precipitates the loss in fractionation was high. Details of the fractionation as well as the reduced viscosities of the fractions are recorded in Table I. Fractionation was duplicated and the fractions obtained were blended on the basis of their reduced viscosity into 8 representative fractions as shown in Table II. Blending was carried out by co-solution and freezedrying. The blended fractions were used in the present study.

TABLE I

Fractionation Data for CMC 7HP, 7MP and 7LP

Fraction No.	CMC 7HP			CMC 7MP			CMC 7LP		
	Volume of ethanol added (ml.)	Weight of fraction (g.)	$\eta_{sp/c}$ (dl.g.$^{-1}$)	Volume of ethanol added (ml.)	Weight of fraction (g.)	$\eta_{sp/c}$ (dl.g.$^{-1}$)	Volume of ethanol added (ml.)	Weight of fraction (g.)	$\eta_{sp/c}$ (dl.g.$^{-1}$)
1	150	5.72	24.52	195	1.10	8.58	220	2.36	5.94
2	70	0.56	16.80	65	0.60	7.98	70	0.43	3.17
3	65	0.97	8.75	70	1.41	7.93	80	1.42	2.94
4	Excess recovered	1.65	6.57	75	3.9	7.70	Excess recovered	4.54	2.18
5	-	-	-	Excess recovered	2.42	5.52	-	-	-
Loss	-	1.10	-	-	0.57	-	-	1.25	-

TABLE II

Blending of CMC Fractions

Fraction No.	7HP			7MP			7LP		
	Weight of fraction (g.)	$\eta_{sp/c}$ (dl.g.$^{-1}$)	Blended fraction	Weight of fraction (g.)	$\eta_{sp/c}$ (dl.g.$^{-1}$)	Blended fraction	Weight of fraction (g.)	$\eta_{sp/c}$ (dl.g.$^{-1}$)	Blended fraction
1	5.90	24.43	H1	1.10	8.58		2.36	5.94	L1
	5.72	24.52		2.20	8.45	M1	2.25	4.59	-
2	0.46	16.83	H2	0.60	7.98		0.43	3.17	-
	0.56	16.80		2.85	8.27		0.71	2.85	-
3	1.43	9.6	H3	1.41	7.93	-	1.42	2.94	L2
	0.97	8.75	-	3.24	6.77	M2	1.24	2.17	-
4	1.62	7.09	-	3.90	7.70	-	4.54	2.18	L3
	1.65	6.57	-	1.69	4.91	-	1.32	1.45	
5	-	-	-	2.42	5.52	-	-	-	-
				0.56	1.80	-	-	-	-

The fractionation was done twice in the case of each sample

APPENDIX II

VISCOMETRY

VISCOMETRY

A suspended level Ubbelohde viscometer of the Schurz-Immergut (1) type was used and is shown in Fig. 1. For clarity the horizontal scale of the diagram has been increased. The dimensions of its different parts are shown in Table I. This viscometer had four bulbs whose dimensions were so chosen as to allow interpolation of viscosity values to a shear rate of 500 sec.$^{-1}$. Also a large reservoir permitted dilution *in situ*. Details of this viscometer were described by Huque (2).

The intrinsic viscosity of the CMC solutions were computed as follows. From the efflux times of the solvent and the solution, Ostwald's formula gives

$$\rho_s t_s / \rho_o t_o = \eta_s / \eta_o = \eta_{rel} \qquad \ldots(1)$$

where ρ_s, ρ_o are the densities and η_s and η_o the viscosities of two liquids having flow times t_s, t_o respectively.

$\frac{\eta_{rel} - 1}{c} = \eta_{sp/c}$ is the reduced viscosity of the polymer. By measuring the reduced viscosity at different shear rates by means of the four bulbs in the viscometer, the reduced viscosity at the shear rate (G) of 500 sec.$^{-1}$ was computed for different concentrations from the graphs of log $\frac{\eta_{sp}}{c}$ vs. log G, as shown in Fig. 2 for M2 at 0.001 M.

The intrinsic viscosity, $[\eta]$ was calculated from

$$[\eta] = \left(\frac{\eta_{sp}}{c}\right)_{c=o} \qquad \ldots(2)$$

Fig. 1

Multi-shear viscometer

(from the Ph.D. Thesis of M.M. Huque

McGill University, 1957)

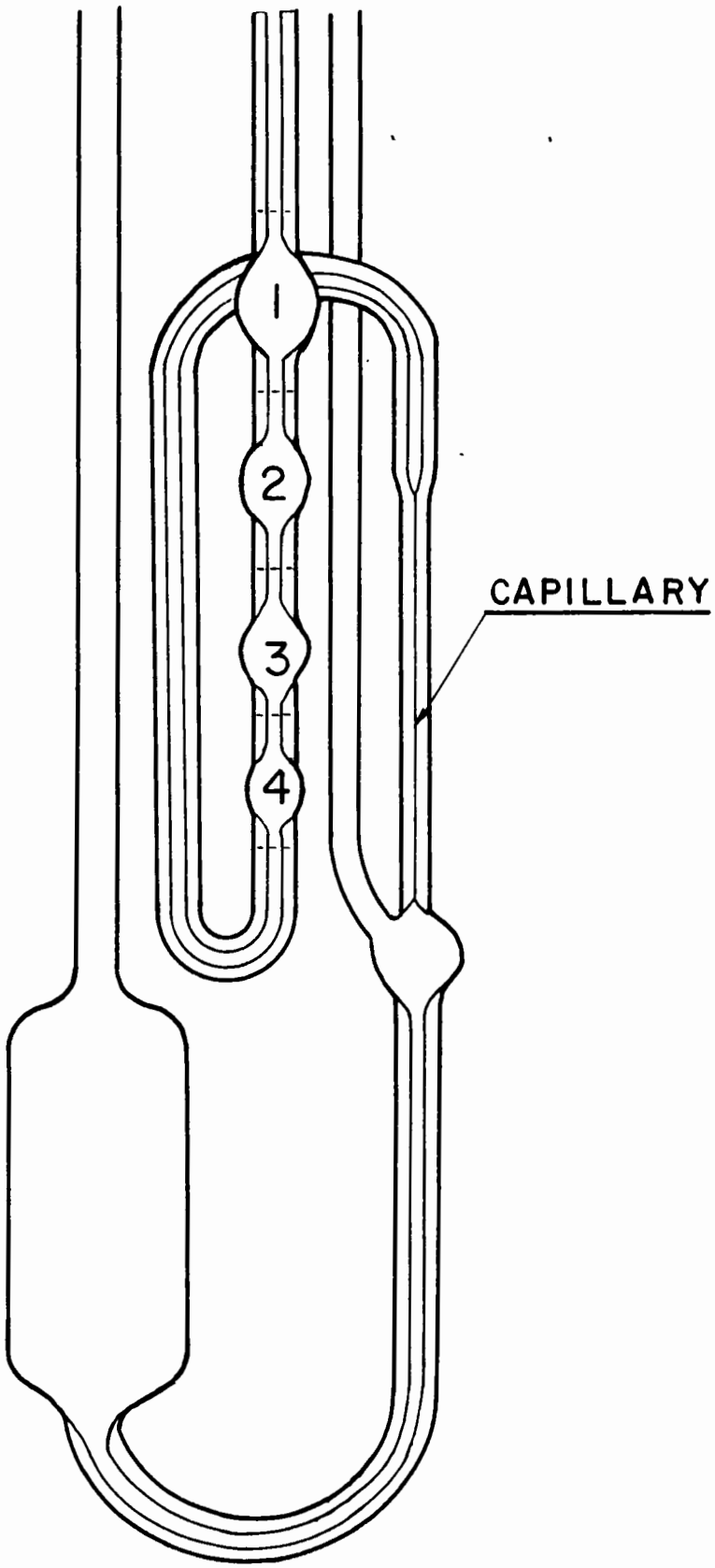
1
2
3
4
CAPILLARY

TABLE I

Data for Multi-Shear Viscometer

Bulb No.	Volume ($cm.^3$)	Mean hydrostatic head, h_m (cm.)	Efflux time of water at 25°C (sec.)
1	2.74	17.0	165.1
2	1.98	12.0	171.0
3	1.75	7.1	254.8
4	0.83	3.1	280.5

Fig. 2

Log $\eta_{sp}/_c$ vs. log G for M2 at 0.001 M at concentrations

$c_1 = 0.0340$ g.dl.$^{-1}$

$c_2 = 0.0204$ g.dl.$^{-1}$

$c_3 = 0.0128$ g.dl.$^{-1}$

$c_4 = 0.0093$ g.dl.$^{-1}$

$c_5 = 0.0060$ g.dl.$^{-1}$

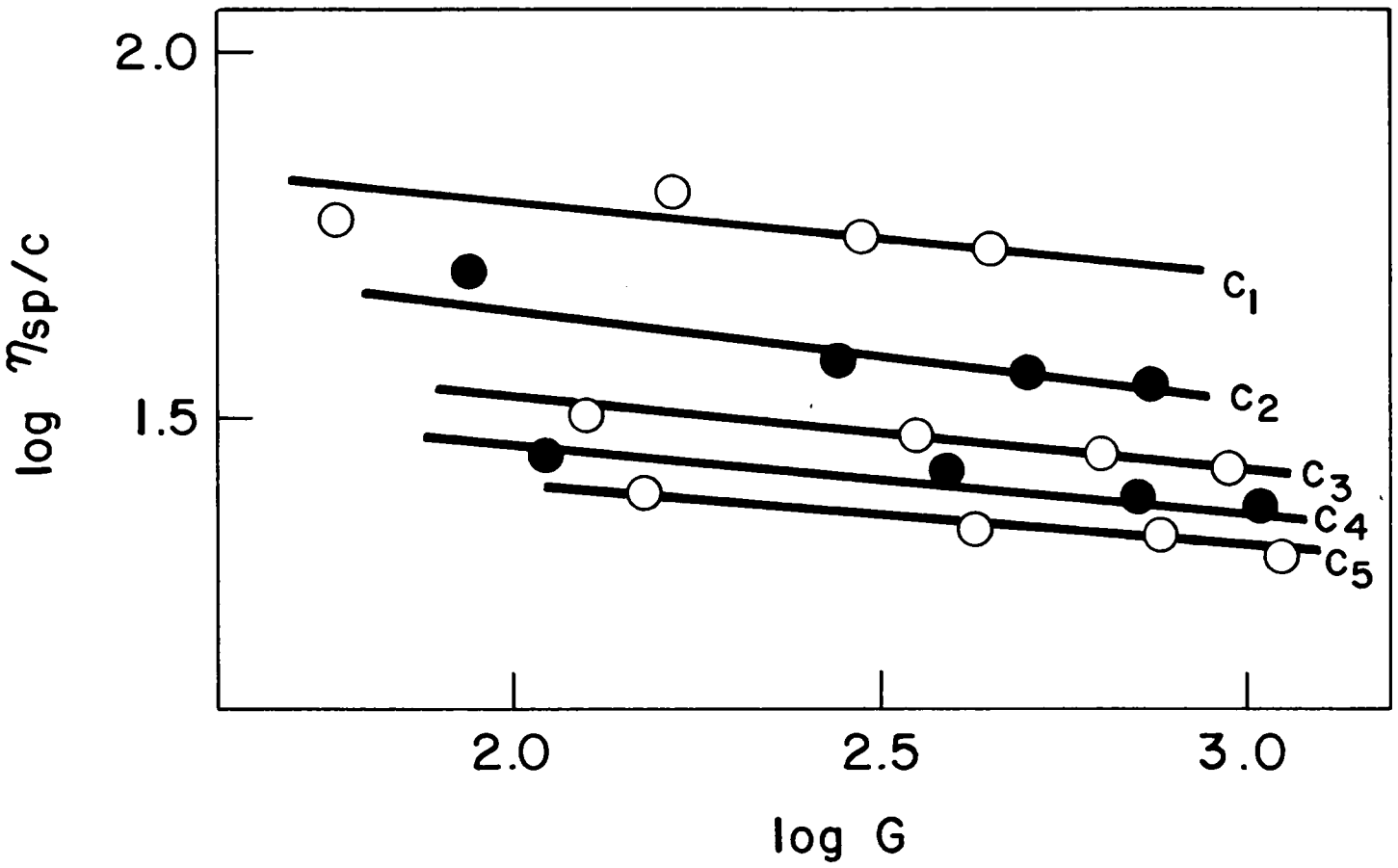
2.0
1.5
log η_{sp}/c
c_1
c_2
c_3
c_4
c_5
2.0
2.5
3.0
log G

Polyelectrolyte Expansion

At low ionic strengths, the reduced viscosity increased with dilution in the case of CMC. The reduced viscosity vs. concentration graphs in aqueous sodium chloride of different ionic strengths as well as in deionized water are shown in Fig. 3. This behavior is typical of polyelectrolytes and similar curves were reported earlier by Fujita and Homma (3) for CMC.

The reduced viscosity in 0.1 M NaCl was found to decrease with increase in temperature, the temperature coefficient being 0.6 dl.g.$^{-1}$ per ^{o}C.

Capillary Adsorption

Ohrn (4) proposed that an adsorbed layer of the polymer in the capillary of the viscometer was responsible for the upward curvature of $\eta_{sp/c}$ vs. c graphs at low concentrations. To assess the magnitude of capillary adsorption, if any, of CMC the viscometer was washed with water 2 to 3 times after measuring the flow times of CMC solutions. However, the difference in efflux times of the solvent before and after the experiment was always within experimental error ($\pm$ 0.1 sec.). In the case of cellulose trinitrate, Huque *et al* (5) observed differences of 0.6 sec. which confirmed that the upward curvature observed by these authors was due to capillary adsorption. Further study of this effect in the viscometry of solutions of cellulose derivatives is required. The viscosity increase with dilution observed in the case of CMC could not therefore be explained as due to capillary adsorption but must have arisen from the expansion of the polyelectrolyte due to a change in the ionic strength of the solution.

Fig. 3

Plot of $\eta_{sp/c}$ vs. conc. for M1 in deionized water and aqueous sodium chloride from 10^{-1} M to 10^{-5} M

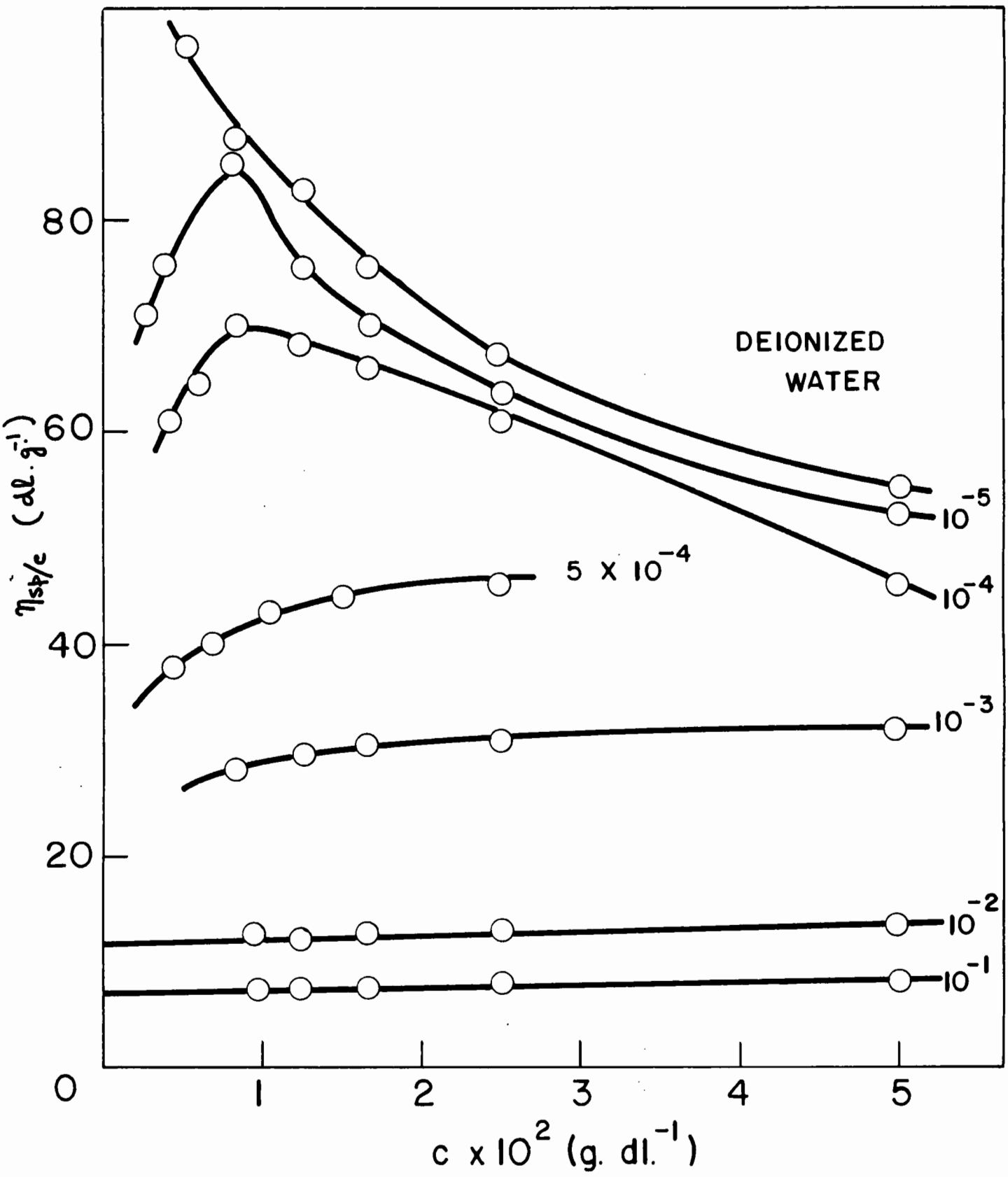
80
60
40
20
0
1
2
3
4
5
η_{sp}/c (dl. g^{-1})
c x 10^2 (g. dl.$^{-1}$)
DEIONIZED
WATER
10^{-5}
10^{-4}
5 x 10^{-4}
10^{-3}
10^{-2}
10^{-1}

Shear Dependence

Shear dependence of viscosity was estimated in the shear rate range of 250 — 1000 sec.$^{-1}$. The intrinsic viscosity, $[\eta]$ was found to be dependent on the shear rate, G particularly at high molecular weights. A typical plot of $\eta_{sp/c}$ vs. c is shown in Fig. 4, for M1 at 10^{-3} M. The intrinsic viscosity is seen to increase with a decrease of the rate of shear. The magnitude of shear dependence increased with the increase of molecular weight, as shown in Fig. 5 and $[\eta]$ varies linearly with G. Further the shear dependence of viscosity increased with the decrease of ionic strength as shown in Fig. 6. Thus it would appear that increased shear effects occur with an increase of chain length and a decrease in ionic strength. In the present study even though the maximum shear effects observed between 500 sec.$^{-1}$ and zero shear were up to 20% at low ionic strengths and high molecular weights, in general the shear effects were less than 5%. Pals and Hermans (6) reported similar shear effects of up to 15% for CMC.

REFERENCES

1. J. Schurz and E.H. Immergut, J. Polym. Sci. 9, 281 (1952).
2. M.M. Huque, D.A.I. Goring and S.G. Mason, Can. J. Chem. 36, 952 (1958).
3. H. Fujita and T. Homma, J. Plym. Sci. 15, 277 (1955).
4. O.E. Ohrn, J. Polym. Sci. 17, 137 (1955).
5. M.M. Huque, M. Fishman and D.A.I. Goring, J. Phys. Chem. 63, 766 (1959).
6. D.T.F. Pals and J.J. Hermans, Rec. trav. Chim. 71, 433 (1952).

Fig. 4

$\eta_{sp/c}$ vs. conc. at different rates of shear for M1 at 10^{-2} M

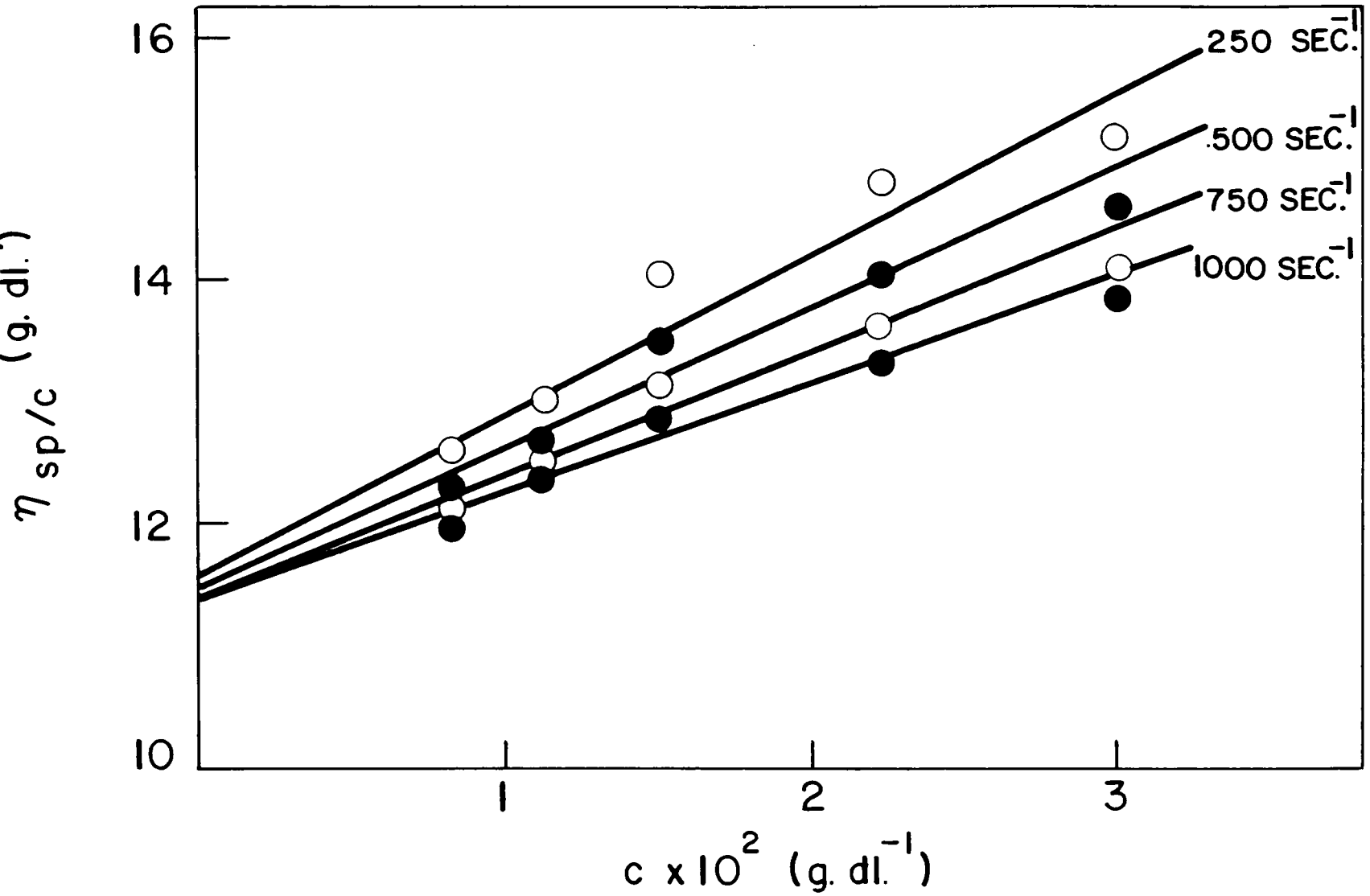
16
14
12
10
1
2
3
250 SEC.-1
500 SEC.-1
750 SEC.-1
1000 SEC.-1
η sp/c (g. dl.-1)
c x 10^2 (g. dl.-1)

Fig. 5

Intrinsic viscosity vs. rate of shear for fractions L3, M1, H3 and H1 at 10^{-3} M NaCl

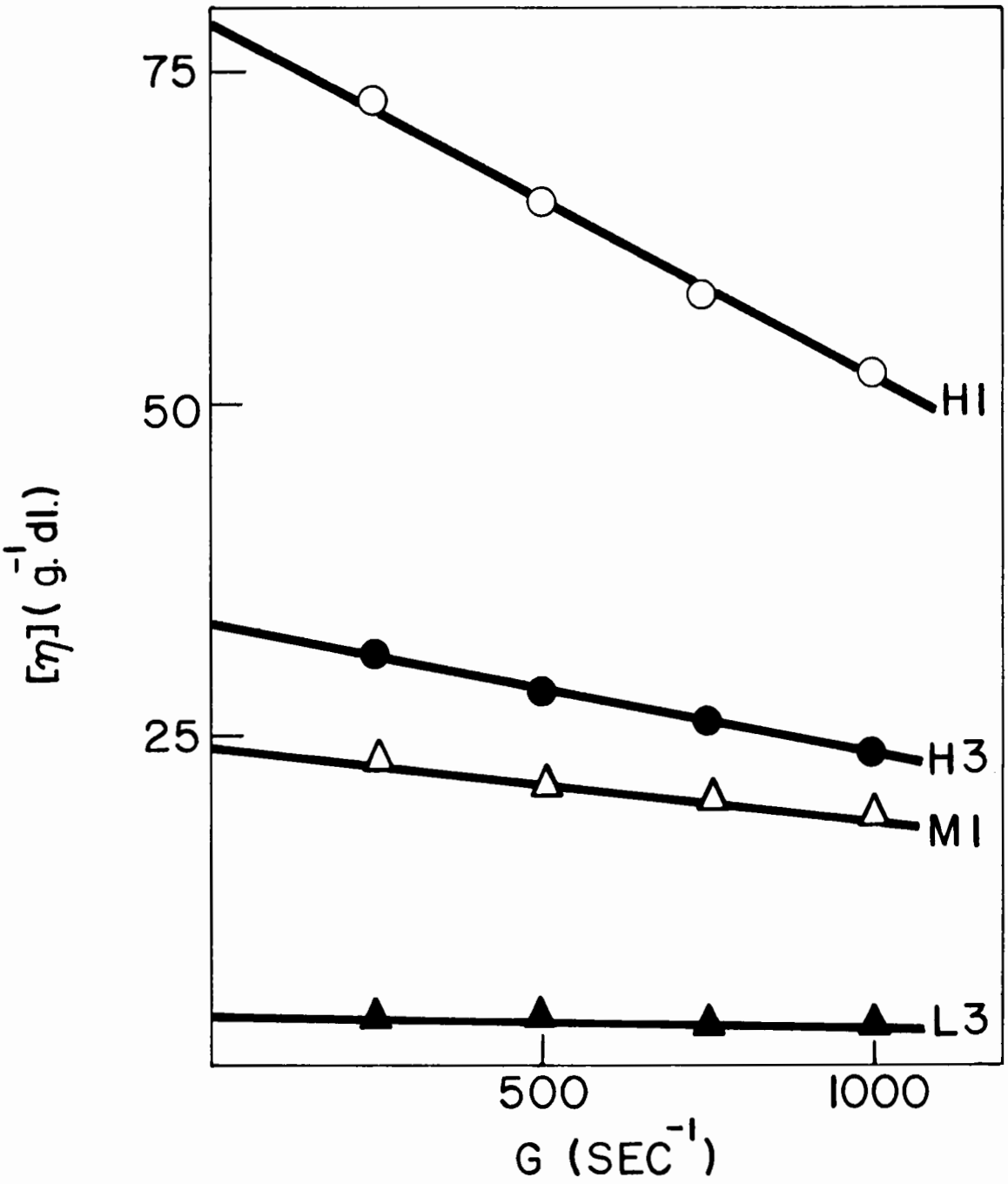
75
50
25
[η] (g⁻¹·dl)
H1
H3
M1
L3
500
1000
G (SEC⁻¹)

Fig. 6

Intrinsic viscosity vs. shear rate for M1 at

10^{-1} M, 10^{-2} M and 10^{-3} M NaCl

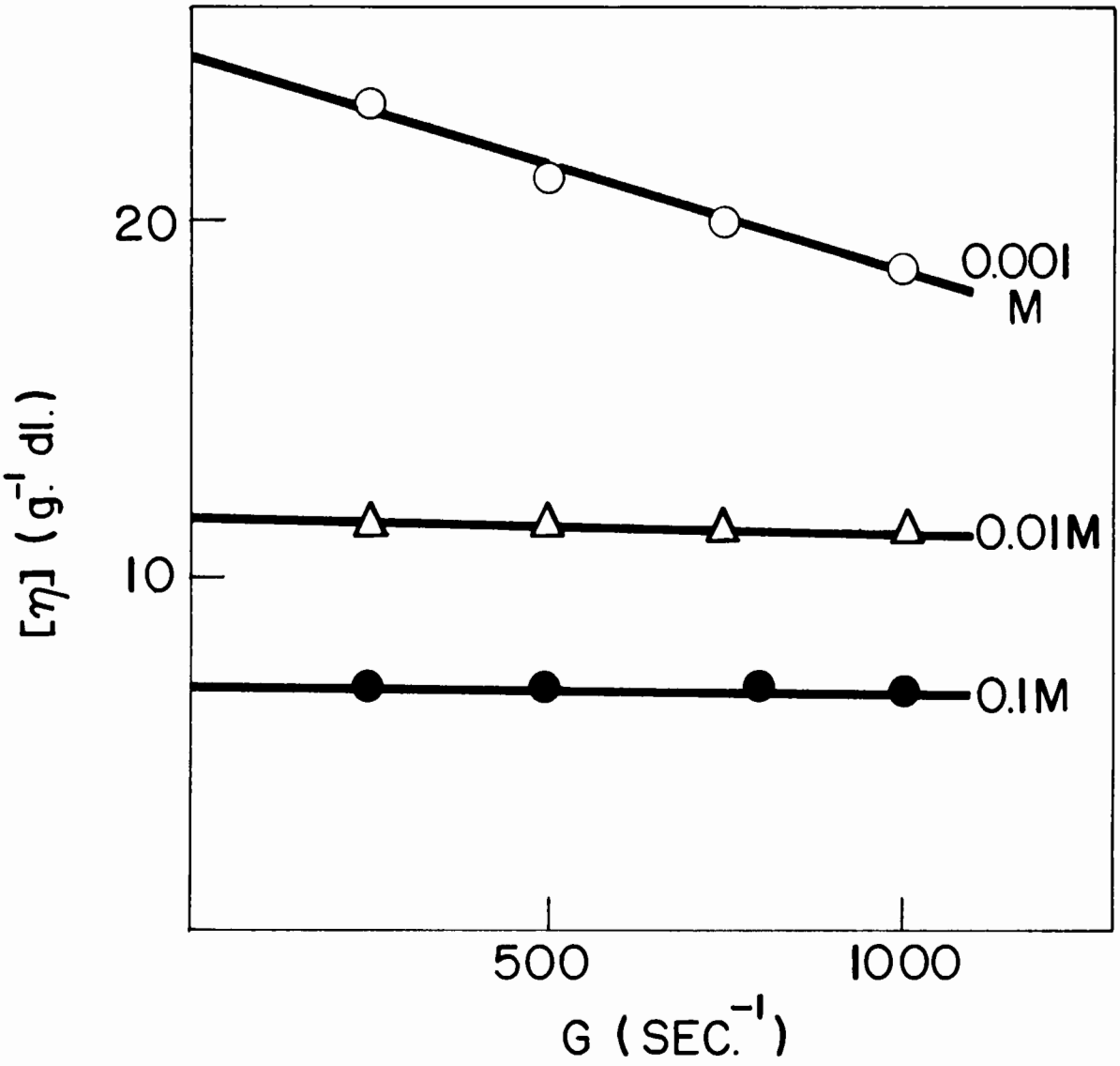
20
10
[η] (g.⁻¹ dl.)
0.001 M
0.01M
0.1M
500
1000
G (SEC.⁻¹)

APPENDIX III

LIGHT SCATTERING

LIGHT SCATTERING

Calibration of the Apparatus

The Brice Phoenix photometer was calibrated with Du Pont Ludox suspensions made up from a 30% stock suspension. The stock was centrifuged at 2000 r.p.m. for half an hour to sediment down larger aggregates. The supernatant liquid was decanted for the preparation of dilute suspensions of Ludox.

The calibration procedure was practically the same as described by Goring et al (1). The solvent used was 0.05 M NaCl which was clarified by filtration through Millipore* filter of 10 m μ stated pore size. The spectrophotometric turbidity, τ was measured with a Beckman DU spectrophotometer using 10 cm. cells at 5461 Å, in the concentration range of 0.5 to 6%. The value of $(c/\tau)_{c=o}$ was obtained by extrapolation of c/τ vs. c plot to zero concentration (Fig. 1).

Light scattering measurements were then made on the Ludox solutions in the concentration range of 0.1 — 6%. The scattering intensity, I_θ, was calculated in the usual manner as the ratio of the filter-corrected galvanometer readings at θ and at $\theta = 0$ (1,2,3). From measurements at 90°, a plot of c/I_{90} was extrapolated to zero concentration and $(c/I_{90})_{c=o}$ was obtained (Fig. 1)

* supplied by Millipore Filter Corp., Bedford, Mass.

Fig. 1

c/τ (Beckman) and $c/_{I_{90}}$ (Light Scattering)

vs. conc. for Ludox suspensions

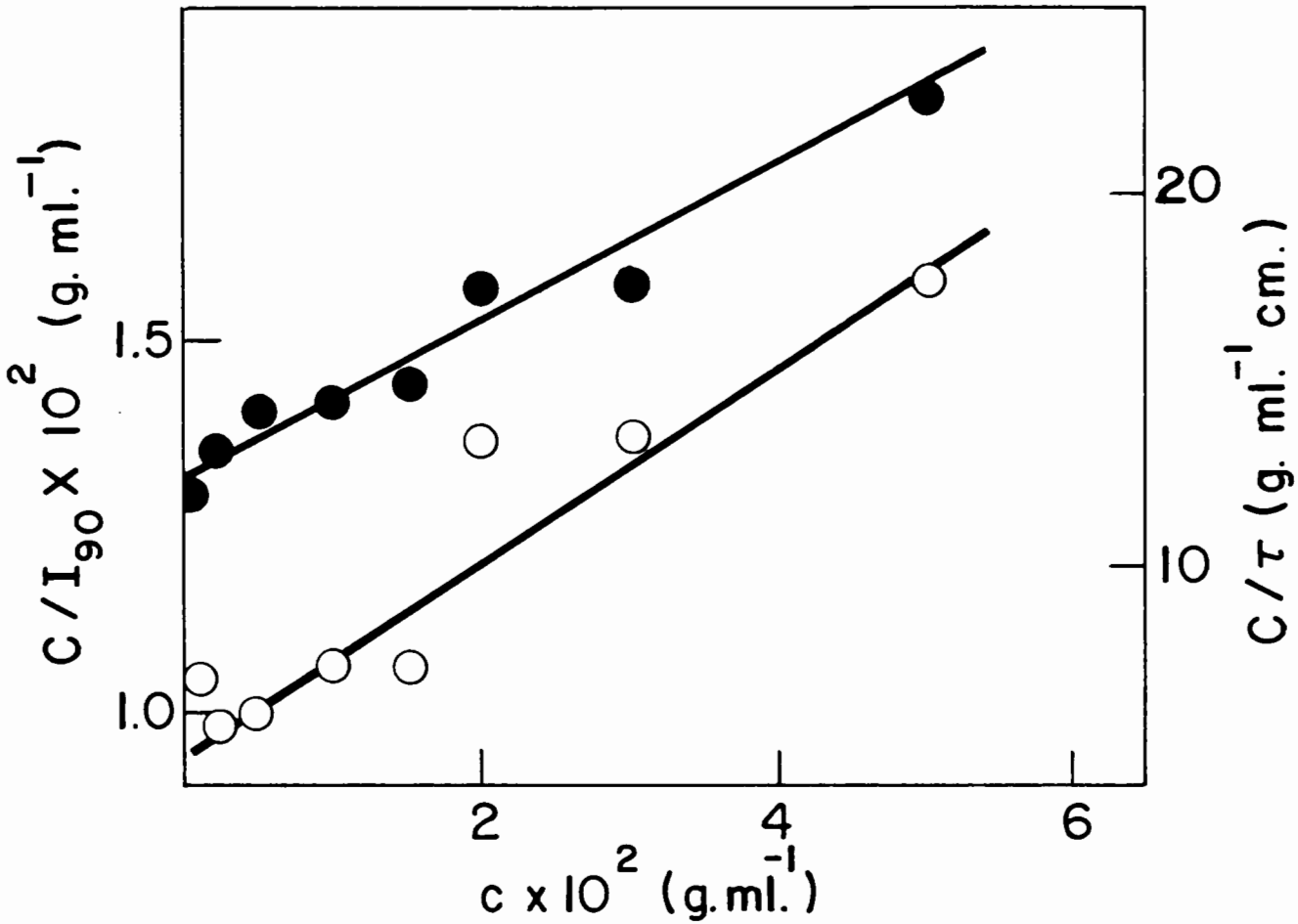
1.5
1.0
20
10
2
4
6
$c/I_{90} \times 10^2$ (g. ml.$^{-1}$)
c/τ (g. ml.$^{-1}$ cm.)
$c \times 10^2$ (g. ml.$^{-1}$)

The calibration constant, C was calculated from the relationship

$$(c/\tau)_{c=o} = C \cdot (c/I_{90})_{c=o} \qquad \ldots(1)$$

The value of C computed was 13.05 which agreed well with recent values (2,4) for the instrument.

Bath Liquid

As most of the light scattering measurements were made in 0.1 M NaCl, this solvent was initially used in the outer bath. The bath liquid clouded quickly perhaps due to the corroding action of the NaCl on the metal baffle, which holds the cell in position (5). Hence a 1.05% solution of ethylene glycol in water, which has the same refractive index as 0.1 M sodium chloride, was used in all subsequent experiments as the bath liquid.

Ultraclarification

Light scattering was done in the modified Dandliker and Kraut cells developed by Timell and Goring (6) (Fig. 2). The cells were floated in a carbon tetrachloride - ethanol mixture and centrifuged at speeds up to 25,000 r.p.m. in the swinging bucket rotor (SW 25-1) of a Spinco Model L ultracentrifuge.

All solvents were adequately clarified by filtration through 10 mμ. Millipore filter and ultracentrifugation in the light scattering cells.

Fig. 2

Light scattering cells according to

(A) Dandliker and Kraut

(B) Modified by Timell and Goring

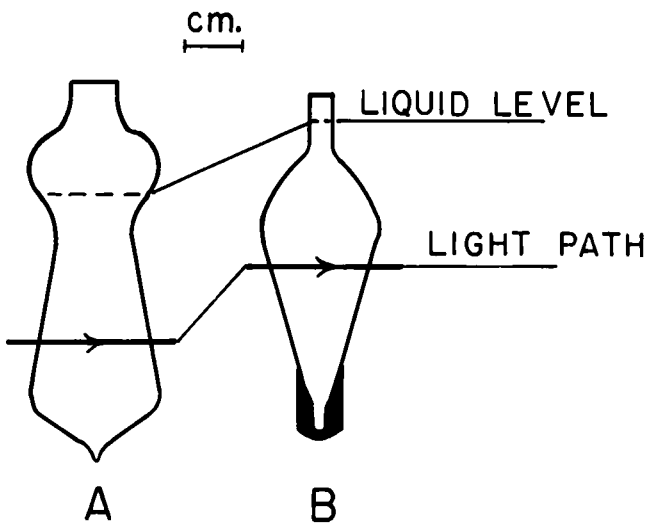
cm.
LIQUID LEVEL
LIGHT PATH
A
B

Ultraclarification of CMC solutions by high speed precentrifugation was necessary. The technique used has been described previously by Timell and Goring in a light scattering study of certain 4-O-methylglucuronoxylans (6). It consists of a 40,000 r.p.m. precentrifugation in the 40 rotor of a Spinco Model L ultracentrifuge prior to ultraclarification in the light scattering cells. Striations (7) were found in CMC solutions of 0.25 $g.dl.^{-1}$ concentration, precentrifuged for 2 hours at 40,000 r.p.m. and further for one more hour in the light scattering cells at 20,000 r.p.m. Striations were generally eliminated by a longer precentrifugation for 4 hours at 40,000 r.p.m. and further for one hour in the cells at 25,000 r.p.m.

As with the xylans (6) the effect of the time of precentrifugation on Kc/R_θ values was investigated. The Kc/R_θ values did not increase by large amounts after 2 hours, as seen in Fig. 3. Hence an arbitrary 4 hour precentrifugation time was fixed in all subsequent experiments.

The concentration loss on centrifugation was generally of the order of 5%. But losses up to 25% were observed with the high molecular weight fractions. It was shown (7) from sedimentation experiments that no fractionation occurred during centrifugation.

Molecular Weights

Molecular weights were computed for eight fractions, using both the Zimm plot and the dissymmetry method.

In the disymmetry method, molecular weights were obtained from the

Fig. 3

Kc/R_θ vs. time of precentrifugation at scattering angles of 40°, 80° and 130° for M1 in 0.1 M NaCl (conc. of M1 = 0.25 g.dl.$^{-1}$)

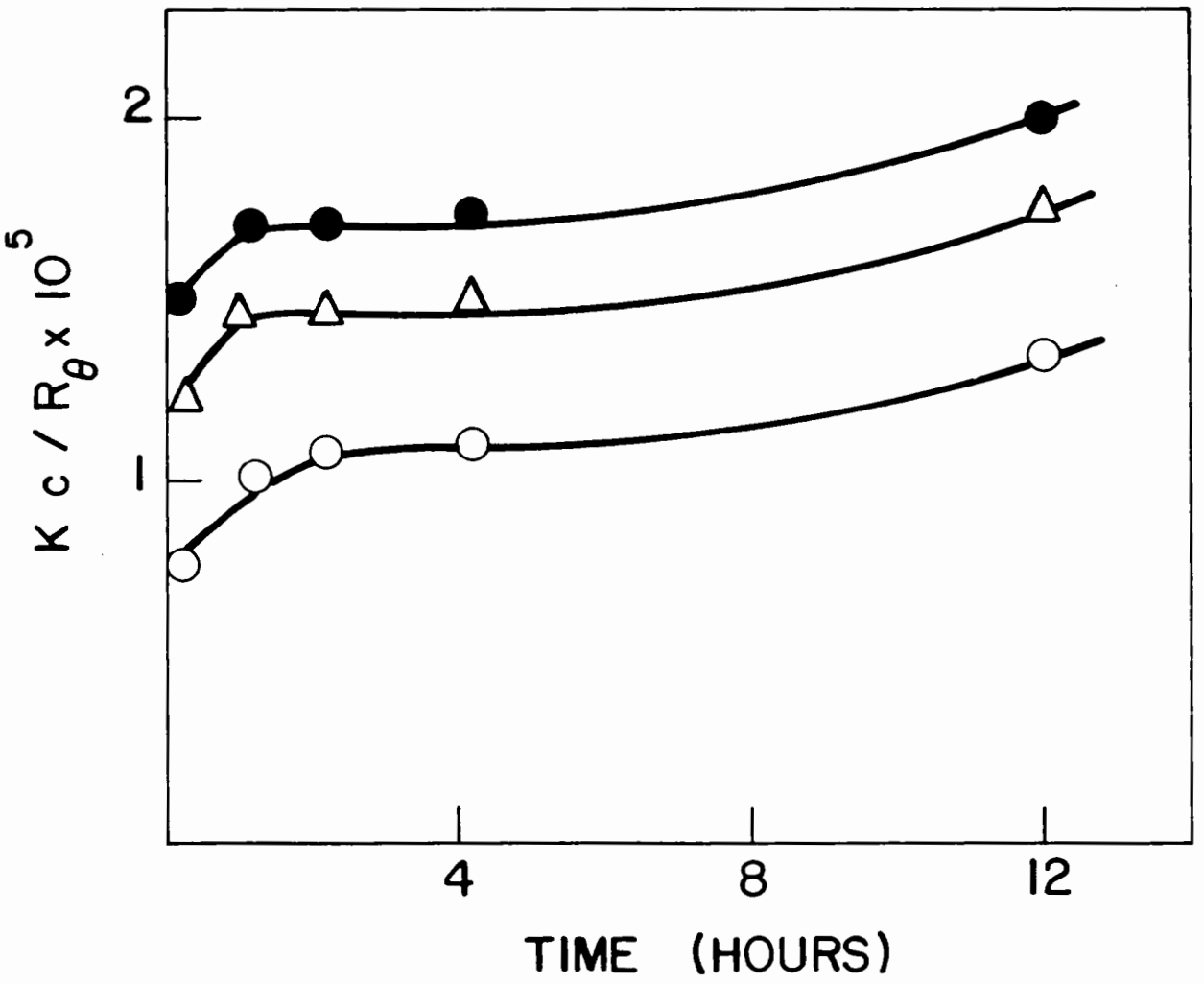
2
1
$Kc/R_\theta \times 10^5$
4
8
12
TIME (HOURS)

Debye's equation (8)

$$Hc/\tau = \frac{1}{M_w} + 2A_2c \qquad \ldots(2)$$

where $H = 32\pi^3 n^2 (dn/dc)^2/3 N\lambda^4$ and the symbols have the usual significance. The value of $(Hc/\tau)_{c=o}$ was derived from the linear extrapolation of the graph of Hc/τ vs. c as shown in Fig. 3. Similarly the intrinsic dissymmetry $(Z^*)_{c=o}$ was obtained by extrapolation of Z* vs. c (Fig. 4). The dissymmetry correction (9) was applied to $(Hc/\tau)_{c=o}$ Molecular weights were then calculated by substituting $(Hc/\tau)_{c=o}$ in Eq. (2).

Zimm plots an example of which is given in Part I were obtained for the fractions by plotting Kc/R_θ vs. $\sin^2\theta/2 + kc$ where $K = 2\pi^2 n^2(dn/dc)/N\lambda^4$ and the symbols have their usual significance. The molecular weight was obtained from the $(Kc/R_\theta)_{c,\ \theta=o}$. The z - average radius of gyration calculated, $\sqrt{\bar{S}_z^2}$, was obtained from the initial slope of the c=o line by means of the expression

$$\frac{\text{Initial slope}}{\text{Intercept}} = \left(\frac{16\pi^2}{3}\right) \cdot \bar{S}_z^2 \cdot (n/\lambda)^2 \qquad \ldots(3)$$

The second virial coefficient, A_2 was computed from the slope of the $(Kc/R_\theta)_{\theta=o}$ vs. c line in the Zimm plot. The values of $\sqrt{\bar{S}_z^2}$ and A_2 are given in Table I. However, in view of the uncertainities of the light scattering data as shown in Part I, further consideration was not given to these values.

As seen in Table I, the molecular weights from Zimm plot technique were generally higher than those obtained by the dissymmetry method. This might probably be due to the polydispersity of the fractions.

As the molecular weights of the fractions showed an irregular trend which was not in the order of the intrinsic viscosities, a particularly careful study was made on M1 as follows:

(a) testing the reproducibility of the results by repeating the experiment

(b) improving the clarification of the solutions by prolonged pre-centrifugation up to 4 hours

(c) making up the solutions and shaking vigorously overnight to facilitate uniform mixing

(d) changing the deionized water earlier used for making up the solutions to laboratory distilled water as it was felt that some fragments of inn-exchange resin might be carried over in the solutions resulting in high scattering.

However, from these experiments the molecular weights obtained for M1, as seen in Table I, were in close agreement with a mean deviation of $\pm$ 7%. A repetition of the experiment for H1, L1 and L3 similarly gave molecular weights in good agreement. Hence the large values of M_{LS} and their irregular trend from fraction to fraction would be due to some reproducible anomaly in each fraction rather than random error. As suggested in Part I this could be due to molecular aggregation.

The intrinsic dissymmetry of the fractions increased with the molecular weight and varied between 1.45 and 3.0.

TABLE I

Molecular Weights and Other Light Scattering Data for the Fractions

Fraction	$M_w \times 10^{-5}$ (Zimm plots)	$M_w \times 10^{-5}$ (Dissymmetry)	$[Z^*]$	$\sqrt{\bar{S}_z^2}$ (Å)	$A_2 \times 10^5$	dn/dc (ml.g.$^{-1}$)
H1	15.87	10.41	2.80	1750	1.63	0.1467
	15.36	11.03	3.00	-	-	-
H2	14.82	9.64	2.65	1610	1.48	0.1467
H3	5.88	3.58	2.0	1180	3.58	0.1482
M1	12.80	-	-	-	-	0.1473
	13.79	10.42	2.66	1430	1.21	-
	11.43	9.97	2.56	-	-	-
	13.89	10.16	2.46	-	-	-
M2	4.35	3.31	1.98	1010	3.06	0.1482
L1	8.00	6.57	2.16	-	1.47	0.1473
	-	5.82	2.27	-	-	-
L2	2.11	1.98	1.50	990	3.47	0.1470
L3	1.82	1.66	1.45	850	3.36	0.1477
	1.94	1.85	1.47	-	-	-

Fig. 4

Hc/τ and dissymmetry, Z* vs. conc. for Hl in 0.1 M NaCl

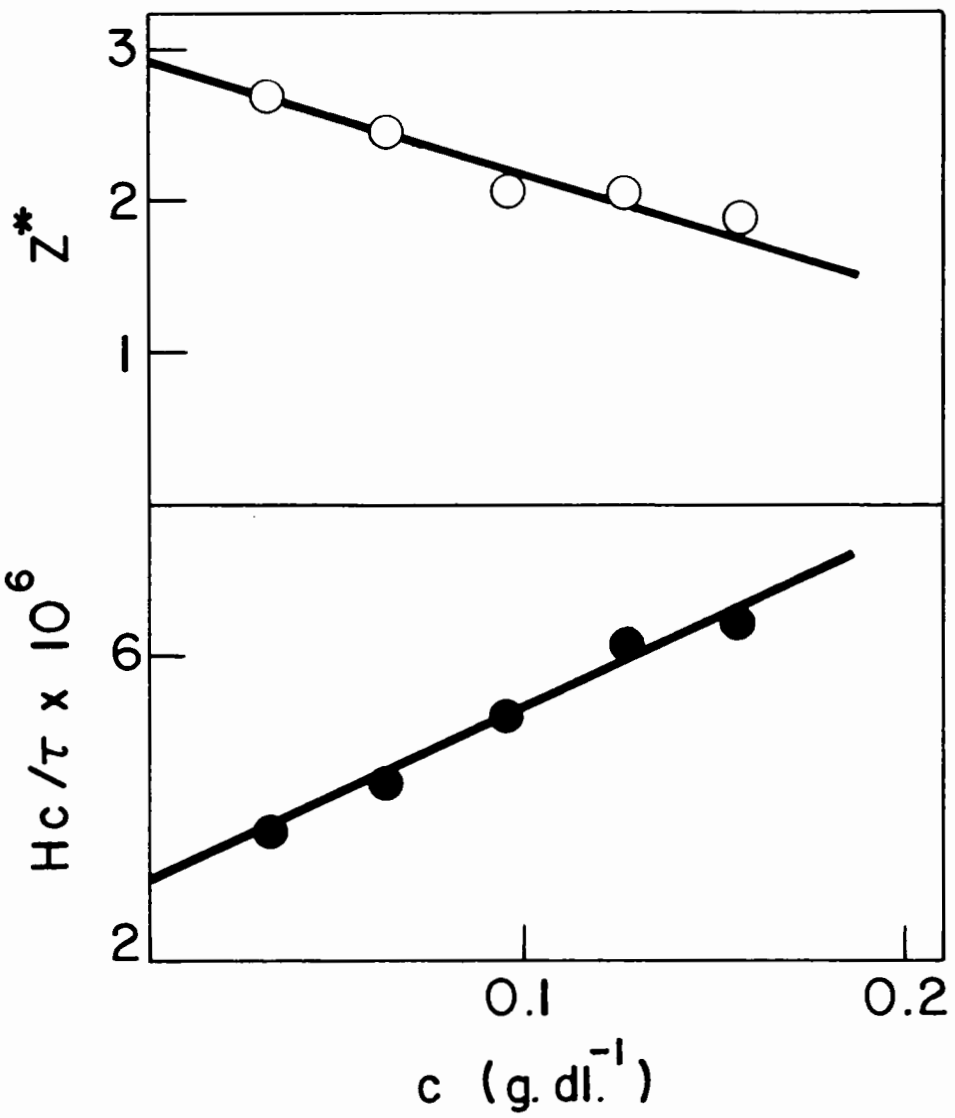
3
2
1
Z*
6
2
Hc/τ x 10^6
0.1
0.2
c (g. dl.^-1)

Ionic Strength

The influence of ionic strength on the light scattering of CMC was studied in a few preliminary experiments. Scattering was measured at different angles of a single low concentration of M1 over a range of I_E values. In Fig. 5, values of Kc/R_θ were plotted against $\sin^2\theta/2$ at different ionic strengths. The slope of Kc/R_θ increases with the decrease of ionic strength. Radii of gyration calculated from Eq. (3) were 1670 Å, 1760 Å, 2180 Å and 2510 Å at I_E = 0.1 M, 0.05 M, 0.01 M and 0.006 M respectively. The increased radius of gyration at low ionic strengths is anticipated from the molecular extension which occurs at low ionic strengths (7). This aspect of light scattering was not pursued as it was found difficult to obtain fairly reproducible scattering values at the very low concentration necessary to achieve the low ionic strengths.

Refractive Index Increment

The refractive index increment, dn/dc, of the CMC fractions was measured on a Brice Phoenix refractometer, as described in Part I. The values of dn/dc shown in Table I do not exhibit any molecular weight dependence and agree well among the fractions. A similar absence of molecular weight dependence of dn/dc has been noted by Huque et al (10). A mean dn/dc value of 0.147 $\pm$ 0.0007 ml.g.$^{-1}$ was obtained for λ = 5461 Å.

Fig. 5

Kc/R_θ vs. $\sin^2 \theta/_2$ at ionic strengths from 0.006 M to 0.1 M

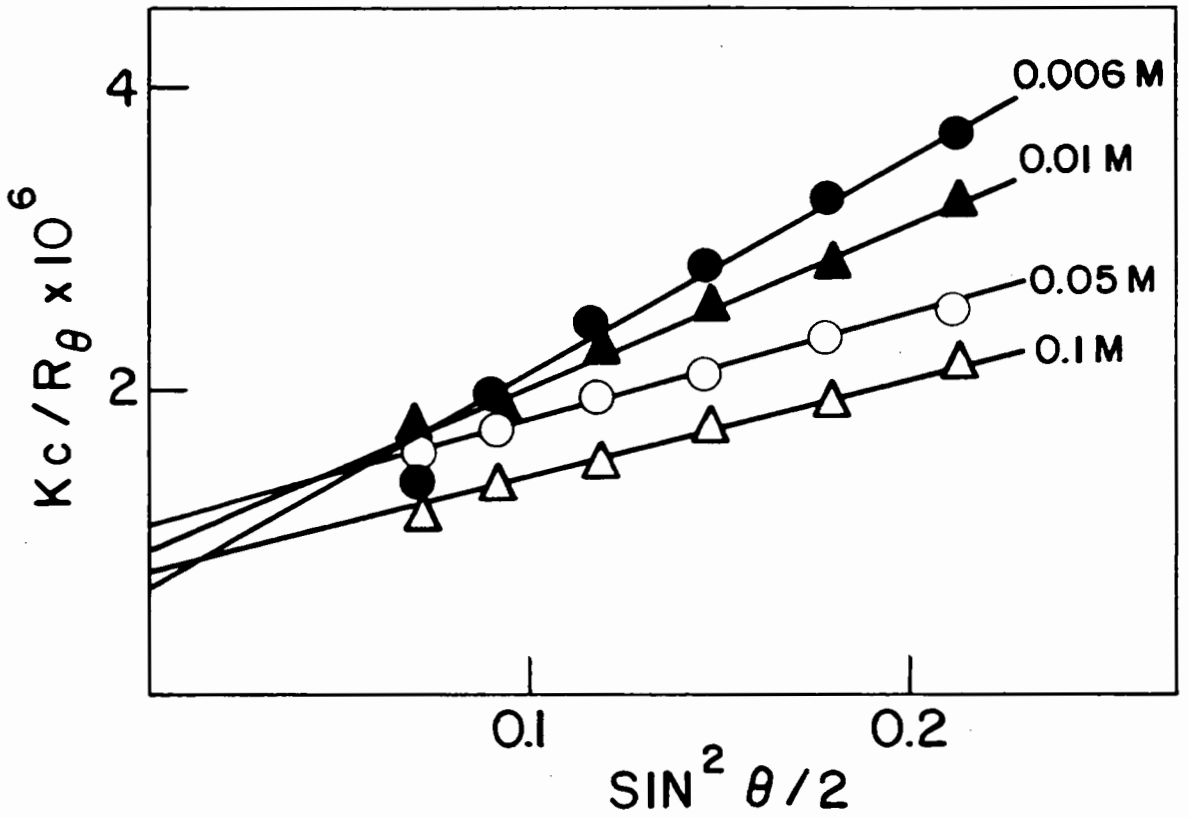
4
2
$Kc/R_\theta \times 10^6$
0.006 M
0.01 M
0.05 M
0.1 M
0.1
0.2
$SIN^2\ \theta/2$

REFERENCES

1. D.A.I. Goring, M. Senez, B. Melansen and M.M. Huque, J. Colloid Sci. 12, 412 (1957).
2. P.R. Gupta, Ph.D. Thesis, McGill Univ. (1959).
3. M.M. Huque, Ph.D. Thesis, McGill Univ. (1957).
4. D.A.I. Goring and J. Jaworzyn, Unpublished data.
5. M.M. Huque, J. Jaworzyn and D.A.I. Goring, J. Polym. Sci. 39, 9 (1958).
6. T. Timell and D.A.I. Goring, J. Phys. Chem. 64, 1426 (1960).
7. Part I of this thesis.
8. P. Debye, J. Phys. and Colloid Chem. 51, 18 (1947).
9. K.A. Stacey, Light Scattering in Physical Chemistry, Butterworths Publications, London. 63 (1956).
10. M.M. Huque, D.A.I. Goring and S.G. Mason, Can. J. Chem. 36, 952 (1958).

APPENDIX IV

SEDIMENTATION

SEDIMENTATION

Certain details of the sedimentation experiments have already been described in Part I and III. The purpose of the present Appendix is to give examples of the sedimentation diagrams and plots from which the sedimentation constants were calculated.

Fig. 1 gives the sedimentation diagrams for M1 at I_E = 0.01 M. The peaks are sharp showing absence of gross aggregation. The upper peaks correspond to a concentration of 0.0236 g.dl.$^{-1}$ and the lower peaks correspond to 0.0158 g.dl.$^{-1}$.

In Fig. 2 are shown the plots of the logarithm of the distance, s_m of the peak from the centre of the rotor against time. Sedimentation constants were calculated in the usual manner from the slope of the linear plots of log 10 x_m vs. time, using the relation

$$s = \frac{dx/dt}{\underline{w}^2 x} \qquad \ldots(1)$$

where $\underline{w}$ is the angular velocity. The sedimentation constant at zero concentration was obtained from

$$s_m = (s_m)_{c=o} \cdot (1 + k_s c)^{-1} \qquad \ldots(2)$$

where the symbols have the usual significance.

Fig. 1

Sedimentation patterns for M1 at 10^{-2} M

Upper peaks $c = 0.236$ g.dl.$^{-1}$

Lower peaks $c = 0.015$ g.dl.$^{-1}$

t_1	= 0 sec.	t_7	= 48 sec.
t_2	= 8 sec.	t_8	= 56 sec.
t_3	= 16 sec.	t_9	= 64 sec.
t_4	= 24 sec.	t_{10}	= 72 sec.
t_5	= 32 sec.	t_{11}	= 80 sec.
t_6	= 40 sec.	t_{12}	= 88 sec.

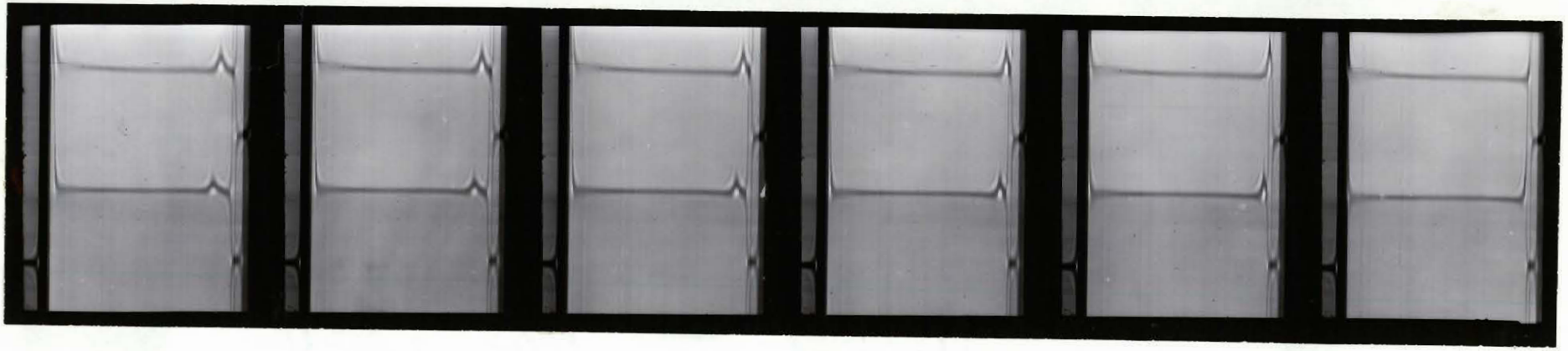

t_6 t_5 t_4 t_3 t_2 t_1

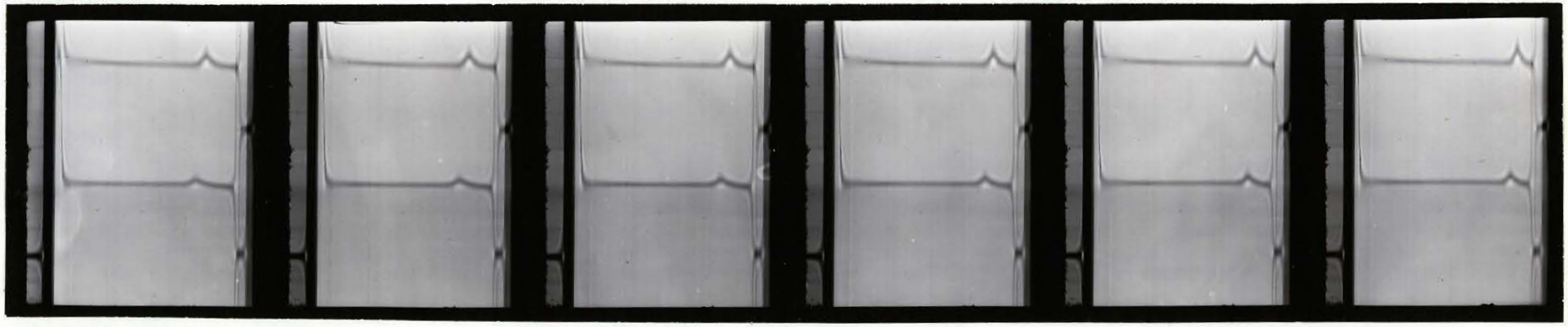

t_{12} t_{11} t_{10} t_9 t_8 t_7

Fig. 2

Log of the distance, x_m of the boundary from the center of the rotor vs. time for fraction, H3 at I_E = 0.1 M

c_1 = 0.3115 g.dl.$^{-1}$

c_2 = 0.1557 g.dl.$^{-1}$

c_3 = 0.0779 g.dl.$^{-1}$

c_4 = 0.0389 g.dl.$^{-1}$

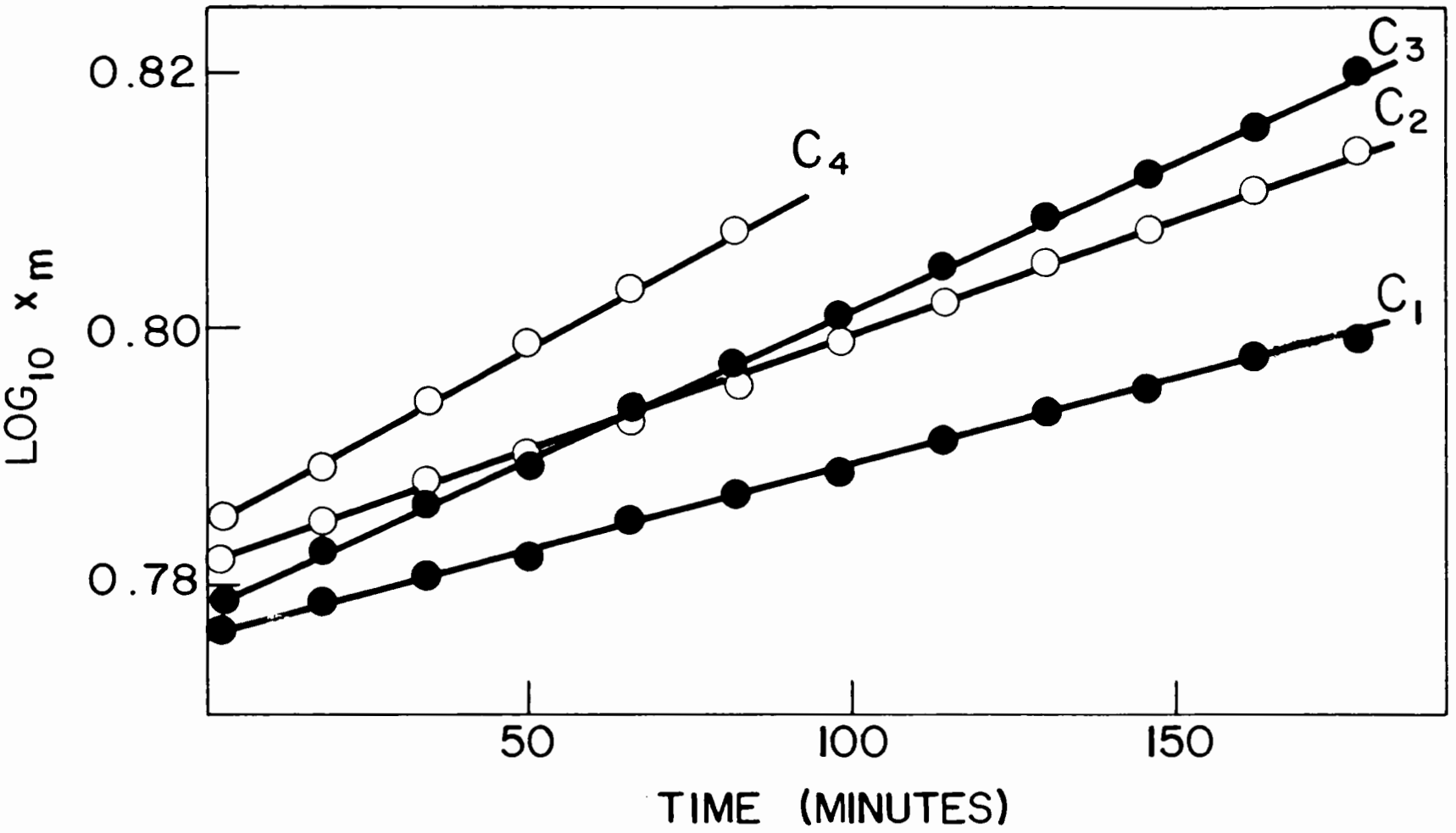
0.82
0.80
0.78
LOG10 x m
C4
C3
C2
C1
50
100
150
TIME (MINUTES)

APPENDIX V

DEVELOPMENT OF DIFFUSION TECHNIQUES

Diffusion was measured on a Zeiss interferometer. The instrument is relatively new and there are few reports on its use. Therefore this appendix will describe the experimental techniques of diffusion in detail.

The interferometer shown in Fig. 1 is manufactured in accordance with the specifications of Prof. H.J. Antweiler of Bonn and can be used for diffusion measurements with reasonable accuracy and speed. The progress of diffusion can be observed visually and the interferograms can be photographed at definite intervals of time.

The quartz micro diffusion cell consists of 4 separate components:- the main section, k, the somewhat smaller sliding section s and the upper and lower cover plates, d and e (Fig. 3a). The main section and sliding section are provided with an equal number of channels of identical dimensions. Channel I is the measuring compartment proper in which diffusion takes place. Channel II is the comparison compartment in which the solvent is filled. Channel III houses the thermometer and channel IV serves only for introducing the solution. In Fig. 3a the cell is ready for filling and in Fig. 3b, the sliding compartment is moved so that solvent and solution come in contact and diffusion takes place. The individual components of the cell are housed in a metal container (Fig. 2), a plate of which can be removed for inserting the cell components. The container has also a cover T with an inlet for the thermometer. By rotating a milled screw W the sliding section s is moved so that the two liquid layers come in contact and start diffusing.

Fig. 1

Zeiss Diffusion Interferometer

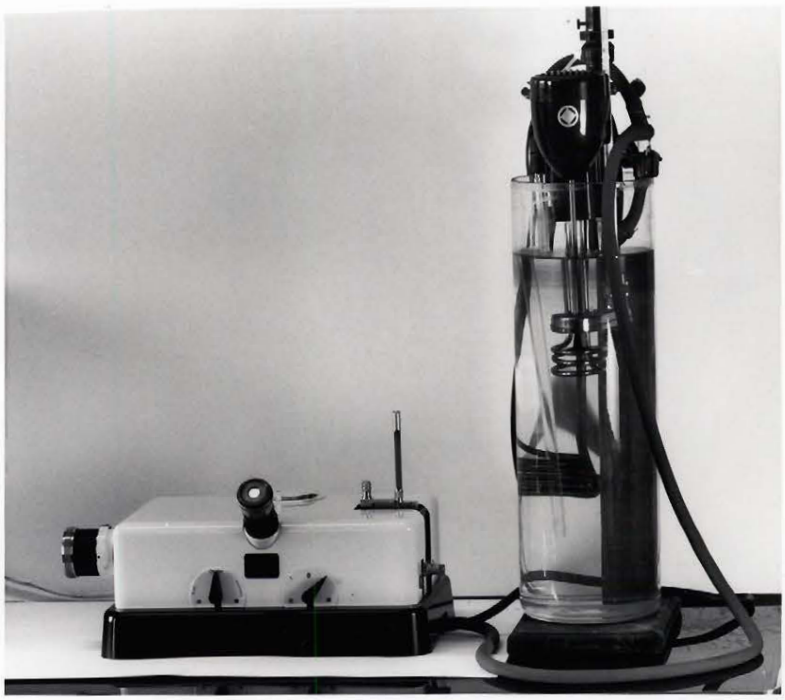

Fig. 2

Diffusion cell assembly

T - container cover with an inlet for thermometer

W - milled screw for moving the sliding section of the cell to start diffusion

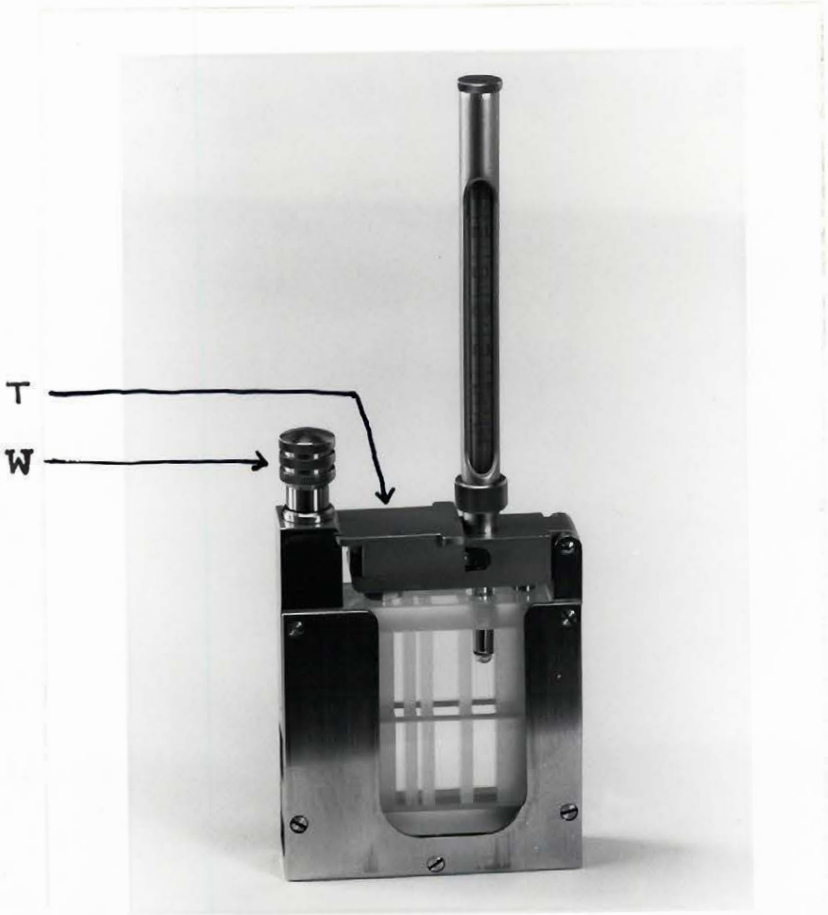
T
W

Fig. 3

Micro-diffusion cell

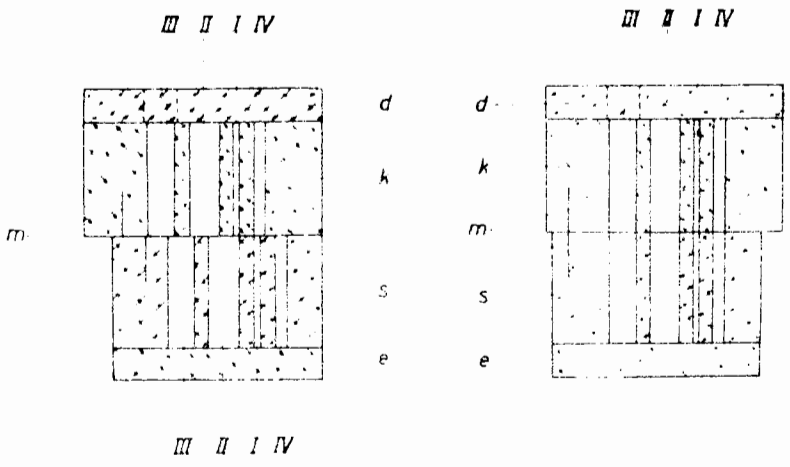

Diagram of diffusion cell, side cut

Fig. 3a Position for charging

Fig. 3b Position for diffusion

I Test compartment
II Comparison compartment
III Charging channel for solvent and space for thermometer
IV Charging channel for solution

d Upper cover plate
e Lower cover plate
k Main section
s Sliding section
m Mark

The optical system is a Raleigh-Jamin interferometer and thus the change in concentration, c resulting from diffusion can be determined from the fringe shift. If dn/dc is assumed constant for change of c

$$\Delta c = \frac{dc}{dn} \cdot \Delta n = \frac{dc}{dn} \cdot \frac{\lambda \Delta C_o}{\ell} \qquad \ldots(1)$$

where Δn is the difference in refractive index between solution and solvent, ℓ is the depth of the diffusion cell (5 mm.), λ the wavelength and ΔC_o the fringe shift. Thus the concentration at any distance, x from the initial boundary is proportional to the fringe shift and can be obtained directly from the interferograms, photographically recorded and suitably magnified.

In Fig. 4 are shown diffusion interferograms for H2 in 0.1 M NaCl at different time intervals. Such interferograms were analysed in various ways to give the diffusion constants.

The "area" diffusion constant, D_A is given by

$$D_A = \frac{A^2}{4 \pi t H^2} \qquad \ldots(2)$$

where A is the area and H is the maximum height of the characteristic bell-shaped diffusion curves of the gradient, dc/dn vs. x. However, it is possible to use directly the C_o vs. x graph of the interferogram and thus avoid recomputation of the gradient curve. For this purpose, H becomes the tangent maximum and is determined by the slope C_o/x of the steepest tangent at the inflection point of an interference curve. Further, the area under the gradient curve expresses the difference in concentration

Fig. 4

Diffusion interferograms for H2 in 0.1 M NaCl,

at c = 0.3 g.dl.$^{-1}$, for different times, shown below:

t_1 - 480 sec. t_5 - 13800 sec.

t_2 - 1800 sec. t_6 - 18120 sec.

t_3 - 4500 sec. t_7 - 20100 sec.

t_4 - 8100 sec. t_8 - 33120 sec.

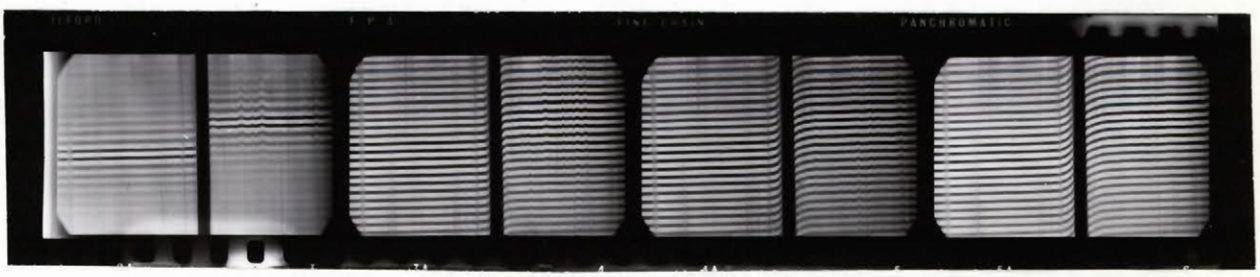

t_1 t_2 t_3 t_4

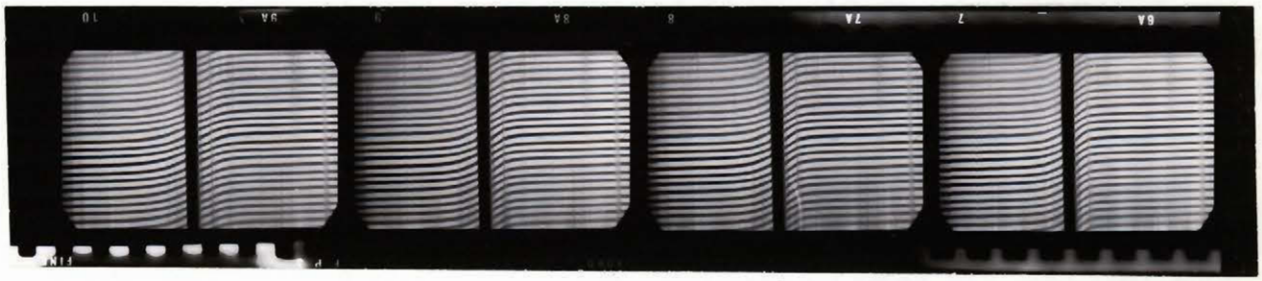

t_5 t_6 t_7 t_8

or the total fringe shift, C_o of the two liquids. Now D_A can be computed from

$$D_A = \frac{C_o^2}{4\pi t H^2} \qquad \ldots(3)$$

In Table I are shown C_o and H at different times for the fraction M1 at the concentration of 0.25 g.dl.$^{-1}$ in 0.1 M NaCl. A plot of H^2 vs. $1/t$ is shown in Fig. 5, the slope of which gives H^2t in Eq. (3). As the value of C_o is known, D_A can be computed by substituting in Eq. (3), the value of $H^2t \; x\beta^2$ where β = 15.6, the magnification of the enlarged interferograms in the x - direction. In a similar manner D_A value at zero concentration was determined by extrapolation.

The "second moment" diffusion constant, D_m is given by

$$D_m = \frac{m_2}{2 t C_o} \qquad \ldots(4)$$

where m_2 is the second moment given by

$$m_2 = \int_{-\infty}^{+\infty} x^2 \frac{d C_o}{dx} dx = \int_{-\infty}^{+\infty} x^2 \, d C_o \qquad \ldots(5)$$

Hence D_m can be written in the form

$$D_m = \frac{1}{2 t C_o} \int_{-\infty}^{+\infty} x^2 \, d C_o \qquad \ldots(6)$$

In Table II, the method of obtaining the second moment, m_2 by graphical

TABLE I

Values of C_o and H for Different Times

in the case of M1 at 0.25 g.dl.$^{-1}$

No.	Time x10^{-4} (sec.)	C_o (cm.)	$H = \Delta C_o / x$
1	0.48	3.6	2.68
2	1.20	3.6	1.63
3	1.56	3.6	1.41
4	1.92	3.7	1.39
5	3.00	3.7	1.10
6	7.32	3.6	0.84

TABLE II

Evaluation of the Second Moment, m_2 for M1 at a Concentration of 0.4 g./dl. for the progress of Diffusion of 10 hrs. 15 min.

Solution Side			Solvent Side		
d C_o (cm.)	x (cm.)	x^2 d C_o ($cm.^3$)	d C_o (cm.)	x (cm.)	x^2 d C_o ($cm.^3$)
0.15	0.18	0.006	0.15	0.20	0.008
0.2	0.48	0.05	0.2	0.43	0.04
0.2	0.70	0.10	0.2	0.75	0.11
0.2	0.90	0.16	0.2	1.00	0.20
0.2	1.15	0.26	0.2	1.45	0.42
0.2	1.40	0.39	0.2	1.95	0.76
0.2	1.60	0.51	0.2	2.85	1.62
0.2	2.00	0.80	0.2	4.10	3.36
0.2	2.85	1.62	0.1	5.60	3.13
0.1	3.40	1.16	-	-	-
0.1	5.30	2.81	-	-	-

$$m_2 = \frac{\text{Total } x^2 \text{ d } C_o}{\beta^3} = 4.62 \times 10^{-3}$$

Fig. 5

H^2 vs. $^1/t$ for the diffusion of M1

in 0.1 M NaCl (conc. = 0.25 g.dl.$^{-1}$)

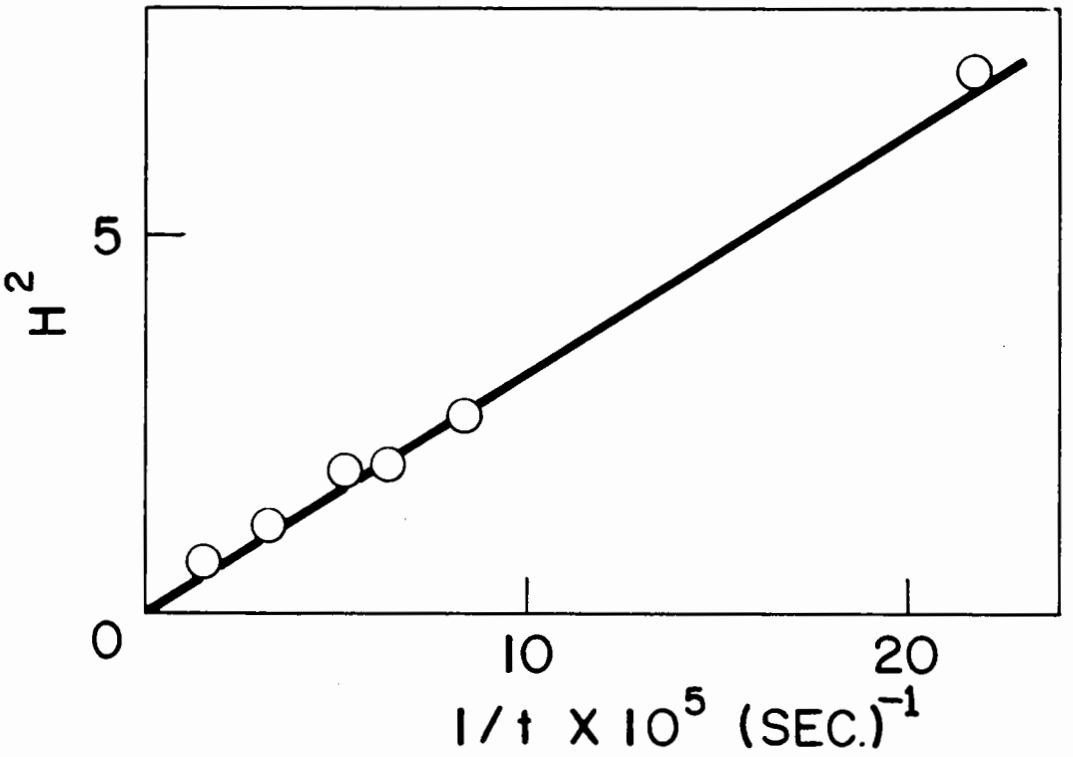
H^2
5
0
10
20
$1/t \times 10^5$ (SEC.)$^{-1}$

integration is shown. By evaluating m_2 at different periods of diffusion, m_2 is plotted against the time (Fig. 6) and the slope gives the value of m_2/t. By introducing this value of m_2/t in Eq. (6), the value of D_m was calculated for a particular concentration of CMC. By carrying out the diffusion runs at a few concentrations, the $(D_m)_{c=o}$ value was obtained by extrapolation to zero concentration (Fig. 7, Part I).

Diffusion constant from Boltzmann Equation

For obtaining the D_m and D_A values at zero concentration it is necessary to do the diffusion runs at 4 or 5 concentrations for extrapolation to zero concentration. By carrying out the diffusion at only one concentration, a method has been developed by the use of the Boltzmann equation (Eq. (1) Part I) by means of which the diffusion constant can be computed over a series of concentrations and extrapolated back to zero concentration. Certain details of this procedure have already been given in Part I. However, a sample calculation for fraction L3 is shown here.

From the enlarged interferograms, values of x corresponding to a particular value of c are determined for the various times, t at which the pictures were taken. Values of c, x and $\sqrt{t}$ are listed in Table III. In Fig. 6 (Part I), c vs. $x/\sqrt{t}$ written as λ is shown. From this curve, by graphical integration of the area under the curve $\int_o^c \lambda \, dc$ for each concentration as well as the tangent, $d\lambda/dc$ were obtained. Diffusion constants were then calculated at each concentration by substitution in Eq. (1) (Part I) and are shown in Table IV. $(D)_{c=o}$ was obtained by extrapolation to zero concentration and $(D)_{c=o}$ values corrected to 25°C were designated as D_o.

Fig. 6

The second moment, m_2 vs. t in the diffusion of M1 in 0.1 M NaCl (conc. = 0.4 $g.dl.^{-1}$)

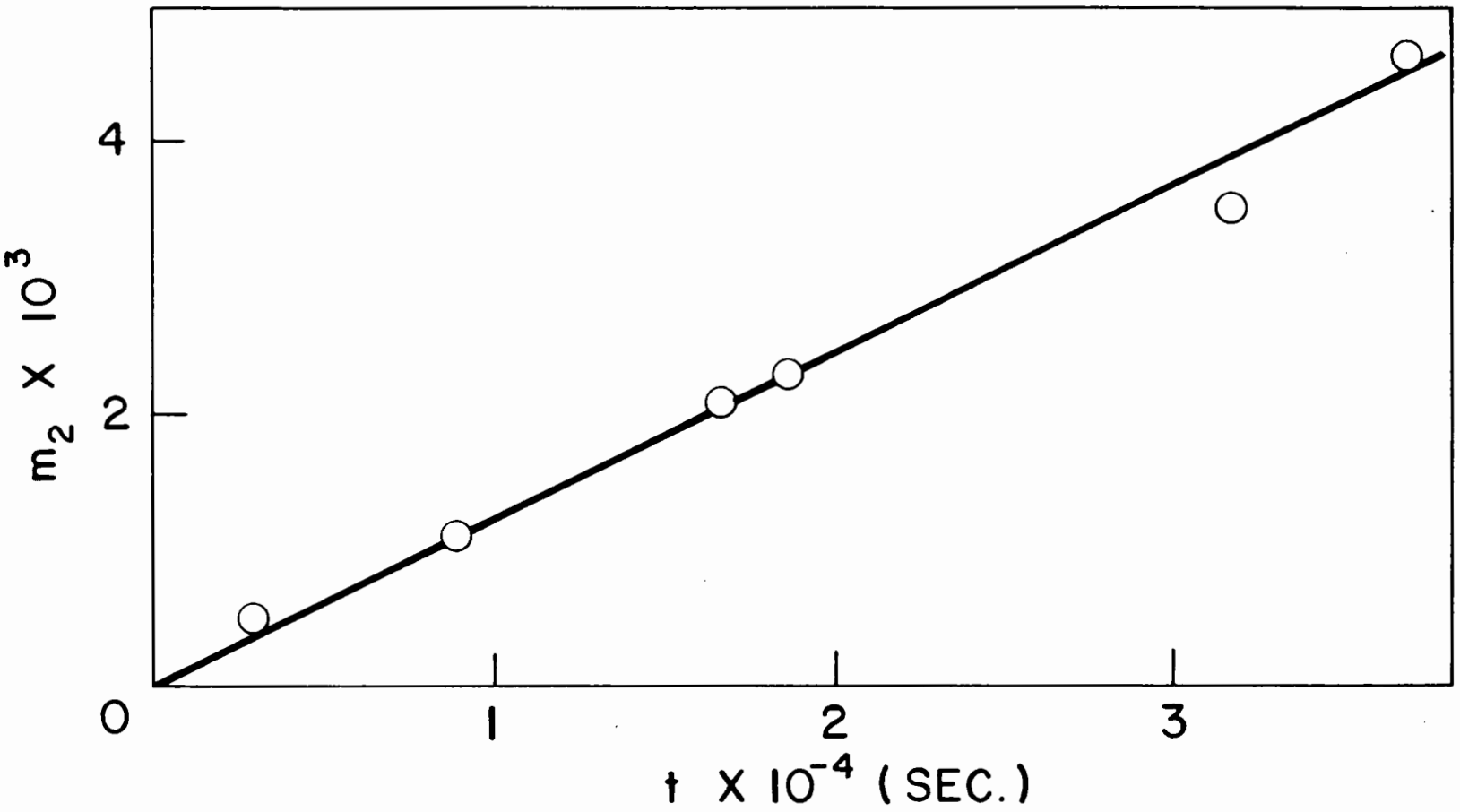
4
2
0
$m_2 \times 10^3$
1
2
3
$t \times 10^{-4}$ (SEC.)

TABLE III

$x/\sqrt{t}$ at Different Concentrations for L3 in 0.1 M NaCl

No.	c ($g.dl.^{-1}$)	$\sqrt{t_1}$ = 57.5 x_1 cm.	$\sqrt{t_2}$ = 84.9 x_2 cm.	$\sqrt{t_3}$ = 106.8 x_3 cm.	$\sqrt{t_4}$ = 126.1 x_4 cm.	$\sqrt{t_5}$ = 139.6 x_5 cm.	$\sqrt{t_6}$ = 164.3 x_6 cm.	$x/\sqrt{t}$ $x10^2$	$x/\sqrt{t}$ $x10^3$ (corrected for magnification)
	0.400	1.50	2.60	2.70	3.60	3.85	5.10	2.79	1.788
	0.385	1.32	2.10	2.20	2.80	3.10	4.00	2.23	1.426
	0.356	0.90	1.40	1.46	1.70	2.15	2.55	1.54	0.984
	0.326	0.60	0.98	1.10	1.35	1.65	1.85	1.13	0.721
	0.296	0.46	0.70	0.73	0.95	1.05	1.25	0.76	0.487
	0.267	0.30	0.45	0.45	0.55	0.75	0.85	0.51	0.327
	0.237	0.15	0.25	0.20	0.32	0.35	0.40	0.25	0.160
	0.178	0.20	0.15	0.28	0.30	0.30	0.35	- 0.24	- 0.154
	0.148	0.35	0.35	0.56	0.65	0.65	0.80	- 0.50	- 0.321
	0.119	0.46	0.60	0.85	0.95	1.05	1.15	- 0.74	- 0.474
	0.089	0.70	0.90	1.25	1.30	1.50	1.60	- 1.05	- 0.673
	0.059	0.95	1.20	1.67	1.85	1.95	2.20	- 1.43	- 0.913
	0.030	1.35	1.70	2.2	2.50	2.70	2.90	- 1.97	- 1.260
	0.000	2.40	2.90	3.80	4.20	4.70	5.10	- 3.38	- 3.163

TABLE IV

$\int \lambda \, dc$, $\frac{d\lambda}{dc}$ and D for Fraction L3 in 0.1 M NaCl

No.	c ($g.dl.^{-1}$)	$\frac{d\lambda}{dc} \times 10^3$	Area $cm.^2$	$\int \lambda \, dc \times 10^5$	D x 10^7
1	0.5925	9.0	12.85	7.61	3.43
2	0.0889	7.1	16.78	9.94	3.51
3	0.1482	5.4	21.51	12.75	3.46
4	0.2074	5.1	22.96	13.61	3.50
5	0.2667	5.8	24.51	14.53	4.18

$$\int \lambda \, dc = \text{Area in sq.cm.} / 5.925 \times 10^6$$

The diffusion runs were made for the eight fractions in 0.1 M NaCl in the concentration range between 0.1 to 0.4 g.dl.$^{-1}$. The D_o values are given in Table V. As the diffusion was measured at only one concentration, except in the case of M1, D_A values were computed at that concentration. The concentration dependence of D_A, in the case of M1, has been shown in Fig. 7 (Part I). Assuming the same concentration dependence for other fractions, D_A values were corrected to give 'area' diffusion constants at zero concentration. This procedure, though arbitrary, may be justifiable in view of Manley's (2) observation that the concentration dependence of D_m and D_A was the same for all the fractions within experimental error.

Values of D_m/D_A for the CMC fractions, given in Table V, are greater than unity. As noted by Jullander the D_m value is a weight average whereas the D_A value approaches a number average diffusion constant. Hence the ratio of D_m/D_A would be expected to be greater than unity. A similar trend has been noted by Manley and Gralen (2,4).

REFERENCES

1. L. Boltzmann, Ann. Physik. 53, 959 (1894).
2. R. St.J. Manley, Arkiv Kemi, 9, 519 (1956).
3. I. Jullander, Studies on Nitrocellulose, Arkiv Kemi, Minerologi Och Geologi, 21 A, 1 (1945)
4. N. Gralen, Sedimentation and Diffusion Measurements on Cellulose and Cellulose Derivatives, Inaugural Dissertation, Uppsala (1944).

TABLE V

D_o, D_A and D_o/D_A values for the Fractions in 0.1 M NaCl

Fraction	$D_o \times 10^7$	$D_A \times 10^7$	D_o/D_A
H1	0.95	0.71	1.34
H2	1.16	1.06	1.09
H3	1.37	1.22	1.23
M1	1.49	1.30	1.15
M2	2.03	1.10	1.85
L1	2.07	1.07	1.93
L2	3.57	2.67	1.34
L3	3.58	2.70	1.33

A P P E N D I X VI

DETAILED DATA FROM VISCOMETRY, SEDIMENTATION, DIFFUSION AND LIGHT SCATTERING

APPENDIX VI

Detailed Data from Viscometry, Sedimentation, Diffusion and Light Scattering

The results described in the main text are derived from the detailed experimental data given in this Appendix.

The concentrations throughout are expressed in $g.dl.^{-1}$. The shear rate, G in the Tables I - VIII is expressed in $sec.^{-1}$. At very low ionic strengths where the concentration of the polymer is small, viscosities were measured only in bulb 3 (Tables I - III).

Sedimentation constant, s_m in Table IX are expressed in Svedberg units and the diffusion constants (Table X) are expressed in $cm.^2$ $sec.^{-1}$.

TABLE I

Specific Viscosities for H1 at Different Ionic Strengths, Concentrations and Rates of Shear

I_E (M)	Bulb No.	c_1 = 0.030		c_2 = 0.0225		c_3 = 0.015		c_4 = 0.0113		c_5 = 0.00818	
		G	η_{sp}	G	η_{sp}	G	η_{sp}	G	η_{sp}	G	η_{sp}
0.1	1	874	0.3967	939	0.3004	1027	0.1896	1074	0.1372	1114	0.0963
	2	599	0.4209	645	0.3189	712	0.1949	744	0.1436	777	0.1033
	3	348	0.4474	381	0.3239	418	0.2067	441	0.1444	458	0.1012
	4	151	0.4443	163	0.3333	179	0.2130	191	0.1408	199	0.0962
		c_1 = 0.030		c_2 = 0.0225		c_3 = 0.0150		c_4 = 0.0113		c_5 = 0.00818	
0.01	1	587	1.096	686	0.7922	834	0.4738	935	0.3145	993	0.2385
	2	372	1.309	457	0.8757	564	0.5222	631	0.3605	681	0.2592
	3	212	1.398	262	0.9423	322	0.5819	363	0.4016	396	0.2843
	4	88	1.503	110	0.9869	136	0.6082	156	0.4084	170	0.2871
		c_1 = 0.015		c_2 = 0.0113		c_3 = 0.0075		c_4 = 0.00562		c_5 = 0.00375	
0.001	1	505	1.436	633	0.9416	808	0.5222	901	0.3645	1007	0.2217
	2	323	1.658	403	1.1274	536	0.6002	607	0.4126	685	0.2534
	3	165	2.075	217	1.3424	294	0.7292	340	0.4985	394	0.2912
	4	64	2.431	83	1.6561	115	0.9056	139	0.5744	164	0.3381

TABLE I Contd

I_E (M)	Bulb No.	c_1 = 0.00466		c_2 = 0.00350		c_3 = 0.00233		c_4 = 0.00175		c_5 = 0.00117	
		G	η_{sp}	G	η_{sp}	G	η_{sp}	G	η_{sp}	G	η_{sp}
0.0001	1	587	1.095	807	0.5231	949	0.2951	1029	0.1951	1105	0.1133
	2	378	1.271	530	0.6199	631	0.3592	700	0.2263	756	0.1354
	3	191	1.667	280	0.8182	356	0.4248	397	0.2835	438	0.1629
	4	69	2.197	105	1.0831	139	0.5737	162	0.3562	182	0.2025
		c_1 = 0.00230		c_2 = 0.00153		c_3 = 0.00115		c_4 = 0.00086		c_5 = 0.00058	
0.00005	3	288	0.7663	374	0.3616	416	0.2249	438	0.1627	466	0.0912
		c_1 = 0.000466		c_2 = 0.000333		c_3 = 0.000259		c_4 = 0.000194		c_5 = 0.000146	
0.00001	3	454	0.1221	472	0.0786	483	0.0530	488	0.0421	495	0.0285

TABLE II

Specific Viscosities for M1 at Different Ionic Strengths, Concentrations and Rates of Shear

I_E (M)	Bulb No.	c_1 = 0.05		c_2 = 0.04		c_3 = 0.03		c_4 = 0.02		c_5 = 0.01	
		G	η_{sp}	G	η_{sp}	G	η_{sp}	G	η_{sp}	G	η_{sp}
0.1	1	878	0.3901	936	0.3041	999	0.2223	1068	0.1431	1143	0.0681
	2	609	0.3966	649	0.3115	693	0.2271	742	0.1462	799	0.07160
	3	359	0.4036	383	0.3168	410	0.2305	439	0.1479	471	0.07042
	4	154	0.3833	164	0.3260	176	0.2374	189	0.1496	202	0.07634
		c_1 = 0.05		c_2 = 0.04		c_3 = 0.03		c_4 = 0.02		c_5 = 0.01	
0.01	1	711	0.7287	793	0.550	880	0.3970	987	0.2458	1099	0.1189
	2	492	0.7447	548	0.5661	611	0.4045	684	0.2547	764	0.1228
	3	289	0.7633	322	0.5821	360	0.4153	403	0.2636	451	0.1294
	4	124	0.7689	138	0.5836	155	0.4136	173	0.2669	194	0.1277
		c_1 = 0.05		c_2 = 0.03		c_3 = 0.02		c_4 = 0.02		c_5 = 0.01	
0.00139	1	323	2.802	429	1.862	568	1.161	751	0.6349	971	0.2645
	2	219	2.895	289	1.953	385	1.221	513	0.6652	668	0.2791
	3	126	3.012	165	2.057	220	1.298	297	0.6992	390	0.2943
	4	52	3.140	68	2.187	90	1.404	124	0.7446	166	0.3073

TABLE II Contd

I_E (M)	Bulb No.	c_1 = 0.0036		c_2 = 0.0027		c_3 = 0.0018		c_4 = 0.0009	
		G	η_{sp}	G	η_{sp}	G	η_{sp}	G	η_{sp}
0.0001	1	949	0.2962	1036	0.1865	1117	0.1013	1184	0.0386
	2	646	0.3281	709	0.2096	771	0.1133	823	0.0430
	3	372	0.3700	412	0.2367	452	0.1267	485	0.0485
	4	150	0.4643	173	0.2686	192	0.1431	208	0.0530
		c_1 = 0.0181		c_2 = 0.0135		c_3 = 0.0090		c_4 = 0.0045	
0.0005	1	610	1.015	763	0.6108	918	0.3392	1076	0.1424
	2	411	1.087	520	0.6515	628	0.3655	745	0.1512
	3	234	1.171	298	0.7076	365	0.3953	438	0.1630
	4	95	1.304	125	0.7551	154	0.4241	187	0.1709
		c_1 = 0.00108		c_2 = 0.00081		c_3 = 0.00059		c_4 = 0.00027	
0.00003	3	465	0.953	479	0.0616	490	0.0381	501	0.0165

TABLE III

Specific Viscosities for L3 at Different Ionic Strengths, Concentrations and Rates of Shear

I_E (M)	Bulb No.	c_1 = 0.150		c_2 = 0.113		c_3 = 0.090		c_4 = 0.065		c_5 = 0.050	
		G	η_{sp}	G	η_{sp}	G	η_{sp}	G	η_{sp}	G	η_{sp}
0.1	1	988	0.2357	1023	0.1933	1060	0.1523	1103	0.1067	1130	0.0808
	2	672	0.2668	712	0.1946	738	0.1523	770	0.1052	787	0.0815
	3	398	0.2676	423	0.1928	437	0.1529	455	0.1084	467	0.0810
	4	171	0.2700	182	0.1954	190	0.1490	197	0.1071	202	0.0787
		c_1 = 0.150		c_2 = 0.113		c_3 = 0.075		c_4 = 0.0563			
0.01	1	832	0.4781	920	0.3363	1021	0.2045	1073	0.1464		
	2	579	0.4823	637	0.3469	712	0.2057	747	0.1487		
	3	343	0.4849	377	0.3507	421	0.2088	443	0.1496		
	4	147	0.4931	162	0.3488	182	0.2068	192	0.1443		
		c_1 = 0.050		c_2 = 0.030		c_3 = 0.020		c_4 = 0.010			
0.00166	1	901	0.3648	1049	0.1722	1119	0.0980	1181	0.0412		
	2	628	0.3673	731	0.1734	781	0.0991	823	0.0430		
	3	372	0.3693	433	0.1744	463	0.1003	488	0.0425		
	4	160	0.3718	187	0.1722	199	0.0997	210	0.0429		

TABLE III Contd

I_E (M)	Bulb No.	c_1 = 0.0151		c_2 = 0.0100		c_3 = 0.0075		c_4 = 0.0050			
		G	η_{sp}	G	η_{sp}	G	η_{sp}	G	η_{sp}	G	η_{sp}
0.0005	1	1066	0.1539	1138	0.0802	1169	0.0515	1195	0.0291		
	2	740	0.1602	791	0.0847	813	0.0557	831	0.0325		
	3	439	0.1601	469	0.0858	482	0.0551	493	0.0324		
	4	189	0.1605	202	0.0857	208	0.0561	212	0.0359		
		c_1 = 0.0030		c_2 = 0.0023		c_3 = 0.0018		c_4 = 0.0015		c_5 = 0.0010	
0.0001	3	502	0.0135	503	0.0120	504	0.0106	505	0.0092	506	0.0067

TABLE IV

Specific Viscosities for H2 at 0.1 M and 0.001 M, for Different Concentrations and Rates of Shear

I_E (M)	Bulb No.	c_1 = 0.0317		c_2 = 0.0190		c_3 = 0.0119		c_4 = 0.0087		c_5 = 0.0056	
		G	η_{sp}	G	η_{sp}	G	η_{sp}	G	η_{sp}	G	η_{sp}
0.1	1	915	0.3872	1037	0.2240	1121	0.1321	1160	0.0942	1199	0.0586
	2	637	0.4041	706	0.2305	759	0.1447	786	0.1050	813	0.0682
	3	345	0.4220	394	0.2449	425	0.1545	442	0.1094	459	0.0695
	4	122	0.4481	140	0.2580	152	0.1576	158	0.1156	164	0.0757
		c_1 = 0.0458		c_2 = 0.0275		c_3 = 0.0172		c_4 = 0.0125		c_5 = 0.0808	
0.001	1	204	5.236	423	2.002	664	0.9130	807	0.5734	962	0.3200
	2	128	5.799	283	2.072	432	1.013	532	0.6328	624	0.3935
	3	67	6.276	138	2.558	229	1.142	285	0.7175	358	0.3686
	4	23	6.694	45	2.903	76	1.297	97	0.8156	122	0.4367

TABLE V

Specific Viscosities for H3 at 0.1 M and 0.001 M for Different Concentrations and Rates of Shear

I_E (M)	Bulb No.	c_1 = 0.0376		c_2 = 0.0226		c_3 = 0.0141		c_4 = 0.0103		c_5 = 0.0066	
		G	η_{sp}	G	η_{sp}	G	η_{sp}	G	η_{sp}	G	η_{sp}
0.1	1	959	0.3237	1029	0.2337	1138	0.1149	1174	0.0811	1208	0.0508
	2	653	0.3305	696	0.2470	778	0.1157	802	0.0828	825	0.0518
	3	366	0.3399	396	0.2400	437	0.1227	448	0.0866	466	0.0542
	4	131	0.3477	141	0.2441	157	0.1176	162	0.0885	166	0.0565
		c_1 = 0.0461		c_2 = 0.0278		c_3 = 0.0173		c_4 = 0.0126		c_5 = 0.0081	
0.001	1	276	3.596	516	1.464	737	0.7241	868	0.4626	1000	0.2706
	2	179	3.854	337	1.576	488	0.7794	580	0.4992	677	0.2832
	3	98	4.008	180	1.717	263	0.8618	317	0.5443	374	0.3090
	4	33	4.281	62	1.823	90	0.9458	110	0.5939	131	0.3387

TABLE VI

Specific Viscosities for M2 at 0.1 M and 0.001 M, for Different Concentrations and Rates of Shear

I_E (M)	Bulb No.	c_1 = 0.0364		c_2 = 0.0219		c_3 = 0.0137		c_4 = 0.0099		c_5 = 0.0064	
		G	η_{sp}	G	η_{sp}	G	η_{sp}	G	η_{sp}	G	η_{sp}
0.1	1	1046	0.2140	1128	0.1255	1176	0.0792	1201	0.0573	1225	0.0361
	2	713	0.2172	770	0.1278	804	0.0799	820	0.0593	837	0.0373
	3	402	0.2201	434	0.1295	454	0.0814	464	0.0583	473	0.0379
	4	144	0.2251	156	0.1317	163	0.0829	166	0.0601	168	0.0461
		c_1 = 0.0340		c_2 = 0.0204		c_3 = 0.0128		c_4 = 0.0093		c_5 = 0.0060	
0.001	1	449	1.829	743	0.7105	945	0.3438	1042	0.2193	1131	0.1236
	2	299	1.910	498	0.7445	638	0.3624	709	0.2252	768	0.1322
	3	165	2.187	277	0.7708	356	0.3774	392	0.2482	431	0.1353
	4	58	2.028	87	1.0230	125	0.4015	140	0.2556	152	0.1518

TABLE VII

Specific Viscosities for Ll at 0.1 M and 0.001 M, for Different Concentrations and Rates of Shear

I_E (M)	Bulb No.	c_1 = 0.0300		c_2 = 0.0180		c_3 = 0.0113		c_4 = 0.0082		c_5 = 0.0053	
		G	η_{sp}	G	η_{sp}	G	η_{sp}	G	η_{sp}	G	η_{sp}
0.1	1	1128	0.1322	1177	0.0850	1210	0.0550	1237	0.0325	1258	0.0146
	2	759	0.1523	803	0.0893	828	0.0557	843	0.0369	857	0.0209
	3	426	0.1643	451	0.0977	466	0.0623	474	0.0460	485	0.0223
	4	148	0.2023	161	0.1055	166	0.0723	168	0.0570	173	0.0256
		c_1 = 0.0330		c_2 = 0.0198		c_3 = 0.0124		c_4 = 0.0090		c_5 = 0.0058	
0.001	1	680	0.8677	924	0.3750	1070	0.1877	1131	0.1229	1188	0.0694
	2	458	0.8961	627	0.3873	727	0.1945	771	0.1266	809	0.0739
	3	254	0.9310	351	0.3955	408	0.1997	435	0.1262	715	0.0722
	4	91	0.9315	126	0.3918	148	0.1884	155	0.1307	164	0.0671

TABLE VIII

Specific Viscosities for L2 at 0.1 M and 0.001 M for Different Concentrations and Rates of Shear

I_E (M)	Bulb No.	c_1 = 0.100		c_2 = 0.050		c_3 = 0.033		c_4 = 0.020	
		G	η_{sp}	G	η_{sp}	G	η_{sp}	G	η_{sp}
0.1	1	1012	0.2543	1131	0.1230	1179	0.0825	1208	0.0508
	2	689	0.2599	771	0.1266	800	0.0855	823	0.0550
	3	385	0.2738	488	0.1361	450	0.0886	462	0.0602
	4	132	0.3371	149	0.1793	154	0.1377	160	0.0929
		c_1 = 0.0297		c_2 = 0.0198		c_3 = 0.0112		c_4 = 0.0064	
0.001	1	893	0.4209	1080	0.1751	1169	0.8578	1221	0.0398
	2	609	0.4265	737	0.1787	798	0.8804	836	0.0379
	3	344	0.4253	416	0.1772	451	0.8496	472	0.0372
	4	124	0.4124	150	0.1656	165	0.7438	171	0.0274

TABLE IX

Sedimentation Constants of the Fractions for Different Concentrations at 0.1 M, 0.01 M and 0.001 M

Fraction	I_E = 0.1 M		I_E = 0.01 M		I_E = 0.001M	
	Conc. x 10^2	s_m	Conc. x 10^2	s_m	Conc. x 10^2	s_m
H1	28.41	1.66	10.67	1.23	4.58	0.604
	14.20	2.37	7.11	1.58	3.82	0.737
	7.10	3.25	5.34	1.80	3.05	0.867
	3.55	4.52	3.56	2.24	2.29	1.56
	1.78	5.08	1.78	3.04	1.53	2.04
	0.887	5.48	1.33	3.43	0.763	2.52
M1	29.32	1.55	4.73	1.49	3.60	0.587
	14.66	2.03	3.15	1.71	3.00	0.793
	7.33	2.35	2.36	2.00	2.40	1.16
	3.67	-	1.58	2.37	1.80	1.62
	1.83	3.69	0.788	2.62	1.20	1.69
	0.916	4.43	0.591	2.76	0.600	2.64

TABLE IX Contd

Fraction	I_E = 0.1 M		I_E = 0.01 M		I_E = 0.001 M	
	Conc. x 10^2	s_m	Conc. x 10^2	s_m	Conc. x 10^2	s_m
L3	39.46	1.42	8.50	2.43	2.50	0.580
	19.73	1.78	5.67	2.92	2.00	1.15
	9.87	1.95	4.25	3.50	1.50	1.38
	4.93	-	2.83	3.83	1.00	1.74
	2.47	2.92	1.41	3.64	0.501	2.18
	1.23	3.24	1.06	4.43	-	-
H2	26.16	1.67	-	-	4.58	0.844
	13.08	2.24	-	-	3.82	0.940
	6.54	3.84	-	-	3.05	1.13
	3.27	4.19	-	-	2.29	1.54
	1.64	4.31	-	-	1.53	2.17
	0.817	5.38	-	-	0.764	3.57

TABLE IX Contd

Fraction	I_E = 0.1M		I_E = 0.001 M		Fraction	I_E = 0.1 M		I_E = 0.001 M	
	Conc. x 10^2	s_m	Conc. x 10^2	s_m		Conc. x 10^2	s_m	Conc. x 10^2	s_m
H3	31.15	1.30	4.61	0.481	M2	25.00	1.68	3.40	0.553
	15.57	1.74	3.82	0.880		12.50	2.21	2.84	0.872
	7.79	2.24	3.05	1.14		6.25	2.64	2.27	1.17
	3.89	2.72	2.29	1.38		3.13	-	1.70	1.54
	1.95	3.92	1.53	2.18		1.56	3.25	1.13	2.19
	0.973	4.20	0.76	2.74		0.78	3.28	0.567	2.59
	0.487	4.58							
L1	38.62	1.31	3.30	1.10	L2	28.40	1.50	2.38	0.909
	19.31	1.73	2.64	1.33		14.20	1.93	1.78	1.16
	9.66	2.52	1.98	1.78		7.10	2.09	1.19	1.44
	4.83	-	1.32	1.83		3.55	-	0.595	2.57
	2.41	2.84	0.66	2.39		1.78	3.01	-	-
	1.20	3.43	-	-		0.89	3.16	-	-

TABLE X

Diffusion Constants at Different Concentrations, of the Fractions in 0.1 M NaCl by the Boltzmann Technique

H1		H2		H3		M1		M2	
Conc.	$Dx10^7$	Conc.	$Dx10^7$	Conc.	$Dx10^7$	Conc.	$Dx10^7$	Conc.	$Dx10^7$
0.1778	1.19	0.210	1.81	0.2769	1.72	0.3000	2.53	0.2963	2.78
0.1259	0.997	0.180	1.55	0.2154	1.43	0.2440	2.10	0.2371	2.22
0.1037	0.971	0.120	1.38	0.1846	1.49	0.2000	2.08	0.1972	2.23
0.0889	1.03	0.090	1.35	0.1231	1.62	0.1000	2.28	0.1630	2.46
0.0592	1.00	0.060	1.39	0.0615	1.32	0.0440	1.72	0.1037	2.43
0.0445	1.01	-	-	-	-	-	-	0.0444	2.20

L1		L2		L3	
0.2615	2.21	0.2500	4.08	0.2667	4.18
0.2308	2.04	0.2000	3.90	0.2074	3.50
0.1539	1.98	0.1000	4.45	0.1482	3.46
0.1077	1.78	0.0667	4.11	0.0889	3.51
0.0462	1.89	0.0333	3.22	0.0593	3.43

TABLE XI

Values of $Kc/R_\theta \times 10^6$ for Different Fractions in 0.1 M NaCl, at Different Concentrations and Angles

Angle		H1					H2				
	$Cx10^2$ =	15.60	12.48	9.36	6.24	3.12	19.89	15.91	11.93	7.95	3.98
30		3.35	2.62	2.48	1.74	1.34	2.95	2.39	2.13	1.81	1.24
35		3.69	3.18	2.79	2.08	1.53	3.20	2.68	2.31	2.09	1.47
40		3.98	3.65	3.06	2.38	1.74	3.41	3.02	2.55	2.34	1.66
45		4.20	3.90	3.31	2.47	1.91	3.58	3.29	2.75	2.51	1.90
50		4.44	4.16	3.33	2.76	2.11	3.84	3.58	2.99	2.76	2.11
60		4.90	4.77	3.83	3.20	2.55	4.16	4.09	3.37	3.17	2.55
70		5.44	5.33	4.11	3.64	2.89	4.58	4.57	3.80	3.53	2.89
80		5.88	5.75	4.69	4.10	3.32	5.01	4.91	4.30	3.86	3.17
90		6.40	6.21	5.10	4.36	3.72	5.26	5.30	4.70	4.18	3.48
100		6.83	6.64	5.41	4.66	4.03	5.48	5.63	5.02	4.51	3.83
110		7.20	7.13	5.86	5.07	4.52	5.99	6.00	5.54	4.89	4.13
120		7.54	7.47	6.16	5.46	4.79	6.31	6.21	5.77	5.08	4.49
130		7.86	7.79	6.61	5.77	5.11	6.70	6.53	5.87	5.28	4.63
135		7.96	7.96	6.81	6.07	5.20	6.79	6.54	5.95	5.40	4.73

TABLE XI Contd

Angle		H3					M1				
	$Cx10^2$ =	27.27	21.81	16.36	10.91	5.45	25.19	20.15	16.42	10.08	5.04
30		7.66	9.19	7.40	6.00	3.87	2.65	2.30	1.91	1.65	1.19
35		8.55	9.45	7.91	6.23	4.21	2.89	2.61	2.25	1.86	1.36
40		8.93	10.03	8.48	6.70	4.70	3.17	2.96	2.62	2.03	1.54
45		9.31	10.32	8.74	6.93	4.85	3.33	3.10	2.60	2.21	1.73
50		9.41	10.61	9.23	7.15	5.16	3.59	3.29	2.86	2.52	1.94
60		9.99	10.85	9.97	7.83	5.81	4.11	3.91	3.04	3.00	2.37
70		10.63	10.85	10.57	8.15	6.24	4.61	4.43	3.51	3.40	2.68
80		11.73	12.02	10.79	8.78	6.71	4.96	4.71	4.17	3.74	2.99
90		12.79	12.77	11.58	9.26	7.10	5.50	5.16	4.22	4.17	3.36
100		13.02	12.96	12.27	9.73	8.41	5.59	5.58	4.54	4.52	3.69
110		14.01	14.03	12.77	10.29	8.12	6.49	5.89	4.71	4.92	4.02
120		15.78	13.97	13.16	10.65	8.45	7.01	6.21	4.82	5.29	4.27
130		16.71	14.93	13.48	10.99	8.66	7.56	6.71	5.35	5.63	4.55
135		15.78	15.16	13.92	11.07	8.84	7.74	6.85	5.41	5.66	4.60

TABLE XI Contd

Angle		M2					L1				
	$Cx10^2$ =	25.36	20.28	15.21	10.14	5.07	20.44	16.35	12.26	8.18	4.09
30		7.64	6.78	6.23	4.72	4.27	3.58	3.43	2.89	2.61	1.97
35		8.28	7.12	6.78	4.93	4.54	3.80	3.65	3.11	2.68	2.11
40		9.11	7.88	6.87	5.42	5.35	4.11	3.91	3.46	2.83	2.36
45		9.69	8.34	7.67	5.66	5.69	4.38	4.18	3.70	2.82	2.65
50		10.12	9.08	8.72	5.98	6.22	4.61	4.47	3.90	2.83	2.92
60		10.73	9.88	9.39	6.35	7.03	5.20	4.98	4.36	3.09	3.39
70		11.59	10.65	10.17	6.64	7.72	5.64	5.55	4.89	3.28	3.76
80		12.40	11.41	10.36	7.35	8.21	5.92	5.84	5.32	3.67	4.16
90		12.97	12.05	9.95	8.05	8.63	6.29	6.29	5.79	4.02	4.51
100		13.50	12.68	10.86	8.56	9.28	6.55	6.59	6.08	4.06	4.91
110		13.87	13.31	11.68	9.02	9.53	6.95	6.99	6.65	4.59	5.24
120		14.33	14.10	12.31	9.48	9.95	7.21	7.24	6.89	4.79	5.58
130		14.66	14.55	13.38	10.13	10.40	7.84	7.73	7.18	5.15	5.95
135		14.86	14.78	13.59	10.34	10.41	7.78	7.80	7.29	5.15	6.21

TABLE XI Contd

Angle		L2					L3				
	$Cx10^2$ =	39.48	31.58	23.69	15.79	7.90	42.48	33.98	25.49	16.99	8.50
30		1.58	1.40	1.09	0.815	0.879	1.48	1.50	1.44	1.11	0.624
35		1.64	1.49	1.15	0.859	0.875	1.49	1.50	1.45	1.18	0.677
40		1.71	1.67	1.28	0.929	0.875	1.54	1.57	1.53	1.28	0.728
45		1.70	1.70	1.42	0.917	0.943	1.59	1.57	1.55	1.28	0.759
50		1.72	1.73	1.46	0.947	1.01	1.57	1.61	1.57	1.33	0.783
60		1.77	1.80	1.58	1.01	1.05	1.66	1.70	1.61	1.39	0.811
70		1.81	1.83	1.63	1.06	1.16	1.72	1.81	1.72	1.43	0.877
80		1.85	1.86	1.65	1.10	1.18	1.81	1.86	1.65	1.51	0.989
90		1.89	1.90	1.65	1.14	1.12	1.90	1.94	1.74	1.55	1.06
100		1.92	1.95	1.67	1.14	1.16	1.95	2.00	1.82	1.58	1.03
110		1.94	1.98	1.74	1.21	1.17	2.06	2.09	1.87	1.62	1.11
120		1.97	2.02	1.80	1.24	1.22	2.10	2.14	1.91	1.66	1.06
130		2.01	2.07	1.88	1.22	1.28	2.17	2.22	2.00	1.69	1.06
135		2.02	2.07	1.95	1.24	1.33	2.20	2.23	2.14	1.68	1.03

TABLE XII

Values of $Kc/R_\theta \times 10^6$ at two Concentrations of M1, for Different Ionic Strengths

Angle	C = 0.0442			C = 0.0165		
	I_E = 0.05 M	0.01 M	0.0012 M	0.05 M	0.01 M	0.0006 M
30	1.76	3.99	9.90	1.60	1.62	1.42
35	2.44	5.04	9.11	1.74	1.88	1.96
40	3.13	5.40	8.77	1.95	2.49	2.27
45	3.57	5.73	8.24	2.13	2.52	2.81
50	3.87	5.73	8.34	2.32	2.80	3.28
55	4.47	6.23	9.05	2.50	3.22	3.71
60	4.76	7.32	9.43	2.51	3.37	4.16
90	6.37	9.05	11.66	3.22	4.23	6.10
135	8.00	11.47	16.38	4.00	5.39	6.83